A SPECTROSCOPIC STUDY OF SOME ORGANIC FREE RADICALS

A thesis presented for the degree of
Doctor of Philosophy in Chemistry
in the University of Canterbury,
Christchurch, New Zealand.

by

F.T. Greenaway

1972

ACKNOWLEDGEMENTS

I wish to sincerely thank my supervisor, Dr R.F.C. Claridge, for the encouragement and help that he has given to me during the course of this project.

I also wish to thank Dr T.J. Seed of the Physics Department, University of Canterbury for his assistance and for the use of his ESR spectrometer for the first two years of this work; and Mr M.A. Collins of the Physics and Engineering Laboratory, DSIR for the use of his spectrometer and for arranging the γ-irradiation of crystals.

I am most grateful to B.P.(N.Z.) Ltd for the provision of a postgraduate scholarship and to the University Grants Committee for the award of a scholarship and for the provision of equipment.

PUBLICATIONS

The following paper relating to research described in this thesis has been published:

'Electron Spin Resonance of x-Irradiated Single Crystals of Thiosemicarbazide', R.F.C. Claridge, F.T. Greenaway, J. Magnetic Resonance, Dec. 1972 (in press).

CONTENTS

Page

Title

Acknowledgements

Publications

Contents

Abstract

CHAPTER 1 INTRODUCTION AND REVIEW

1.1 The Effect of High Energy Radiation Upon Organic Solids 1

1.2 Application of ESR to the Study of Trapped Organic Radicals 9

1.2.1 The ESR Condition 9

1.2.2 The g-Tensor 10

1.2.3 The Nuclear Hyperfine Tensor 12

1.2.4 The Nuclear Zeeman Interaction 14

1.2.5 The Nuclear Electric Quadrupole Interaction 14

1.2.6 Linewidth and Lineshape 15

1.3 Review of ESR Studies of Organic Radicals Containing Sulphur and Nitrogen 16

1.3.1 Sulphur Radicals 16

1.3.2 Nitrogen Radicals 21

1.4 Introduction to the Present Study 27

CHAPTER 2 EXPERIMENTAL

2.1 Chemicals 29

2.2 Irradiation 32

2.3 ESR Equipment and Experimental Procedure 33

2.4 Calculations 34

2.5 Computational Procedures 35

2.6 Analytical 36

Page

CHAPTER 3 RESULTS FOR THIOACETAMIDE

3.1 Crystal Structure 37

3.2 Irradiation 38

3.3 ESR Spectra 38

CHAPTER 4 RESULTS FOR SODIUM DIETHYLDITHIOCARBAMATE

4.1 Crystal Structure 43

4.2 Irradiation 44

4.3 Temperature Dependence of ESR Spectra 44

4.4 Saturation of ESR Lines 45

4.5 Interpretation of ESR Spectra 46

CHAPTER 5 RESULTS FOR THIOSEMICARBAZIDE

5.1 Crystal Structure 56

5.2 Irradiation 56

5.3 Saturation 57

5.4 Temperature Dependence 57

5.5 Interpretation of ESR Spectra 58

CHAPTER 6 RESULTS FOR SEMICARBAZIDE DERIVATIVES

A Thiosemicarbazide Hydrochloride 69

6A.1 Crystal Structure 69

6A.2 ESR Spectra 69

6A.3 Interpretation of ESR Spectra 71

B Thiosemicarbazide Hydrobromide 77

C Semicarbazide Hydrobromide 78

D 3-Phenyl Thiosemicarbazide 78

E Carbazide 80

F Thiocarbazide 81

G Thiocarbazide Hydrochloride 81

		Page
CHAPTER 7	SUMMARY OF RESULTS AND CONCLUSIONS	82
APPENDIX 1		
A	The g-tensor	93
B	Correction for Anisotropy of g	94
	Computer Program FOE	95
APPENDIX 2		
	Nuclear Zeeman Interaction	98
	Computer Program ANGCALC	101
APPENDIX 3		
	Spectral Simulation	104
	Computer Program LINPLT	104
APPENDIX 4		
A	Anisotropy Curves	109
	Computer Program ROADMAP	109
B	Calculation of Direction Cosines	112
	Computer Program DIRCOS	112
REFERENCES		

ABSTRACT

Several organic compounds which contain an unsaturated carbon-sulphur bond and amino or hydrazino groups have been x-irradiated at room temperature and at 105°K. Electron spin resonance has been used to identify the radical products of irradiation. The unsaturated carbon-sulphur bond is found to be resistant to irradiation damage, which generally occurs at another site in the molecule. In thiosemicarbazide and related compounds the major products of irradiation are nitrogen-centred π radicals and the structure of one such radical has been fully determined. In sodium diethydithiocarbamate, which has a delocalised Π-electron system the ionic products of irradiation are stabler and the radical cation has been characterised. Upon irradiation at room temperature however, the molecule undergoes structural deformation and the extended π-structure is destroyed. Mechanisms for the radiation damage which explain the observed products have been discussed.

CHAPTER 1

INTRODUCTION AND REVIEW

1.1 The Effect of High Energy Radiation upon Organic Solids

Ever since the discovery of x-rays by W.C. Roentgen in 1895 there has been a great deal of interest in the processes by which high energy radiation interacts with matter. No brief review can hope to summarise the wealth of information that has been collected and this introduction will therefore attempt no more than to summarise the major points in one small branch of this wide field, namely the effects of such radiation upon organic solids (1).

The principal characteristic of high energy radiation is that it causes ionisation in all materials. Such a definition distinguishes the field of radiation chemistry from that of photochemistry and although the boundary between the two is not sharp it may be considered to fall at the point where the incident photons have energies greater than the ionisation energy of the most firmly bound outer electrons. This is about 30 eV/molecule which corresponds to radiation with a wavelength of about 40 nm. In radiation chemistry the absorption of energy is not in multiples of the incident photons since only part of the photon energy may be transferred at an interaction. Furthermore, the process is not selective so that different amounts of energy may be absorbed from the photons by different processes. There is always sufficient energy available to break any bond although in practice certain bonds may be broken preferentially. One incident photon may affect many thousands of molecules by secondary effects.

In this project the ionising radiation used was x-rays with energies of 6-8 keV or ^{60}Co γ-rays with energies of 1.17 and 1.33 MeV. When a suitable target is hit by a stream of fast moving electrons x-rays are produced in an energy continuum upon which peaks characteristic of the target material are superimposed. Metal filters may be used to help improve the quality of the radiation by absorbing most of the lower energy photons. γ-rays of discrete energies are emitted from many radioactive nuclei.

The effect of radiation is dependent upon both its energy and its electrical charge. Highly energetic neutral radiation such as 1 MeV γ-rays or neutrons after passing through 10 cm of solid material will have lost only about 50% of its initial intensity whereas charged species such as electrons, protons, or alpha particles penetrate to a depth of only a few millimetres. Low energy neutral radiation of the type used in this project penetrates intermediate distances. Except in the case of neutrons, radiation interacts with electrons and therefore the degree of interaction is dependent upon the electron density of the material, for which mass density is a good approximation.

The mechanism of transfer of energy to the system depends upon the energy of the incident radiation. Photons with energies of 100 keV or more lose energy initially by Compton scattering whereby part of the photon energy is used to eject an electron from an orbital with considerable kinetic energy and the remainder of the energy remains in the scattered photon. For photons with energies less than 60 eV the photo-electric effect becomes the predominant process. With such low energy radiation all of the photon energy is used in

ejecting an electron, usually from an inner orbital. The filling of the inner orbital vacancy from an outer orbital releases further energy which often appears as a number of low energy electrons ejected from one atom, the Auger effect, or as a characteristic fluorescent x-radiation. In addition to these processes a photon may be coherently scattered, but as this scattering is not accompanied by any significant transfer of energy to the molecules it is not necessary to consider it here in any detail.

The primary effect of high energy radiation is therefore to cause ionisation of molecules. The cations and electrons produced in the primary process interact further with the system in what are termed secondary processes. Since a quantum of high energy radiation loses only part of its energy at each interaction a single photon will produce several primary ions. The primary ions will therefore be concentrated along the track of each ionising species, the length of which will depend upon the energy of the photon and the electron density in the material. The secondary products will be centrally distributed about each track. The rate at which energy is transferred to the material is called the Linear Energy Transfer (L.E.T.). This rate is inversely dependent upon the energy of the ionising species, ranging from 0.20 eV/Å for 10 kV x-rays to 0.02 eV/Å for cobalt γ-rays near the surface of the material, and varies in a non-uniform manner as the radiation penetrates further into the solid material. A non-uniform distribution of radiation products within the irradiated material is also observed, because as the ionising species lose energy the concentration of ions increases. The amount of energy absorbed by the system is measured in terms of the rad,

which corresponds to one hundred ergs of energy absorbed per gram of irradiated material.

Following the initial ionisation a number of processes may occur. The secondary electrons or photons which are produced may cause further ionisation or electronic excitation, or by a combination of both, electronically excited ions. Slow moving electrons are especially likely to produce electronic excitation provided that they have sufficient energy to do so. Such electronically excited molecules may return to the ground state by radiationless transition or by luminescence. They may dissociate in three different ways:

$$M^* \rightarrow A\cdot + B\cdot$$

$$M^* \rightarrow A^+ + B^-$$

$$M^* \rightarrow A + B$$

Electrons that are not sufficiently energetic to produce electronic excitation slowly transfer energy to the crystal lattice as vibrational, rotational and translational excitation until they finally reach thermal energies, when they may either recombine with ions to produce neutral species or may be trapped in the crystal by some other species.

The radical cations which are formed in the initial ionisation may dissociate to form an ion and a neutral radical:

$$M^{\cdot +} \rightarrow A^+ + B\cdot$$

or may react with some other species:

$$M^{\cdot+} + M \rightarrow M_2^{\cdot+}$$

$$M^{\cdot+} + M \rightarrow MA^{+} + B\cdot$$

$$M^{\cdot+} + e^{-} \rightarrow M^{*}.$$

The species which are formed in these processes may react together to form either new products or the original species. These processes are summarised in Table 1.1.

In spite of this diversity of possible reactions only a few of them are important in any one irradiated compound. This is because the crystal lattice presents a barrier to the diffusion of species and can absorb excess energy, which means that the probability of recombination is high (liv) and only a few of the reactions will lead to the formation of species that have lifetimes greater than a few molecular vibrations. This inhibition is known as the 'cage effect'. Because hydrogen atoms are small and can escape from a site quite readily one of the most common processes in the irradiation of organic solids is homolytic dissociation of an electronically excited species to produce a hydrogen atom.

$$M^{*} \rightarrow A\cdot + H\cdot$$

Organic compounds vary widely in their susceptibility to radiation, from aromatic systems which are highly resistant to radiation to some olefins and vinyl compounds where radiation may initiate chain reactions. The number of product molecules formed for each 100 eV of energy absorbed by the system is called the G-value, and this may range from 0.1 for some aromatic molecules to 10^6 in systems where chain reactions occur, although for most organic systems G has a value between one and ten.

TABLE 1.1

Reaction Processes in Irradiated Organic Crystals

Primary Ionisation

$$M \rightsquigarrow M^{\bullet+} + e^-$$

Recombination

$$M^{\bullet+} + e^- \rightarrow M^*$$

Electronic Excitation

$$M + e^- \rightarrow M^* + e^-$$

$$M + h\nu \rightarrow M^*$$

Decay of Electronically Excited Species

$$M^* \rightarrow M + h\nu$$

$$M^* \rightarrow A\bullet + B\bullet$$

$$M^* \rightarrow A^+ + B^-$$

$$M^* \rightarrow A + B$$

Formation of Anions

$$M + e^- \rightarrow M^{\bullet-}$$

Decay of Radical Cations

$$M^{\bullet+} + M \rightarrow M_2^{\bullet+}$$

$$M^{\bullet+} + M \rightarrow MA^+ + B\bullet$$

$$M^{\bullet+} + e^- \rightarrow M^*$$

$$M^{\bullet+} \rightarrow A^+ + B\bullet$$

(similarly for anions)

Reactions of Secondary Electrons

$e^- \rightarrow e_t^-$ (thermalisation)

$e_t^- + A^+ \rightarrow A^{\bullet *}$

$e_t^- + A \rightarrow A^{\bullet -}$

$e_t^- + A\bullet \rightarrow A^-$

$e_t^- + A^{\bullet +} \rightarrow A$

Radical Reactions

$A\bullet + B\bullet \rightarrow M$

$A\bullet + B\bullet \rightarrow C + D$

$A\bullet + B \rightarrow BA\bullet \rightarrow C + D\bullet$

Since most organic compounds have low dielectric constants there is less solvation of ions and electrons and greater attractive forces between the two than is the case for polar media. This results in a considerable degree of cation-electron recombination so that reactions involving the primary cations with other species are relatively less important than in a medium which has a high dielectric constant. As a consequence the main mode of formation of radicals is likely to be the decomposition of excited molecules formed in the recombination process rather than the decomposition of the primary ions.

Thus while the initial ionisation and excitation processes are random, the final products are determined by their stability, by the bond strengths of the molecules and by the probability of recombination at any step in the irradiation mechanism. The influence of these factors generally results in there being relatively few products at the attainment of equilibrium which occurs about 10^{-3} seconds after irradiation, although slow thermal reactions of fairly stable species may continue for weeks.

Irradiation of organic crystals at low temperatures may enable some of the primary products to be identified and by careful annealing experiments it is possible to find threshold energies for some of the secondary processes. Experiments at liquid nitrogen ($77^{o}K$) temperatures and even at liquid helium temperatures ($4.2^{o}K$) have become increasingly common and have led to direct observation of every type of radical species mentioned in the foregoing discussion (2-8). It has been shown that irradiation at low temperature followed by heating at higher temperature frequently gives the same products as

irradiation at the higher temperature (9-11). In many other cases it has been possible to deduce reaction mechanisms from a knowledge of the products and of the general molecular properties of the material being irradiated (12-15), even when the irradiation is performed at room temperature.

1.2 Application of ESR to the Study of Trapped Organic Radicals

1.2.1 The ESR Condition

The possession of both spin and charge confers on an electron a magnetic moment, $\bar{\mu}_s$, given by

$$\bar{\mu}_s = -g\beta\bar{S} \qquad (1\text{-}1)$$

where:

g is the Landé splitting factor or g factor,

β is the electronic Bohr magneton, equal to $\frac{e\hbar}{2mc}$ where -e and m are the charge and mass of the electron,

$\hbar S$ is the spin angular momentum of the electron,

$\hbar$ is Planck's constant divided by 2π,

c is the velocity of light.

The interaction between the electron magnetic moment and an applied magnetic field, $\bar{H}$, is expressed by the Hamiltonian

$$\mathcal{H} = -\bar{\mu}_s \cdot \bar{H} \qquad (1\text{-}2)$$

This interaction causes the two previously degenerate electron spin levels to differ in energy and the application of an oscillating magnetic field perpendicular to $\bar{H}$ enables transitions to occur between the two levels, described by the quantum numbers $m_s = \pm\frac{1}{2}$. These transitions may occur if the frequency, ν, is such that

$$h\nu = g\beta H. \qquad (1\text{-}3)$$

In addition to this simple Zeeman interaction, the electron spin may interact with the nuclear spins, I_i, of nearby nuclei, and the magnetic field may also interact with these nuclear spins. Nuclei that have nuclear spins greater than ½ give rise to a nuclear electric quadrupole interaction.

These are the only important interactions affecting the energy of the transition in the case of organic free radicals in the doublet state. Together they may be expressed in the form of a Hamiltonian (16).

$$\mathcal{H} = \beta\bar{H}\cdot\bar{\bar{g}}\cdot\bar{S} - \sum_i \beta_N \bar{H}\cdot\bar{\bar{g}}_{N_i}\cdot\bar{I}_i + \sum_i \bar{S}\cdot\bar{\bar{A}}_i\cdot\bar{I}_i + \sum_i \bar{I}_i\cdot\bar{\bar{Q}}_i\cdot\bar{I}_i \qquad (1\text{-}4)$$

where $\bar{\bar{g}}$ is the g-tensor,

β_N is the nuclear magneton,

$\bar{\bar{g}}_{N_i}$ is the nuclear g-factor tensor,

$\bar{\bar{A}}_i$ is the nuclear hyperfine tensor for nucleus i,

$\bar{\bar{Q}}_i$ is the nuclear electric quadrupole coupling tensor for nucleus i.

1.2.2 The g-tensor

As an electron possesses both spin and orbital angular momentum, the interaction of the magnetic field with the total angular momentum of the electron may be written

$$\mathcal{H} = \beta\bar{H}\cdot\bar{L} + g_e\beta\bar{H}\cdot\bar{S}_T \qquad (1\text{-}5)$$

where $\bar{\bar{S}}_T$ is the true spin angular momentum

and $\bar{L}$ is the orbital angular momentum.

When the electron possesses only spin angular momentum, the g-tensor is isotropic and has the free electron g value, $g_e = 2.0023$. However, even when the electron possesses orbital angular momentum equation 1-5 may be reduced to

$$\mathcal{H} = \beta \bar{H} \cdot \bar{\bar{g}} \cdot \bar{S} \qquad (1\text{-}6)$$

where $\bar{S}$ is an artificial spin vector usually know as the 'effective spin' of the electron,
and $\bar{\bar{g}}$ is a symmetric second rank tensor which incorporates the anisotropy due to the orbital angular momentum.

It is found (16) for molecules which have an orbitally non-degenerate ground state that the only way the odd electron can acquire some orbital angular momentum is through the effect of spin-orbit coupling which can be represented as

$$\zeta \bar{L} \cdot \bar{S} \qquad (1\text{-}7)$$

where ζ is the spin-orbit coupling constant. Because this effect is small, particularly for organic radicals where the orbital levels are well separated, it is considered as a perturbation of the Hamiltonian (1-5) and the resulting energy levels and wave functions can be calculated using perturbation theory. This calculation shows that excited electronic states are mixed into the ground state function to produce new states that are no longer eigenstates of the true spin, $\bar{S}_T$. Thus $\bar{S}$ is redefined so that it operates on the new wavefunctions exactly as $\bar{S}_T$ does on the spin functions. It is found that L_z is unaffected by excited states with spin opposite to that of the ground state and that to first order in ζ the value of S_z is still $\frac{1}{2}$.

The effect of this procedure is that the g-tensor is used to incorporate the anisotropy of the energy levels arising from the effects of the orbital angular momentum of the electron. It can be deduced that

$$g_{zx} = g_e - 2\zeta \sum_n \frac{\langle\psi_0|L_z|\psi_n\rangle\langle\psi_n|L_x|\psi_0\rangle}{E_n - E_0} \qquad (1\text{-}8)$$

where $E_n - E_0$ is the energy difference between levels described by the wavefunctions ψ_n and ψ_0 where ψ_0 is the ground state wave function. For a molecule the molecular orbitals may be expressed as a linear combination of atomic orbitals, ϕ_k,

$$\psi_i = \sum_k c_{ki}\phi_k \qquad (1\text{-}9)$$

and the elements of the g-tensor reduce to the form

$$g_{zz} = g_e - 2 \sum_n \sum_{k,j} \frac{\langle\psi_0|\zeta_k L_{zk}\delta_k|\psi_n\rangle\langle\psi_n|L_{zj}\delta_j|\psi_0\rangle}{E_n - E_0} \qquad (1\text{-}10)$$

where the summation is over all pairs of atoms k,j and over all states, n; and where δ_k means that the result of L_{zk} operating on an atomic orbital is zero unless the orbital belongs to atom k.

Thus a knowledge of the molecular orbitals and their energies enables the g-tensor to be calculated, or alternatively from knowledge of the g-tensor it may be possible to deduce information about the molecular orbitals and thus the geometry of the radical.

1.2.3 The nuclear hyperfine tensor

The nuclear hyperfine term, $\bar{S}\cdot\bar{\bar{A}}_i\cdot\bar{I}_i$, consists of two parts:

(1) an isotropic part, $a_i\bar{S}\cdot\bar{I}_i$, arising from the Fermi contact interaction and related to the electronic wave function, $\psi_i(0)$, at the nucleus i by the equation

$$a_i = \frac{8\pi}{3} g\beta g_N\beta_N |\psi_i(0)|^2 \qquad (1\text{-}11)$$

(2) an anisotropic part, $\bar{S}\cdot\bar{\bar{A}}'_i\cdot\bar{I}_i$. The anisotropic tensor $\bar{\bar{A}}'$ may always be reduced to diagonal form by a suitable similarity transformation to give principal values a'_1, a'_2 and a'_3.

The anisotropic part, or dipolar hyperfine interaction is essentially the interaction of two dipoles, $\bar{\mu}_I$ and $\bar{\mu}_S$ separated by a distance $\bar{r}$. For one electron and one nucleus this interaction is represented by

$$\mathcal{H}' = gg_N\beta\beta_N \frac{\bar{I}\,\bar{S}}{\bar{r}^3} - \frac{3(\bar{I}\,\bar{r})(\bar{S}\,\bar{r})}{\bar{r}^5}, \qquad (1\text{-}12)$$

where the anisotropy arises from the orientation dependence of the vector $\bar{r}$. Because of the orbital motion of the electron this expression reduces to

$$\mathcal{H}' = gg_N\beta\beta_N \left\langle \frac{(1 - 3\cos^2\phi)}{r^3} \right\rangle \qquad (1\text{-}13)$$

which is zero for spherically symmetric orbitals and which averages to zero for rapidly tumbling molecules.

The effect of the hyperfine interaction is to split the $m_s = \pm\frac{1}{2}$ energy levels into $\prod_i (2n_i I_i + 1)$ sublevels, where n_i is the number of magnetically equivalent atoms with nuclear spin $\bar{I}_i$. To a first approximation this produces $\prod_i (2n_i I_i + 1)$ lines in the spectrum, each line associated with a transition between states where $\Delta m_I = 0$. Lines arising from the same nuclear interaction are equally spaced, although the spacing depends upon the orientation of the crystal in the magnetic field. In this approximation the components of $\bar{I}_i$ and $\bar{S}$ that lie perpendicular to the magnetic field are neglected. If they are not neglected it is found (17) that the energy of the states for the case of one interacting nuclear spin, I, becomes

$$E = \beta g H M_S + A M_S m_I + \frac{A^2 M_S}{2g\beta H}\left[I(I+1) - m_I^2\right] \qquad (1\text{-}14)$$

where the third term arises from the second order correction. For a single interacting nucleus the inclusion of this term merely causes a small shift in the hyperfine energy levels without altering their separation and these effects are negligible compared with the effects of the nuclear Zeeman energy. Slight changes in intensity also result from the second order correction.

1.2.4 Nuclear Zeeman interaction

The term $\beta_N \overline{\overline{H}}\, \overline{\overline{g}}_{N_i}\, \overline{I}_i$ may be regarded as isotropic since the anisotropic terms arising from the diamagnetic shielding of the nucleus are only 10^{-5} times the isotropic terms. While the magnitude of the nuclear Zeeman interaction is usually quite small at X-band frequencies (9000 MHz) it does produce shifts in the energy levels and also allows transitions between states where $\Delta m_I \neq 0$ to have appreciable intensity. The result is that additional weak satellite lines may be observed. The procedure for calculating the effects of the interaction is discussed in Appendix 2.

1.2.5 The nuclear electric quadrupole interaction

The deviation of nuclear charge from spherical symmetry is reflected in the nuclear quadrupole interaction which causes small shifts in the energy levels. These cause the spacings of the nuclear hyperfine lines to be unequal but as the nuclear quadrupole moments of ^{14}N, ^{35}Cl and ^{37}Cl are all small it was not expected that this inequality could be observed, as was indeed the case, and no calculation was required.

1.2.6 Linewidth and lineshape

Associated with each line in a spectrum is a position, a width and a shape, and information about the radical and its environment may be obtained from each of these.

The linewidth is dependent upon the lifetime, τ, of the spin state undergoing the observed transition in a manner described by the Heisenberg Uncertainty Principle:

$$\Delta H \propto \frac{1}{\tau} .$$

Thus all relaxation processes which shorten the lifetime of the spin state will cause an increase in linewidth. Such processes include interaction of the electronic dipole with surrounding electronic or nuclear dipoles and quadrupoles, either spatially fixed or varying with the rotational, vibrational or translational motions of the crystal lattice. Electron exchange and chemical reactions between species may also be important.

Line broadening may also be caused by unresolved hyperfine structure, by variations in the frequency of the oscillating field or by an inhomogeneous magnetic field as well as by the effects of saturation or modulation broadening which can be eliminated by suitable tuning of the spectrometer. A detailed study of linewidth can therefore yield information about relaxation processes and unresolved hyperfine interactions.

For organic radicals the line shape is generally approximately Gaussian because the predominant broadening effect is the dipole interaction with neighbouring dipoles which are arranged in an approximately Gaussian distribution.

When energy is supplied to the spin system more rapidly than it can be transferred to the lattice the system is said to be 'saturated' and the result is a reduction in signal height which is greatest at the centre of the signal and which therefore causes line broadening. As different species relax in different manners deliberate saturation of one of the spin systems may clarify the spectrum in cases where more than one radical is present.

1.3 Review of ESR Studies of Organic Radicals containing Sulphur and Nitrogen

1.3.1 Sulphur radicals

From the very beginnings of esr spectroscopy attention has been focussed on radicals containing sulphur because of their importance in the radiolysis of natural products like proteins, enzymes and such components of cell nuclei as DNA and RNA. The early work of Gordy and coworkers (18-22) showed that irradiation of amino acids, proteins and thiols frequently gave rise to a characteristic esr signal which was attributed to radicals that had an unpaired electron localised primarily on a sulphur atom. Subsequent single crystal studies of radicals formed by irradiation at room temperature have verified this assignment and have shown that sulphur-sulphur and sulphur-hydrogen bonds are readily cleaved to produce stable radicals in which the unpaired electron normally occupies a non-bonding p-orbital of the sulphur atom (23-27). Kurita and Gordy (23) developed this model in their study of the $HOOCCH(NH_2)CH_2S\cdot$ radical formed by γ-irradiation of L-cystine dihydrochloride and were able to deduce electronic transition energies from the theory of the g-tensor. The model

has been successfully applied to several similar radicals formed by cleavage of sulphur-hydrogen (25), sulphur-sulphur (27) and sulphur-carbon (24) bonds. Isotropic hyperfine interactions with the β-hydrogen atoms, arising through hyperconjugation are generally observed.

More recent experiments carried out at lower temperatures show that the precursors of these radicals are radical ions that again have an unpaired electron located primarily on the sulphur atom (3,5-8,10,28,29). Studies of crystals of L-cystine dihydrochloride at 77°K and 4.2°K by Box and Freund (8,28) and Akasaka et al. (3,29) have shown that both cations and anions are formed corresponding to a loss or gain of an electron in the region of the sulphur-sulphur bond. As the temperature is raised above 77°K the sulphur-sulphur bond cleaves to produce radicals which when reoriented to their stablest configuration are identical to the radicals formed upon irradiation at room temperature. Both ions are unstable to light but the anion decays more slowly and also persists to higher temperatures than the cation. The hyperfine interaction of the nearby protons is better resolved in the anion than in the cation but is almost isotropic in both. The g-values are also different, with only the anion possessing axial symmetry. Akasaka et al. (29) have explained these properties in terms of a model where the unpaired electron is in an antibonding σ* orbital in the anion, and in a nonbonding orbital in the cation.

Ionic species have also been observed in irradiated dithioglycollic acid (6), D-L methionine (132), thiodiglycollic acid (5) and in several thiols (10,30,31) and it has been established that the species decay by cleavage of a sulphur-sulphur or sulphur-hydrogen bond where one exists, or of a

carbon-hydrogen bond adjacent to the sulphur atom when the sulphur is bonded to two carbon atoms. Although cleavage of a sulphur-carbon bond under irradiation at room temperature has been observed in N-acetyl methionine (24) it is more common for C-H bond cleavage to occur (32-35). The resulting radical is stabilised by some delocalisation of the unpaired electron onto the sulphur atom on which the unpaired spin density may be as high as 0.22, as observed in the $HOOCCH_2\dot{S}CHCOOH$ radical formed from thiodiglycollic acid (34).

The major processes following irradiation of saturated sulphur compounds are:

$$M \rightsquigarrow M^{\cdot+} + e^{\cdot-}$$

$$M + e^{\cdot-} \rightarrow M^{\cdot-}$$

$$RSSR^{\cdot+} + e^{\cdot-} \rightarrow 2RS\cdot$$

$$RSH^{\cdot+} + e^{\cdot-} \rightarrow RS\cdot + H\cdot$$

$$RSCH_2R^{\cdot+} + e^{\cdot-} \rightarrow RS\dot{C}HR + H\cdot$$

$$RSCH_2R^{\cdot+} + e^{\cdot-} \rightarrow RS\cdot + \cdot CH_2R$$

together with simple recombination processes.

Many of the early experiments on sulphur-containing systems were concerned with the transfer of spin from one part of a molecule to another (36) or from one molecule to another (37,38). Such work is of interest because of the protective action of sulphur towards radiation damage in biological systems. In many irradiated compounds or mixtures of compounds where there is a sulphur atom it is found that alkyl radicals formed soon after irradiation gradually decay and that the number of sulphur radicals increases. These processes

generally involve transfer of a hydrogen atom and the rate of this process is found to depend upon the temperature and upon the nature of the sample (30,39-44).

Very few esr studies have been made upon irradiated compounds which have unsaturated carbon-sulphur bonds. Luck and Gordy (19) observed a broad signal in irradiated thioacetamide and Jaseja and Anderson (45) reported the lack of signals in thiourea. Carbon disulphide gains an electron to form CS_2^- (46) which is similar to the CO_2^- radical ion and whose structure agrees with that predicted by a Walsh diagram for a 17-electron molecule.

Anions and cations were observed in thiourea, allyl thiourea and 1,2-dimethyl thiourea which are planar molecules but not in the non-planar tetramethyl or 1,2-diphenyl thioureas which gave nondescript spectra near the g value of a free electron (7). Such anions have nearly isotropic g values ($g \sim 2.003$) whereas the cations have highly anisotropic g values. (For example, the principal values of the g tensor of the thiourea cation are 2.067, 2.009 and 2.003). The difference between the g-values of the two ions is due to the difference in the energy required to excite a ground state molecule to the lowest electronic excitation level, which is much greater for the anion ($n \rightarrow \Pi^*$) than for the cation ($n \rightarrow \Pi$). This means that there is less admixture of the excited states into the ground state for the anion. In addition to the signals due to these ions, a signal attributed to a hole shared between two thiourea molecules was observed. All the radicals disappeared on momentary warming to room temperature showing that recombination processes are much more

important than radical-producing reactions. Even though thiourea is a conjugated system and the unpaired electron was expected to have been delocalised over both nitrogen atoms the unpaired spin density on the nitrogen atoms was too low for resolvable hyperfine splittings to be observed.

Perhaps the most important general observation concerning the irradiation of sulphur compounds is that there is a preference for sulphur as the site of radiation damage and that radicals of the general form RS· are more stable than analogous radicals having the odd electron concentrated mainly on a carbon or oxygen atom. Because of the 'cage effect' mentioned in chapter 1.1, loss of a hydrogen atom from a molecule is generally the major radical forming process. In the presence of a mercaptan group this may be followed by intermolecular or intramolecular transfer of a hydrogen atom from a sulphur to a carbon or oxygen atom. This transfer is generally energetically favourable since the dissociation energy of the sulphur-hydrogen bond is less than that of the oxygen-hydrogen or carbon-hydrogen bond as shown in Table 1.2.

TABLE 1.2

Bond Dissociation Energies ($kJ.mole^{-1}$) (47,48)

HS-H	376	HO-H	498	H-H	435
CH_3S-H	368	CH_3O-H	427	CH_3-H	435
C_2H_5S-H	368	C_2H_5O-H	435	C_2H_5-H	410
CH_3-SH	306	CH_3-OH	381		
C_2H_5-SH	293	C_2H_5-OH	381	C_2H_5-CH_3	337

1.3.2 Nitrogen radicals

Because of the importance of nitrogen in amino acids many studies of radicals containing nitrogen have been performed, although only a few of these radicals have the unpaired electron centralised on the nitrogen atom.

Much of the early work on irradiated amino acid powders (19) did not lead to the identification of the radicals, and in many later experiments the nitrogen atom was far removed from the unpaired electron (23,24,26,32,33,43). Loss of the amino or protonated amino group as in α-alanine (49-52), α-aminoisobutyric acid (53-56), glycine (52,57,58) and many other amino acids (44,54,59,60) is also common. Other radicals which have the amino group sufficiently close to the unpaired electron to produce an observable nuclear hyperfine interaction have been studied. In some cases the hyperfine lines are resolved, as in the cases of the $CH_3\dot{C}HNHCOC_6H_5$ and $CH_3\dot{C}(COOH)NHCOC_6H_6$ radicals produced upon irradiation of N-benzoyl alanine (61) and the $\cdot CH(NH_3^+)COO^-$ radical formed in glycine crystals (62-67). In other cases, such as for the $^+H_3NCH_2CONH\dot{C}HCOO^-$ radical formed from α-glycyl glycine (68), the hyperfine splittings are too small to be resolved and contribute to the linewidths.

Some low temperature studies of the effect of radiation on amino acids (50,53,57-59,69) have identified the major primary radical as an anion which has the unpaired electron on the COO^- functional group. This decays upon heating by loss of ammonia from the alpha carbon. Cationic species have not been positively identified although they probably are the precursors of radicals like $^+NH_3\dot{C}HCOO^-$ which has been observed in glycine (50,62,70).

Several radicals formed from amines have been observed in solution and in frozen matrices. Wardman and Smith (71,72) observed the $\cdot CH_2NH_2$ radical upon irradiation of methylamine but found that $CD_3\dot{N}H$ was formed in deuterated methylamine. They attribute this difference to slight changes in crystal structure, hydrogen bonding and in bond strengths which become important because of the similarity of the C-H and N-H bond strengths. They postulate the mechanism:

$$CH_3NH_2 \rightsquigarrow CH_3NH_2^+ + e$$

$$CH_3NH_2^+ + CH_3NH_2 \rightarrow CH_3NH_3^+ + CH_3NH\cdot$$

$$CH_3NH_2^+ + CH_3NH_2 \rightarrow \cdot CH_2NH_2 + CH_3NH_3^+$$

$$CH_3NH\cdot + CH_3NH_2 \overset{\Delta}{\rightleftarrows} \cdot CH_2NH_2 + CH_3NH_2$$

Wood and Lloyd (73) have studied the effects of radiation on a wide variety of primary, secondary and tertiary amines in adamantane matrices and have observed many radicals of the type $R_1R_2\dot{C}NR_3R_4$. The stability of such species increases in the order $H_2\dot{C}NH_2 > HR\dot{C}NH_2 > R_2\dot{C}NH_2$ (R = alkyl) which is the reverse of the order for alkyl radicals. The hyperfine splitting of the nitrogen atom decreases with increasing alkyl substitution on the carbon but increases for increasing substitution on the nitrogen. These effects are attributed to slight shifts in Π electron density caused by the difference in electronegativity between hydrogen and alkyl substituents (74). The hyperfine splitting due to the hydrogen atoms bonded to the nitrogen decreases upon alkyl substitution for one of these atoms and is attributed to twisting about the C-N bond away from a planar CNH_2 equilibrium position.

Upon illumination with light of wavelength less than 540 nm $R_2\dot{C}NH_2$ radicals form alkylimino radicals, $R_2C{=}N\cdot$, that have an unpaired spin density greater than 0.8 in a nitrogen p orbital (75). Where such radicals have a β hydrogen they are characterised by a very large (80-90G) hydrogen hyperfine splitting. Similar radicals have been observed when tetrazene solutions are photolysed (76).

There have been many studies of radicals formed from amides. Most irradiated amides lose a hydrogen or a halogen atom from the α carbon to form radicals of the type $\cdot CXHCONH_2$ (77-82) where the nuclear hyperfine splittings due to the amine group are small or not observed. Only in the $CH_3\dot{C}HCONH_2$ radical formed in crystals of propionamide (30) is the nitrogen hyperfine splitting well enough resolved to enable the principal values to be determined (3.18, 0.40, 0.23G). N-alkyl substituted amides may be reduced by abstraction of a hydrogen atom from the substituent as in the case of N,N dimethylformamide which yields $\cdot CH_2(CH_3)NCHO$ radicals as well as $(CH_3)_2N\dot{C}O$ (83,84). Acetamide initially forms anions upon irradiation at 77°K (85) but at room temperature only the $\cdot CH_2CONH_2$ radical is observed (86). Trifluoroacetamide (81,87) produces the analogous $\cdot CF_2CONH_2$ radical as well as $H_2N\dot{C}O$ and $\cdot CF_3$ radicals from cleavage of a carbon-carbon bond.

Several cases where nitrogen centred radicals were thought to explain the spectra have later been reinterpreted. The carbamoyl radical, $O\dot{C}NH_2$, was originally assigned the structure $OHC\dot{N}H$ (86), but it was later deduced that the orbital of the unpaired electron was centred upon the carbon atom (88). Originally it was thought that $NH_2CONH\cdot$ was formed upon

x-irradiation of hydroxyurea (89) but subsequent studies showed it to be $NH_2CONHO\cdot$ (90-92). $CF_3CF_2\dot{C}ONH$ was observed as a minor product in irradiated pentafluoropropionamide crystals (93) but the g and hyperfine tensors could not be determined.

A radical remarkable for a very large (80G) and almost isotropic hydrogen hyperfine coupling was observed in x irradiated crystals of malonamide and assigned as $H_2NCOCH_2\dot{C}ONH$ (94,95). Similar signals were observed upon irradiation of cyanoacetylurea (96) and dicyandiamide (97,98) and were assigned to the $NCCH_2CONHC\dot{O}NH$ and $NCNC(NH_2)\dot{N}H$ radicals respectively. To account for the large hydrogen hyperfine coupling it was originally considered that these were either σ radicals or π radicals where the hydrogen was not in the nodal plane of the π orbital. The common dominant feature of these radicals suggests that they are similar but Symons (99) was not able to resolve the problem and considered that the malonamide radical might be NH_3^+ while suggesting a new structure, $RHC{=}N\cdot$, to explain the signals in cyanoacetylurea. Radicals of this type have been produced in solution from nitriles (100) and amines (75). Recent experiments on cyanoacetic acid crystals (101,102) γ-irradiated at 77^oK show that $\cdot NCHCH_2COOH$ is formed by hydrogen addition and that the parameters of the Hamiltonian are similar to those of the malonamide, cyanoacetylurea and dicyandiamide radicals. The unpaired electron is in a nitrogen p orbital whose axis is in the plane of the carbon-hydrogen bond and there is an unpaired spin density of 0.65 on the nitrogen atom. It therefore seems reasonable to reassign the other species to radicals of this type. The crystal structure of dicyandiamide has been

determined (103) but because the directions of the principal axes of the g and nuclear hyperfine tensors have not been published it is not possible to determine whether $(NH_2)_2CNCHN\cdot$ or $\cdot NH(NH_2)CNCN$ is the most reasonable assignment. The former, however, seems more probable in view of the observation that only one hydrogen atom and two nitrogen atoms give observable hyperfine interactions with the unpaired spin.

The relative orientations of the various principal axes for the radicals in malonamide and cyanoacetic acid are very similar which suggests that the radicals are both $\cdot NCHR$ radicals. In malonamide the orbital of the unpaired electron (A^N_{max}) appears to be directed along the a axis of the crystal (104) at an angle of 70^o from the nitrogen-hydrogen bond direction (A^H_{max}). This angle is much smaller than the angle expected for a $R\dot{N}H$ radical and is in good agreement with the results for $\cdot NCHCH_2COOH$. It therefore appears that the radical in irradiated malonamide is $\cdot NCHCH_2CONH_2$ formed by loss of OH from the parent molecule. Toriyama and Lin (102) have proposed the following mechanism for radical formation in cyanoacetic acid.

$$NCCH_2COOH \xrightarrow[77^oK]{\gamma} [NCCH_2COOH]^+ + e$$

$$[NCCH_2COOH]^+ \rightarrow NCCH_2C(=O)(-O\cdot) + H^+$$

$$NCCH_2C(=O)(-O\cdot) \rightarrow NCCH_2\cdot + CO_2$$

$$NCCH_2\cdot + NCCH_2COOH \rightarrow NCCH_3 + NC\dot{C}HCOOH$$

$$NCCH_2COOH + e^- \rightarrow NCCH_2\dot{C}(-O^-)(-OH)$$

$$NCCH_2\dot{C}(-O^-)(-OH) + H^+ \rightarrow NCCH_2\dot{C}(OH)_2$$

$$NCCH_2\dot{C}(OH)_2 \rightarrow \cdot N{=}CCH_2COOH$$

Any comparable mechanism for radical formation in amides would involve the formation of RNH· radicals which normally decay by hydrogen abstraction from a C-H bond and therefore low temperature irradiation studies are necessary to resolve the problem of explaining the presence of a cyano radical in malonamide.

In cyanoacetylurea the principal axes of the tensors are directly in a slightly different manner but until the crystal structure is determined no positive identification of the radical can be made.

The only other nitrogen compounds that have been found to produce nitrogen radicals are the ureas. Urea itself forms the radical $H_2NCO\dot{N}H$ upon irradiation at 77°K (105). This has the unpaired electron in a π orbital but is not stable at room temperature, when $O\dot{C}NH_2$ forms (133). Alkyl substituted ureas form alkyl radicals (45,106) and thiourea forms ionic sulphur-centred radicals (7), which recombine at temperatures below 77°K. Ionic species have also been observed in O-methyl isouronium chloride crystals x irradiated at 77°K (107).

Semicarbazide hydrochloride forms the $\cdot NHNH_3^+$ radical by cleavage of a carbon-nitrogen bond (108) but carbazide crystals irradiated at 77°K lose hydrogen atoms to form $NH_2NHCONHNH\cdot$ radicals and radical pairs (109).

Thus while many nitrogen compounds have been irradiated only a very few form radicals that have an unpaired electron centred upon the nitrogen atom. This is presumably because the abstraction of a hydrogen atom by cleavage of a C-H bond is energetically favourable. The nitrogen radicals that have been observed have been formed in systems where no C-H bonds occur or where the radical is stabilised by extensive delocalisation over two or more atoms. The only exceptions

(71,76,110) were observed at low temperatures when the available energy was presumably less than the activation energy for hydrogen transfer, or in urea inclusion crystals (111) where intermolecular transfer is impossible.

1.4 Introduction to the Present Study

In view of the paucity of information on unsaturated non-aromatic radicals containing sulphur it was decided to investigate the results of irradiation of organic compounds which contain a carbon-sulphur double bond. Because of the difficulty of predicting exactly which radicals are likely to be formed it seemed desirable to allow for the possibility that the sulphur radicals might not be stable, as the results for thiourea indicated, and to incorporate another functional group of interest. Recent controversy over the structures of radicals formed from organic compounds containing nitrogen decided us to limit the study to compounds containing both sulphur and nitrogen. It was envisaged that the results of such studies could be compared to results obtained from irradiation of amides and that the comparison of the two might lead to a better understanding of the radiation processes and of the structure of the radicals.

The technique of electron spin resonance is a highly sensitive means of studying small concentrations (as low as 10^{-8}M under favourable conditions) of free radicals and leads to information about bonding and the electron distribution throughout the radical. It has the additional advantages that the parent molecule makes no contribution to the observed spectrum except by way of weak intermolecular interactions which sometimes complicate the spectrum, and that unstable species may be observed by working at low temperatures. This

study was primarily concerned with the products of irradiation at room temperature although some experiments were performed at lower temperatures. Lack of very low temperature facilities precluded the observation of primary products which often decay at temperatures below 77°K. It was however anticipated that the reaction mechanism could probably be deduced from a knowledge of the stable products by comparison with the results of other studies at low temperatures. Single crystals were used because the maximum amount of information can be obtained from single crystal spectra.

The compounds selected for study were thioacetamide, which bears comparison with both amides and thiourea, thiosemicarbazide which may be compared with thiourea and semicarbazide, and sodium diethyl dithiocarbamate wherein the unpaired electron was expected to be highly delocalised. Studies were also envisaged on compounds related to these, and a number of additional compounds were irradiated.

Such compounds have the advantages of being stable in air and of forming large suitably shaped crystals. Other possible subjects for study such as thioacetanilide, potassium xanthate and thiopropionic acid were excluded because they did not conform to these requirements.

CHAPTER 2

EXPERIMENTAL

2.1 Chemicals

Thiosemicarbazide (BDH Laboratory Reagent) was twice recrystallised from water. Crystals, mp. 182-183°C (lit. 181-183°C) (112), were colourless needles with poorly defined edges so that it was not possible to identify the crystal faces. Partially deuterated crystals were grown by slow evaporation of a solution of recrystallised thiosemicarbazide in 99.8% deuterium oxide (Stohler Isotope Chemicals). Deuterated crystals had a similar appearance to undeuterated crystals.

Mass spectrographic analysis of deuterated thiosemicarbazide showed 34% d_5-, 55% d_4-, 10% d_3- and 1% d_2-thiosemicarbazide in the crystal from which the final parameters were obtained but it was not possible to identify the position of deuteration by this means. The infrared spectrum of the partially deuterated compound showed none of the peaks associated with the vibrational modes of the amine group and only very weak residual peaks in the region of the N-H bending modes near 336 nm.

Thiosemicarbazide Hydrochloride was prepared by dissolving recrystallised thiosemicarbazide in water acidified with excess dilute hydrochloric acid. Light green transparent crystals, mp. 183-186°C (lit. 186-190°C) (112), with well developed faces readily formed upon slow evaporation of the solution. The infrared spectrum agreed well with published results (113,115). Crystals of deuterated thiosemicarbazide hydrochloride were obtained by slow evaporation of a solution of thiosemicarbazide

hydrochloride in 99.8% deuterium oxide. Mass spectrographic analysis of these crystals showed an average of 32% d_5-, 44% d_4-, 22% d_3- and 2% d_4-thiosemicarbazide hydrochloride although this varied from crystal to crystal. Infrared spectra of the deuterated sample showed only faint peaks in the regions where the NH_2 and NH vibrational modes occur.

Analysis:

	N	H	C	Cl	S
calc. for SCH_3H_6Cl	32.93%	4.74%	9.41%	27.79%	25.13%
found	32.90%	4.74%	9.73%	28.13%	

Thiosemicarbazide Hydrobromide was prepared by dissolving recrystallised thiosemicarbazide in water acidified with excess dilute hydrobromic acid. Crystals, mp. 170-173°C, were very similar to those of the hydrochloride. The infrared spectrum agreed well with published results (113,116).

Analysis:

	C	H	N	S	Br
calc. for SCN_3H_6Br	6.98%	3.49%	24.42%	18.61%	46.50%
found	7.02%	3.57%	24.27%	18.52%	46.43%

Thiosemicarbazide Hydriodide crystals could not be prepared and although a powder was obtained by slow evaporation of an aqueous solution of thiosemicarbazide acidified with excess dilute hydriodic acid, mass spectrographic analysis showed it to be impure. Attempts to produce the hydrofluoride by similar methods were unsuccessful.

Semicarbazide Hydrochloride (Hopkin and Williams Ltd, England) crystals were grown by slow evaporation of aqueous solutions of the material. Large colourless prisms were readily obtained, mp. 172-3°C (lit. 175°) (112).

Semicarbazide Hydrobromide was prepared by the addition of a large excess of dilute hydrobromic acid to an aqueous solution of semicarbazide hydrochloride. Slow evaporation of this solution yielded elongated prisms, mp. 172-176°C (lit. 174°), (117), which were a faint brown colour. Infrared spectra agreed well with published results (118).

Sodium Diethyldithiocarbamate (BDH Laboratory Reagent) crystals were grown by slow evaporation of aqueous solutions. Large well formed colourless crystals, mp. 95-97°C (119) were readily grown.

Thioacetamide (L. Light and Co. Ltd, England) crystals were grown by slow evaporation of benzene solutions. Crystals, mp. 111-112°C (lit. 115-116°C), (120) were slightly yellow and readily cleaved across the axis of elongation.

Zinc bis(diethyldithiocarbamate) (BDH Laboratory Reagent) crystals were grown by slow evaporation of benzene solutions. Very large light brown transparent crystals were obtained, mp. 179.5-182°C (lit. 180°C) (112).

Thiocarbazide was prepared by the reaction of carbon disulphide with hydrazine hydrate (121) but only very small crystals, mp. 168-169°C (lit. 168°C) (122), with ill-defined faces could be obtained. Large colourless crystals of thiocarbazide hydrochloride were grown from an aqueous solution of thiocarbazide acidified with hydrochloric acid.

Carbazide was prepared by the reaction of diethylcarbonate with hydrazine hydrate (123). Large elongated colourless crystals mp. 155-158°C (lit. 153-154°C) (124), were obtained by crystallisation from aqueous solution. The crystals cleaved readily across the axis of elongation.

Analysis:

	C	H	N
calc. for OCN_4H_6	13.33%	6.67%	62.22%
found	13.48%	6.37%	62.58%

3-Phenyl Thiosemicarbazide was prepared by heating phenylhydrazine with thiourea (125) for four hours at 150-160°C following the method of Pinner (125i). Pinkish plates, mp. 201-203°C (lit. 200-1°C) (112), were obtained by crystallisation from ethanol.

Analysis:

	C	H	N	S
calc. for $SC_7N_3H_9$	50.25%	5.43%	25.14%	19.18%
found	50.11%	5.49%	24.92%	18.92%

Fremy's Salt was prepared by the method described by Zimmer, Lankin and Horgan (126).

2.2 Irradiation

Crystals were irradiated in air at room temperature using a Phillips P.W.1009 x-ray generator operating at 35 kV and 20 mA. Nickel filtered copper Kα radiation was generally used although unfiltered CuKα radiation gave identical products.

Samples of all compounds were also sealed in glass tubes and γ-irradiated, both in air and under vacuum, using a ^{60}Co γ-irradiation source at a dose rate of 0.14 Mrad/hr. Dosages were of the order of 1-10 Mrad but in no case did the size of the dose cause a variation in the radiation products. Samples irradiated under vacuum gave identical results to samples irradiated in air.

Low temperature irradiation was achieved by placing the crystals in contact with a copper rod that was placed in a large reservoir of liquid air or liquid nitrogen so that the

crystals lay in the x-ray beam just above the surface of the liquid coolant. The temperature of the crystal was determined by a chromel-constantan thermocouple and was found to vary between 95°K and 105°K depending on the quantity of coolant in the reservoir. Crystals irradiated by this method were attached to a quartz rod by silicone grease and rapidly transferred to the cavity of the esr spectrometer.

In some cases crystals were glued to a quartz rod which was cooled in a similar manner while in the x-ray beam. This afforded a greater degree of accuracy in orienting the crystal but the difficulty of placing the crystal in the centre of the x-ray beam while maintaining good thermal contact with the coolant and the fairly high frequency with which the glue failed to hold meant a much lower rate of success. In addition, radicals were produced in the glue and in the quartz rod. The signals due to these radicals, although generally weaker than the signals of interest did sometimes obscure them.

2.3 ESR Equipment and Experimental Procedure

ESR spectra were taken on a Varian E12 esr spectrometer operating at 9.5 GHz with 100 kHz modulation and 12" magnet. Variable temperatures were achieved by using the Varian V4557 variable temperature accessory. Early results were obtained from a similar spectrometer built by Dr T.J. Seed of the Physics Department, University of Canterbury (127).

Samples were mounted on the quartz rod of a Varian E229 goniometer which was attached to a Varian general purpose cavity. In the case of thiosemicarbazide, crystals were first mounted in a perspex cube to facilitate rotation about three orthogonal axes. For all other crystals rotation was

about directions defined by the crystal faces. Crystals were mounted by eye with the aid of a magnifying glass and glued into position with a glue made by dissolving perspex in chloroform. Large crystals could be mounted with an accuracy of at least 2^{o} as evidenced by good agreement between spectra from different crystals. Data were normally recorded at intervals of $1\text{-}5^{o}$ depending on the complexity of the spectra. Relative alignments in a single rotation were correct to $\pm\frac{1}{2}^{o}$. Rotation was about three orthogonal axes with the axial directions consistent for all three rotations. Checks were also made in a few orientations not in these planes.

The effect of varying microwave power was determined for each crystal, and spectra were taken at power levels that gave negligible saturation effects. In some cases additional sets of spectra were taken at power levels where a high degree of saturation was occurring, as this enabled the signals of different radicals to be separated. The effect of temperature on the spectra of each radical was also observed.

Powdered 2,2'-diphenyl-1-picrylhydrazyl (DPPH) recrystallized from carbon disulphide (mp. 127^{o} sharp) was used to calibrate g-values ($g_{DPPH} = 2.0036$) and solutions of naphthalene with potassium in 1,2-dimethoxyethane (130), or Fremys salt in water (128,129) were used to check the calibration of the field scan.

2.4 Calculations

All calculations were performed on an IBM 360 Model 44 (32K word core storage) computer. Output from this computer was used to drive an IBM1627 plotter.

2.4.1 Spectral simulation

Spectra were simulated using a simple first order calculation to generate line positions. A line shape function was used to calculate intensities at small intervals around the line positions. These intensities were summed for each increment on the magnetic field and the pairs of coordinates so obtained were used to plot the spectra. The computer program used to calculate and plot spectra is discussed in Appendix 3.

An adaptation of a program provided by J.A. Weil (131) enabled spectral simulation using second order equations to calculate line positions and intensities but as this took considerably more computer time and as the effects were barely observable little use was made of it.

2.5 Computational Procedures

2.5.1 g tensor

For each spectrum the g value was calculated from the microwave frequency and the magnetic field at the centre of the spectrum of each species. These experimental g-values together with two angles defining the orientation of the field relative to axes related to the crystal faces were used as input for a computer program that calculated the elements of the g^2 tensor (Appendix 1, part A).

2.5.2 Nuclear hyperfine splitting tensor

The experimentally observed hyperfine splitting due to each nucleus was calculated at each orientation by measuring the difference in magnetic field strength between the hyperfine lines. In cases where $I > \frac{1}{2}$ the splittings between the lines were averaged as they were always equal, within experimental error. A hyperfine tensor was then calculated by the

procedure used to calculate the g tensor.

Once the g tensor had been determined it was used to obtain a more accurate hyperfine tensor by the procedure outlined in Appendix 1, part B.

2.5.3 Nuclear Zeeman interaction

The effect of the nuclear Zeeman interaction is considered in Appendix 2. The g and hyperfine tensors derived from first order calculations were used as input for a computer program which adjusted the tensor elements to obtain a least squares fit to the observed hyperfine splittings using the second order equations. The corrections were again generally small when compared with the experimental error in the measured splittings.

2.5.4 Computer programs

The computer programs used in the course of this work are discussed in the appendices.

2.6 Analytical

Microanalytic analyses for carbon, hydrogen, nitrogen, sulphur, chlorine and bromine were carried out in the Microanalytical Laboratory of the University of Otago.

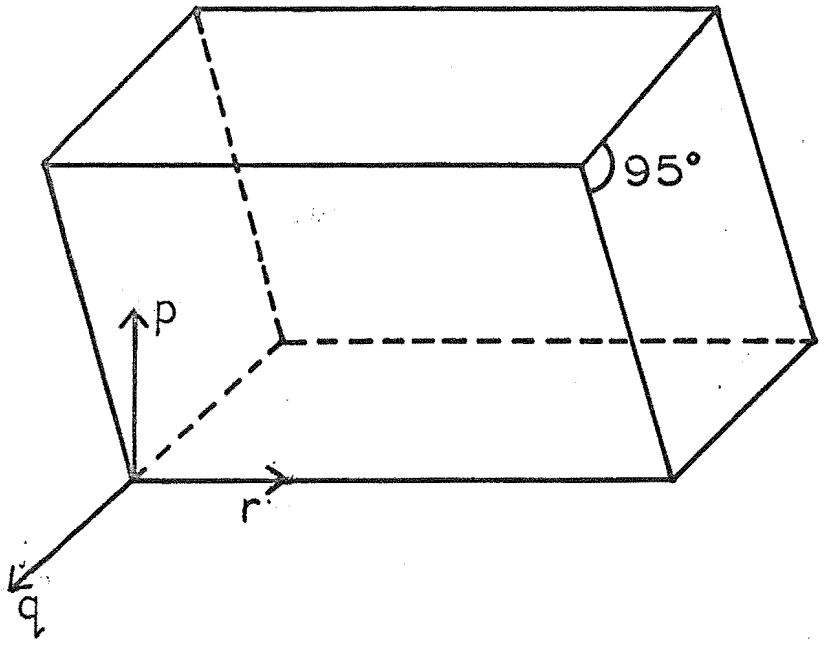

FIG. 3.1 Crystal habit of thioacetamide, with laboratory axes.

CHAPTER 3

RESULTS FOR THIOACETAMIDE

3.1 Crystal Structure

Crystals of thioacetamide were faintly yellow with well defined edges and readily cleaved across the axis of elongation, which caused some difficulties in obtaining esr spectra at low temperatures. Axes were assigned to coincide with the crystal faces as shown in Fig. 3.1.

The crystal structure has been determined (134) by x-ray diffraction methods. The crystals are monoclinic, space group $P2_1/a(C_{2h}^5)$, with eight molecules in a unit cell of dimensions $a = 11.065\text{Å}$, $b = 10.005\text{Å}$, $c = 7.170\text{Å}$, $\beta = 99.5^\circ$. The carbon, nitrogen and sulphur atoms of each molecule are coplanar and the molecular planes of the two inequivalent molecules in the asymmetric unit meet at an angle of 24.6°. The symmetry unrelated molecules differ slightly in their rotational modes, which may be due to the closer proximity of one of these to its centrosymmetrically related molecule. The normals to the molecular planes of the two sets of molecules make angles of 5.1° and 28.6° respectively with the crystal c-axis.

Single crystal x-ray precession photographs were taken to relate the laboratory axis system to the crystal axes. The direction of elongation (r axis) was found to be the crystal c-axis, as deduced from the ready cleavage across this axis. The crystal a-axis was found to be 47.5° from the normal to the broader face (q axis) and 42.5° from the p axis. These angles show that the broad face is the $1\bar{1}0$ face of the crystal and that the other face is the 110 face of the crystal, there being an angle of 95° between them.

The direction cosines of the bond directions in the a'bc crystal axis system were calculated from crystallographic data and transformed to the laboratory axis system. The important direction cosines are given in Table 3.1 where the two unrelated species are designated I and II.

The unit cell has a centre of symmetry and there will therefore be only four magnetically inequivalent radicals in a general orientation. When the magnetic field is along the crystal axes two magnetically inequivalent crystal sites are expected.

3.2 Irradiation

Crystals became green when they were irradiated for long periods with x- or γ-rays at room temperature. Exposures of about 100 hours were required to produce sufficient concentration of radicals to give an adequate signal to noise ratio, and exposures of less than 40 hours resulted in little colouration of the crystals and only very weak esr signals. As far as could be determined the radicals resulting from irradiation for 60 hours were the same as those produced upon irradiation for 150 hours.

Upon irradiation for six hours at 105^{o}K the crystals become olive, but this colour disappeared when the crystals were warmed to room temperature.

3.3 ESR Spectra

3.3.1 Low Temperature Irradiation

Crystals x-irradiated at 105^{o}K and immediately transferred to an esr cavity at 120^{o}K gave a many lined, orientation dependent spectrum centred at g = 2.003. The spectra were never symmetrical about their centre even when the magnetic

TABLE 3.1

Thioacetamide

Direction Cosines of Bond Directions[a]

Molecule I (site 1)			
C_1-S_1	0.0118	-0.9991	-0.0406
C_1-N_1	0.08549	-0.5121	-0.0832
C_1-C_2	-0.8600	-0.5072	0.0553
$\perp$	-0.0733	0.0396	-0.9965
Molecule I (site 2)			
C_1-S_1	-0.9943	0.0988	-0.0406
C_1-N_1	-0.4356	0.8963	-0.0832
C_1-C_2	-0.5803	-0.8125	0.0553
$\perp$	-0.0331	0.0764	-0.9965
Molecule II (site 1)			
C_3-S_2	0.0320	-0.9966	0.0757
C_3-N_2	0.7677	-0.5292	-0.3613
C_3-C_4	-0.7330	-0.5167	0.4423
$\perp$	0.4701	0.0818	0.8788
Molecule II (site 2)			
C_3-S_2	-0.9900	0.1188	0.0757
C_3-N_2	-0.4603	0.8109	-0.3614
C_3-C_4	-0.5787	-0.6852	0.4423
$\perp$	0.1225	0.4611	0.8788

[a]Relative to laboratory axes, pqr.

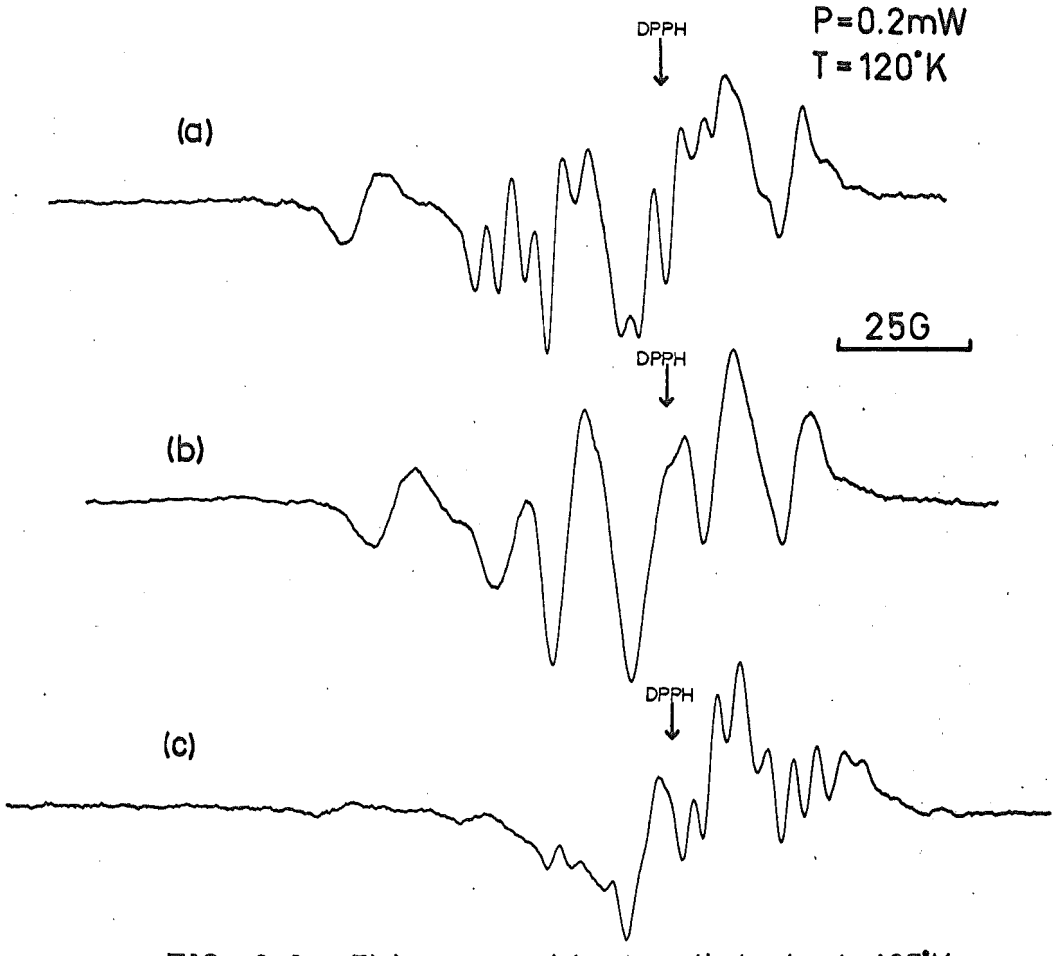

FIG 3.2 Thioacetamide, irradiated at 105°K.

field was along the crystal axes, which indicates that there are at least two inequivalent species present. Examples of spectra are given in Fig. 3.2 but it was not possible to follow the variation of line position as the orientation of the crystal in the magnetic field was altered and no assignment could be made to the various lines. At some orientations a single line (Fig. 3.2b) separated from the main set of lines which extended over a range of sixty gauss at all orientations. In a few orientations spectra became almost symmetrical about their centre and were composed of five broad lines of relative heights 1:3:4:3:1. These could arise from interaction of the unpaired electron with one nitrogen and two equivalent hydrogen nuclei, where all the nuclear hyperfine splittings lie between ten and fifteen gauss.

The complexity of the spectra precludes the definite identification of the radicals formed upon low temperature irradiation, but the g-value shows little evidence of spin-orbit coupling which indicates that there is little spin density in orbitals centred upon the sulphur atom. The simplest spectra suggest the presence of the $\cdot CH_2CSNH_2$ radical although the nuclear hyperfine coupling of the nitrogen is much larger than has been observed in the $\cdot CH_2CONH_2$ (84,86) radical or in any similar halogen substituted radical where the hyperfine splitting of the nitrogen nucleus is always less than three gauss. Molecular orbital calculations for amides and thioamides (163) however, show that there is a greater π-electron density on the nitrogen atom in the thio compounds and that the carbon-nitrogen bond has greater double bond character, so that a greater hyperfine splitting from the nitrogen atom is expected for the $\cdot CH_2CSNH_2$ radical.

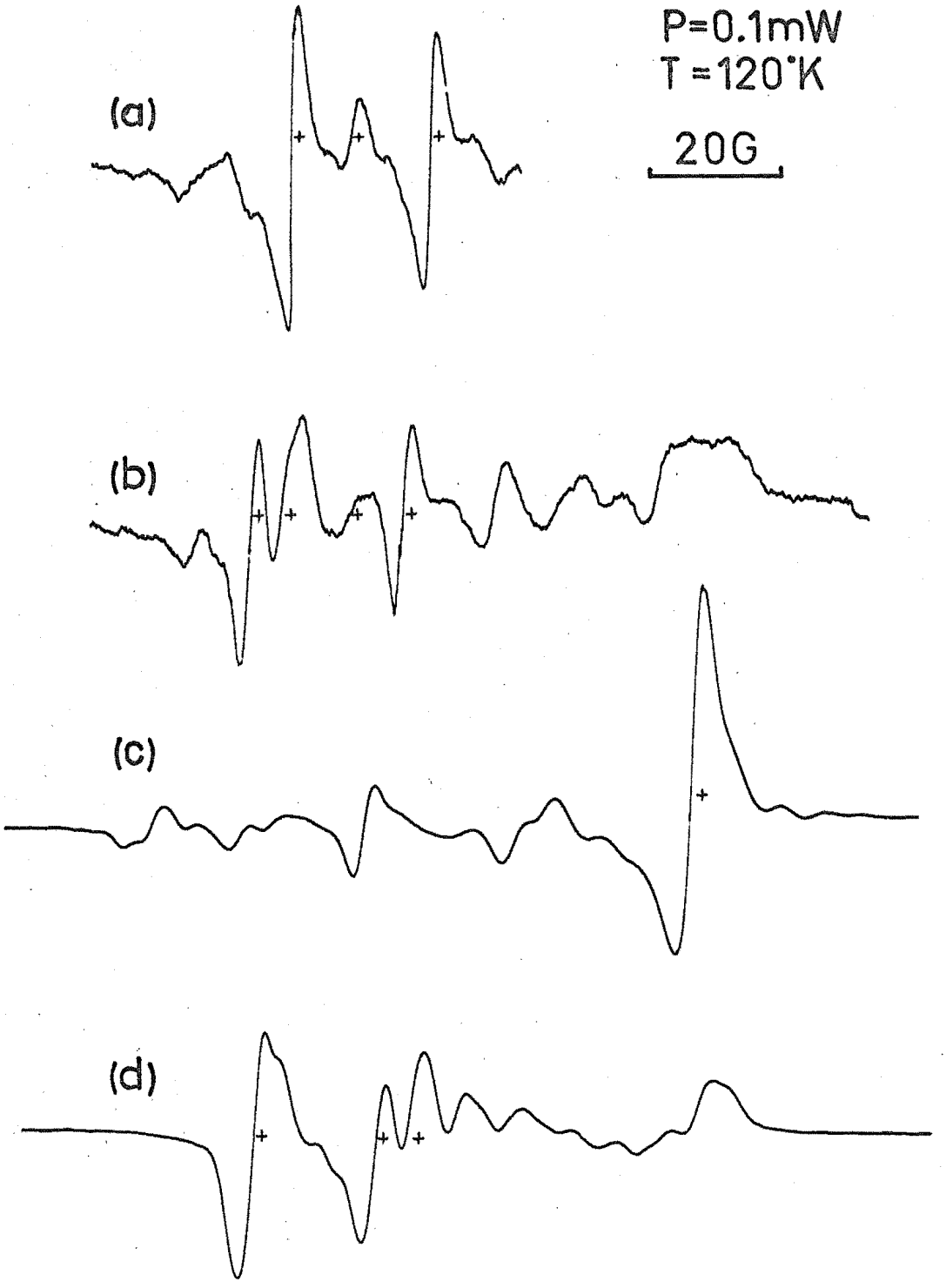

FIG 3.7 Thioacetamide irradiated at 290°K showing main peaks(+) with the magnetic field along (a) (1,0,0), (b) (0,1,0), (c) (0,0,1), (d) (0.5,0.87,0.0) in the pqr-axis system.

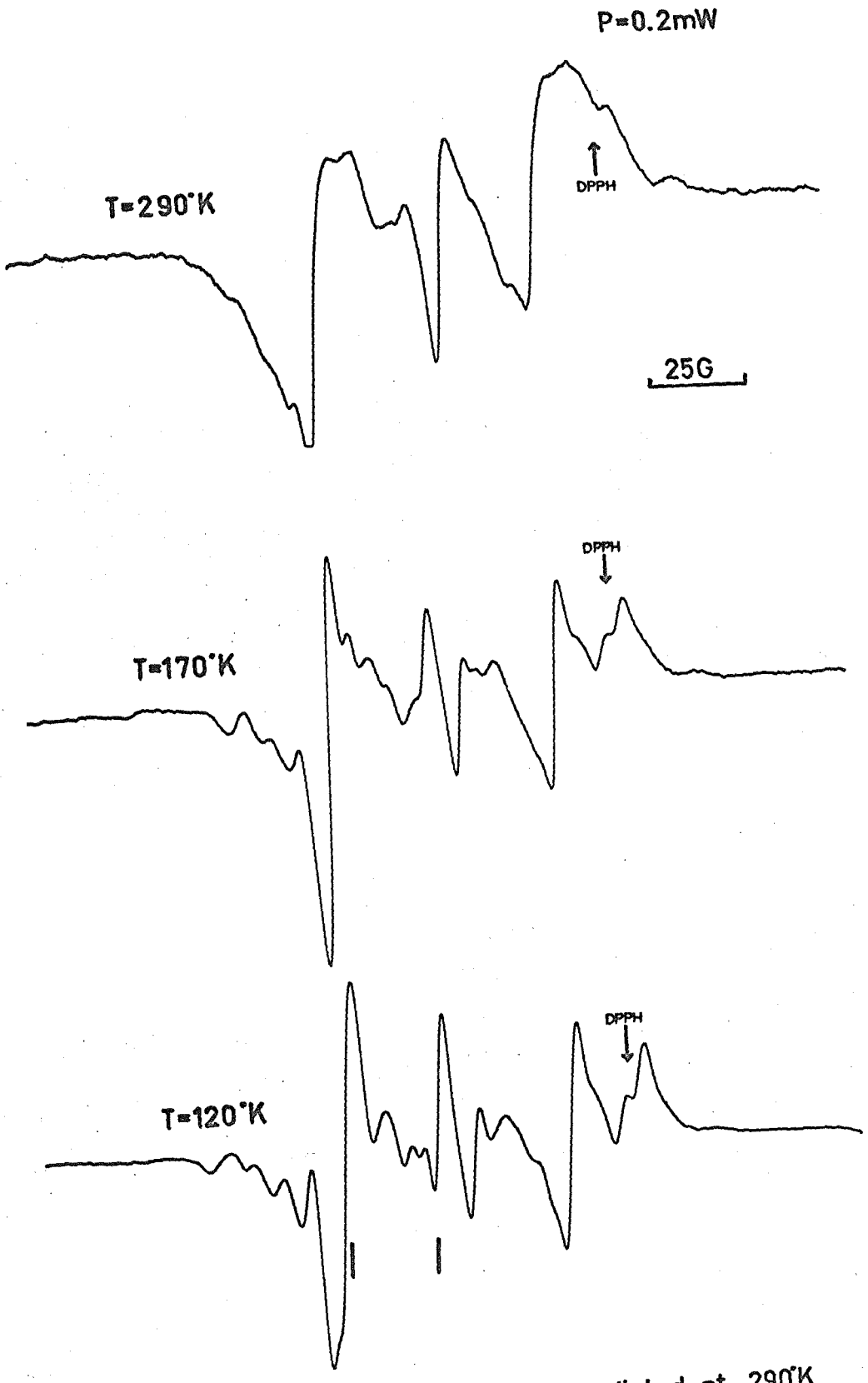

FIG 3.3 Thioacetamide, irradiated at 290°K. Temperature dependence.

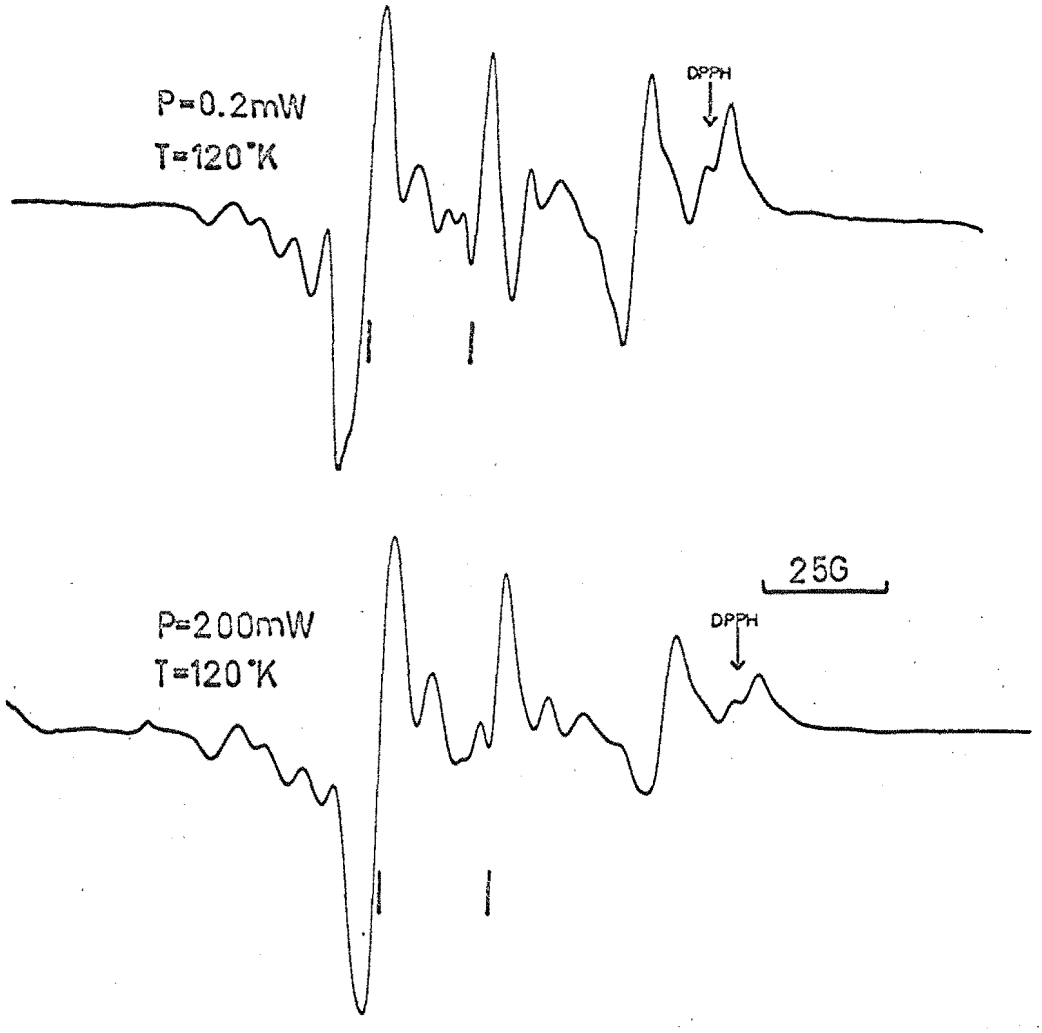

FIG 3.4 Thioacetamide, irradiated at 290°K. Power saturation.

3.3.2 Room temperature irradiation

The esr spectra of crystals irradiated at room temperature were generally composed of many overlapping broad lines (Fig. 3.7) spanning a range of about 150G on the low field side of g = 2.000. Such spectra were markedly temperature dependent (Fig. 3.3). As the temperature was decreased some lines became dominant and it was possible to determine the anisotropy in the g-value. No major attempt was made to analyse the less intense lines because while the angular variation of such lines could be established over small changes in orientation of the crystal, it was not possible to obtain a complete set of orientation data. Since all of these lines had g > 2.003 it appears that they generally involve spin-orbit coupling of the electron to an atom with a large spin orbit coupling constant, probably sulphur.

Spectra of the major lines were recorded at 120°K and at low microwave power (0.2 mW) in three orthogonal planes at 1.8° intervals. The effect of increasing the microwave power level to 200 mW was not very great (Fig. 3.4) although all lines saturated and some of the weaker lines appeared to broaden more than others.

When the magnetic field was parallel to the crystal c-axis the esr spectrum showed only one line due to the major species, but in the general orientation there are four lines and spectra taken with the magnetic field in the pq plane show clearly that there are two sets each of two symmetry related species (Fig. 3.5). These different sets have similar g-values but unrelated orientations. The g-tensors calculated for these lines are given in Table 3.2 and the anisotropy curves are shown in Fig. 3.5.

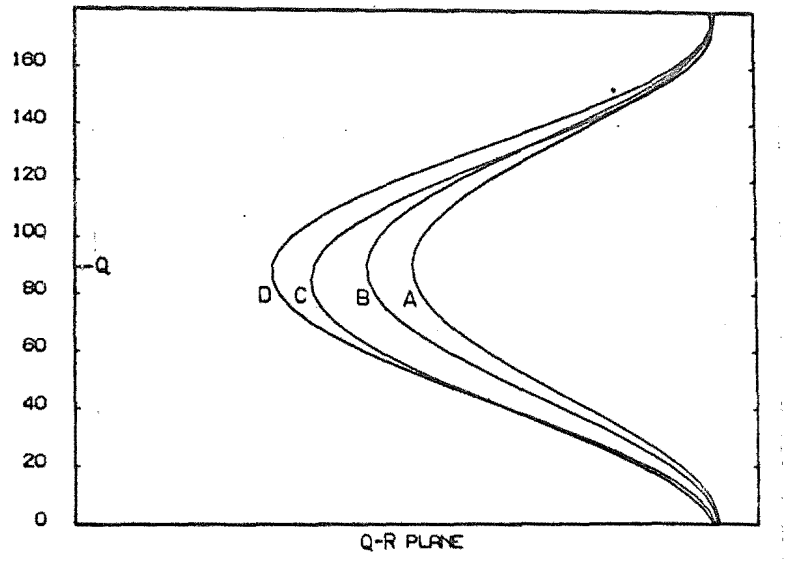

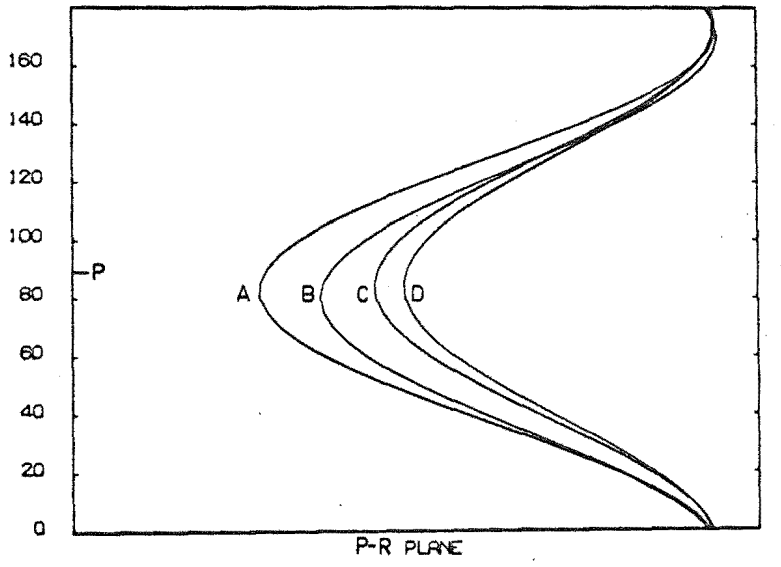

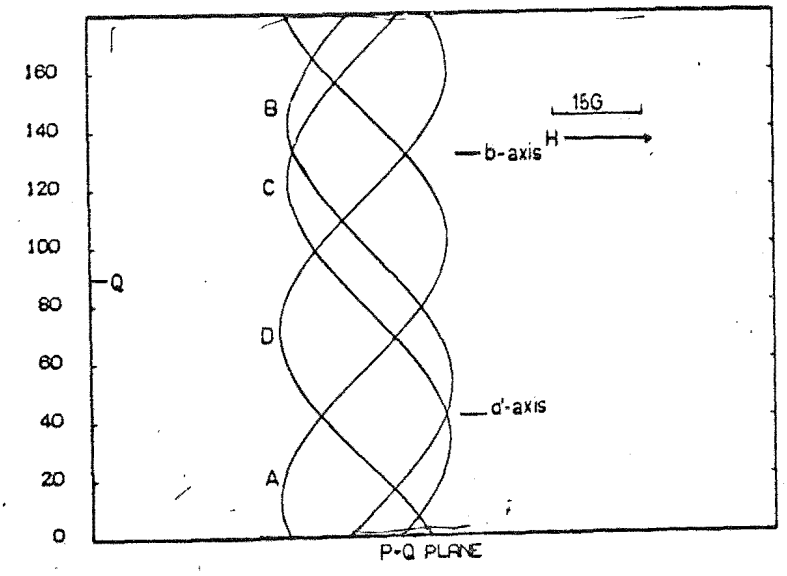

FIG 3.5 Thioacetamide

TABLE 3.2

Thioacetamide

	Principal Value[b]	Direction Cosines[a]		
A	2.0507	0.978	0.207	0.032
	2.0334	-0.203	0.975	-0.095
	2.0028	-0.050	0.087	0.995
B	2.0496	0.796	-0.599	0.091
	2.0327	0.601	0.799	0.005
	2.0029	-0.076	0.051	0.996
C	2.0496	-0.545	0.838	-0.003
	2.0329	0.838	0.545	0.027
	2.0031	-0.024	-0.012	0.9996
D	2.0506	0.323	0.946	-0.033
	2.0331	0.946	-0.322	0.039
	2.0032	-0.026	0.044	0.9987

[a]With respect to laboratory axes, pqr

[b]Standard deviation = 0.0004

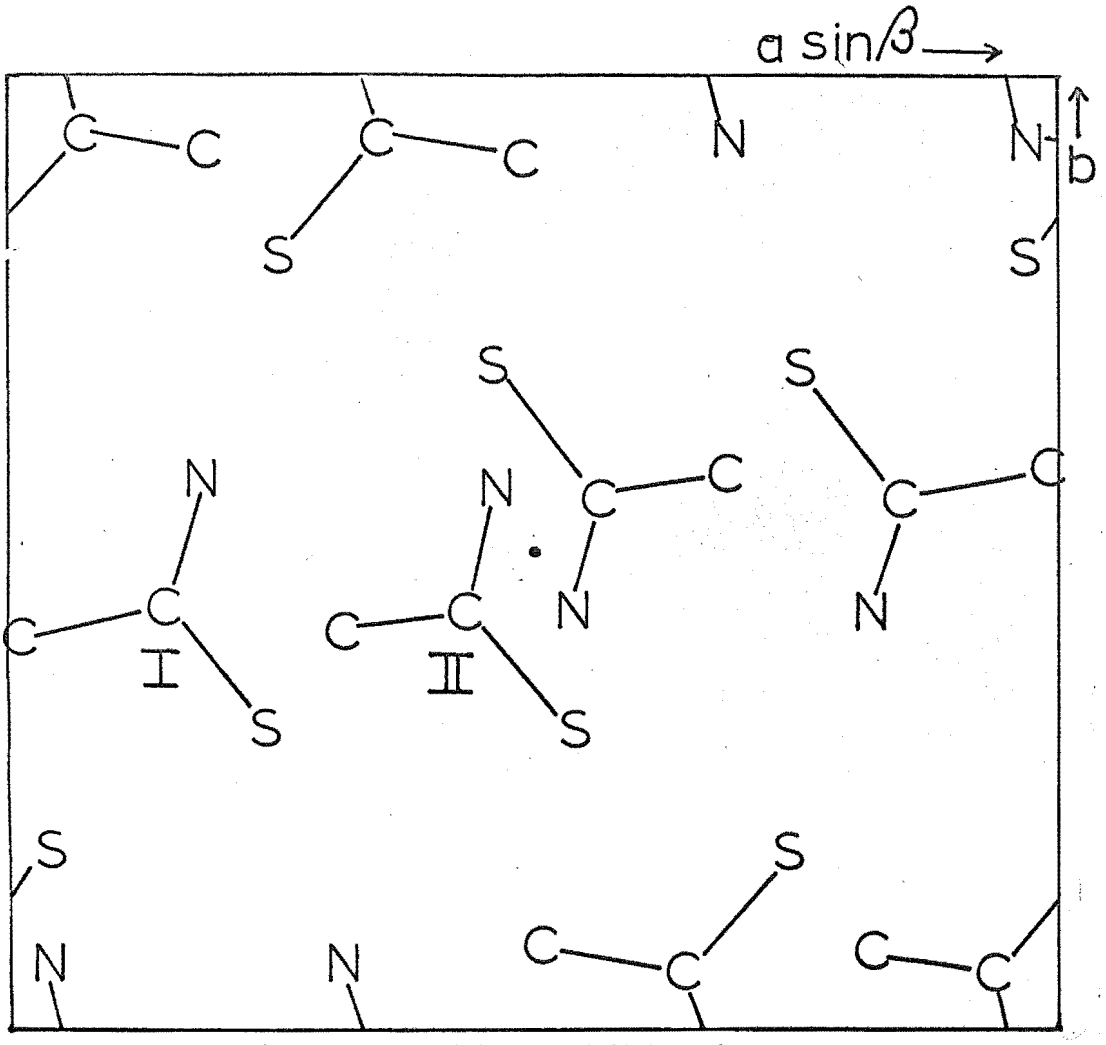

CRYSTAL STRUCTURE

DIRECTION COSINES

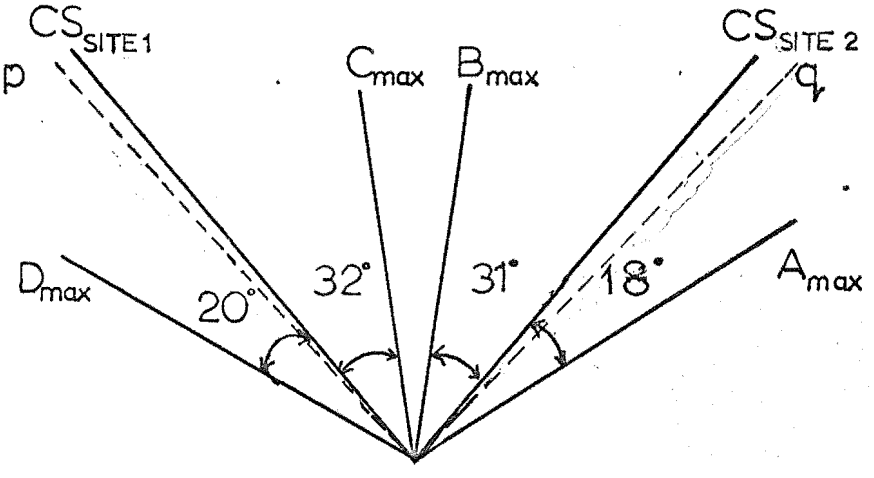

THIOACETAMIDE

FIG 3.6

The large deviation of the principal values of the g-tensor from the free spin value suggests that the electron is localised primarily on the sulphur atom, and the close comparison of these values to those found for a number of thiol radicals where the unpaired electron is in a π orbital (Table 3.3) localised mainly on a sulphur atom indicates that a similar radical has been formed in thioacetamide.

This conclusion is supported by the orientation of the principal axes of the g-tensor. The minimum principal value is directed in a direction close to the crystal c-axis or normal to the molecular plane. According to the model of Kurita and Gordy (23) for a radical with the unpaired electron in a sulphur 3p orbital normal to the molecular plane there should be little mixing of this orbital with other orbitals and the g-value should be close to the free spin value, as observed. This model predicts the maximum principal value to be directed along the carbon-sulphur bond. The calculated direction of the maximum principal value in the four observed radicals is shown in Fig. 3.6 where it can be seen that the principal axis associated with the maximum g-value occurs at an angle from the carbon-sulphur bond of about 19° for the A and D radicals and of about 32° for the B and C ardicals. The similarity of the direction cosines of the carbon-sulphur bond direction for the two inequivalent molecules I and II (Table 3.1), means that it is not possible to determine which set of molecules should be associated with the radicals, but the significant although small difference between the principal values of the g-tensors suggests that A and D are associated with one site and that B and C are associated with the other.

TABLE 3.3

Literature Data for g-Values of Thiol Radicals

Radical	Principal Values	Reference
$HOOCCH_2CH_2S\cdot$	2.055, 2.025, 2.003	27
$HOOCCH(NH_3Cl)CH_2S\cdot$	2.29, 1.99, 1.99	26
$CH_3CONHCHCOOH$ with $CH_2CH_2S\cdot$ on the central CH	2.064, 2.029, 2.004	24
$HOOCCH_2CH(COOH)S\cdot$	2.054, 2.026, 2.003	25
$HOOCCH(NH_2)CH_2S\cdot$	2.053, 2.025, 2.003	23
Radical I	2.0507,2.0332,2.0030	this work
Radical II	2.0496,2.0328,2.0030	this work

The complete absence of hyperfine structure and the lack of correspondence of the principal axes of the g-tensor with the bond directions in the undamaged crystal makes assignment to a structure uncertain. The large radiation dose required to produce observable quantities of the radical indicates that the radical may have been formed from an unobserved product of the irradiation. It is unlikely that the radical is either $CH_3\dot{C}=S$ or $NH_2\dot{C}=S$ as this type of radical is expected to have the unpaired electron in a σ-orbital (154), in which case the minimum principal value of the g-tensor is expected to be in the plane of the molecule.

The stability of the radical at 290°K and higher temperatures discounts the possibility that the radical is an ionic species of the type:

$$CH_3 - \overset{\overset{S^{\pm}}{\|}}{C} - NH_2$$

since comparable ionic species formed from other compounds such as thiourea (7) decay at much lower temperatures. The most probable assignment is to a radical of the form:

$$R - \overset{\overset{CH_3}{|}}{\underset{\underset{NH_2}{|}}{C}} - S\cdot$$

where the unpaired electron is in a p orbital on the sulphur atom and where R is most likely to be a hydrogen atom. The formation of such a radical would be accompanied by a considerable reorientation of the bonds about the central carbon atom.

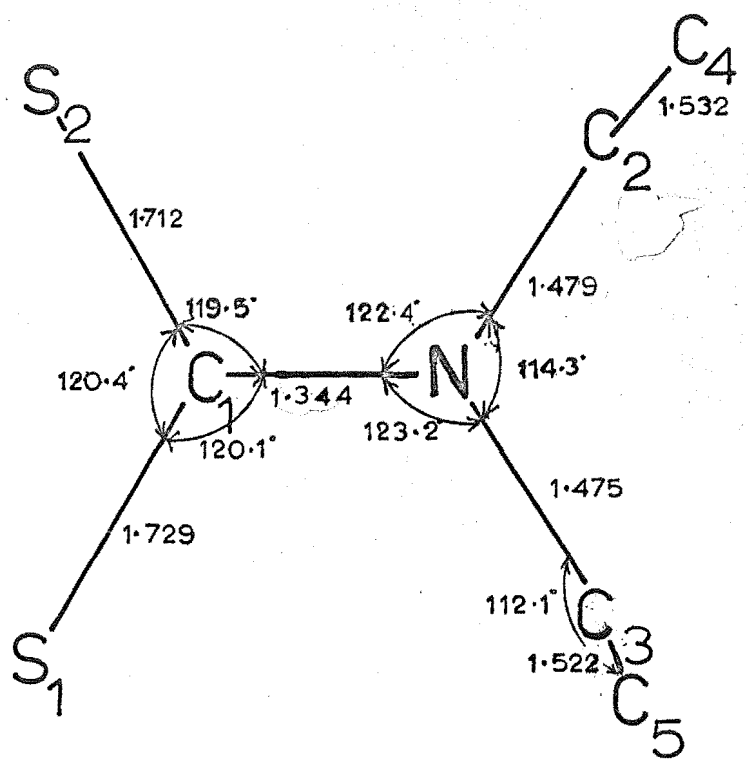

FIG. 4.1 Bond lengths (A) and angles (degrees) in the N,N-diethyldithiocarbamate anion.

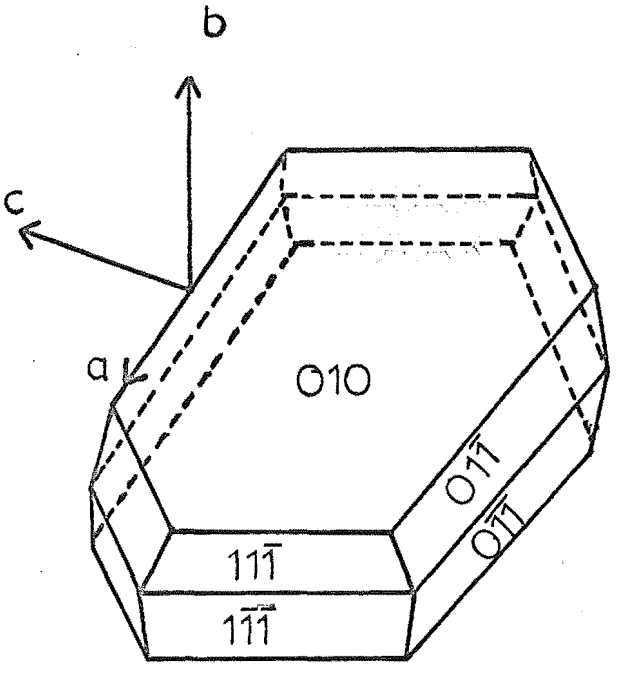

FIG. 4.2 Crystal habit of Sodium N,N-diethyldithiocarbamate. $3H_2O$

CHAPTER 4

RESULTS FOR SODIUM DIETHYLDITHIOCARBAMATE

4.1 Crystal Structure

Preliminary results have been published (135,136) for the crystal structure of sodium N,N-diethyldithiocarbamate ($NaS_2CN(CH_2CH_3)_2.3H_20$) but not the atomic coordinates. Crystals are orthorhombic, space group Pbca(D_{2h}^{15}), with eight molecules in a unit cell of dimensions a = 7.591Å, b = 28.632Å, c = 10.470Å. The structure consists of infinite layers of coordination polyhedra of sodium ions extending parallel to the ac-plane and connected on both sides with layers of organic anions. Each sodium ion is situated at the centre of a distorted octahedron of five water molecules and one sulphur atom (at 3.05Å). The other sulphur atom is 4.15Å from the sodium ion. The anion is planar within ±0.04Å except for the terminal methyl groups. The three angles at C1 are all equal to 120° and the two carbon-sulphur bond lengths are almost equal in spite of the fact that one of them, S1, is within the sodium coordination sphere. The carbon-sulphur and carbon-nitrogen bond lengths indicate a high degree of double bond character (Fig. 4.1).

The axis system used for this study is shown in Fig. 4.2. Crystallographic axes were determined by single crystal x-ray precession photographs and the crystal faces were indexed from these results. For convenience, laboratory and crystal axes were made to coincide. Crystals were of two forms, corresponding to development of either the 001 or the $\bar{1}01$ face. The crystal symmetry is such that there should be only two magnetically distinguishable sites when the magnetic field is

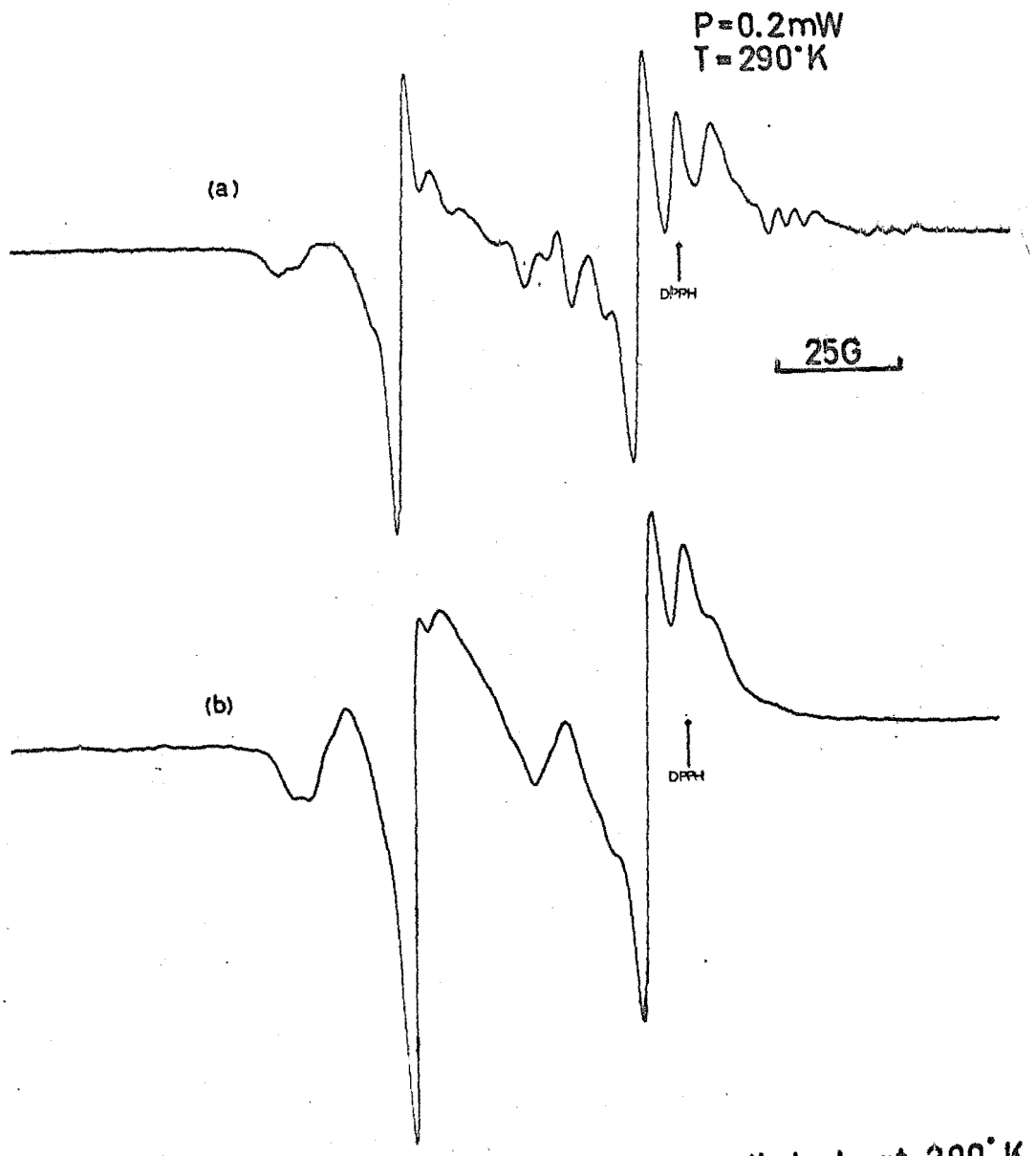

FIG 4.3 Spectrum of crystal, x-irradiated at 290°K, after (a) one day, (b) four months.

in the ab, bc or ac planes and these sites should become equivalent when the magnetic field is along a crystal axis. In a general orientation four sites are expected.

Preliminary atomic coordinates (137) provided by Professor Domenicano have been used to calculate the direction cosines of the bond directions, which are tabulated in Table 4.1. Direction cosines of symmetrically related molecules may be generated by reversing the signs of each column in turn. These results show that the normal to the molecular plane lies 17° from the crystal c-axis and that the bisector of the $S_1C_1S_2$ angle lies almost in the ab-plane 45° from the a-axis.

4.2 Irradiation

Crystals turned green upon x- or γ-irradiation at room temperature both in air and in vacuo. When crystals were irradiated at 105°K they became a very dark colour which faded as the temperature was raised above 150°K until they became light pink and finally colourless. There were no observable differences in the esr spectra of crystals irradiated at room temperature for six hours from crystals irradiated for twenty five hours nor between crystals irradiated in air or in vacuo.

4.3 Temperature Dependence of ESR Spectra

The esr signals produced in crystals irradiated at room temperature faded irreversibly when the crystals were annealed by heating to 60°C in a stream of nitrogen, but a number of weak spectral lines faded more rapidly than the other lines. The same lines disappeared when the crystals were stored at room temperature for four months (Fig. 4.3). Spectra of crystals irradiated at room temperature but cooled to 120°K in the cavity of the esr spectrometer were similar to spectra

TABLE 4.1

Sodium Diethyldithiocarbamate

Direction Cosines of Bond Directions[ab]

Bond	Direction Cosines		
C_1-S_1	0.2103	-0.9637	0.1647
C_1-S_2	-0.9150	0.2742	-0.2959
C_1-N	0.7070	0.6965	0.1231
S_1-S_2	0.6465	-0.7154	0.2651
N-C_2	0.1761	-0.9740	0.1423
N-C_3	-0.9477	0.2175	-0.2336
$\perp$	0.2782	-0.1025	-0.9550
Na-S_1	0.1327	-0.9506	-0.2805

[a]With respect to crystal axes, abc.

[b]Data from ref. 137.

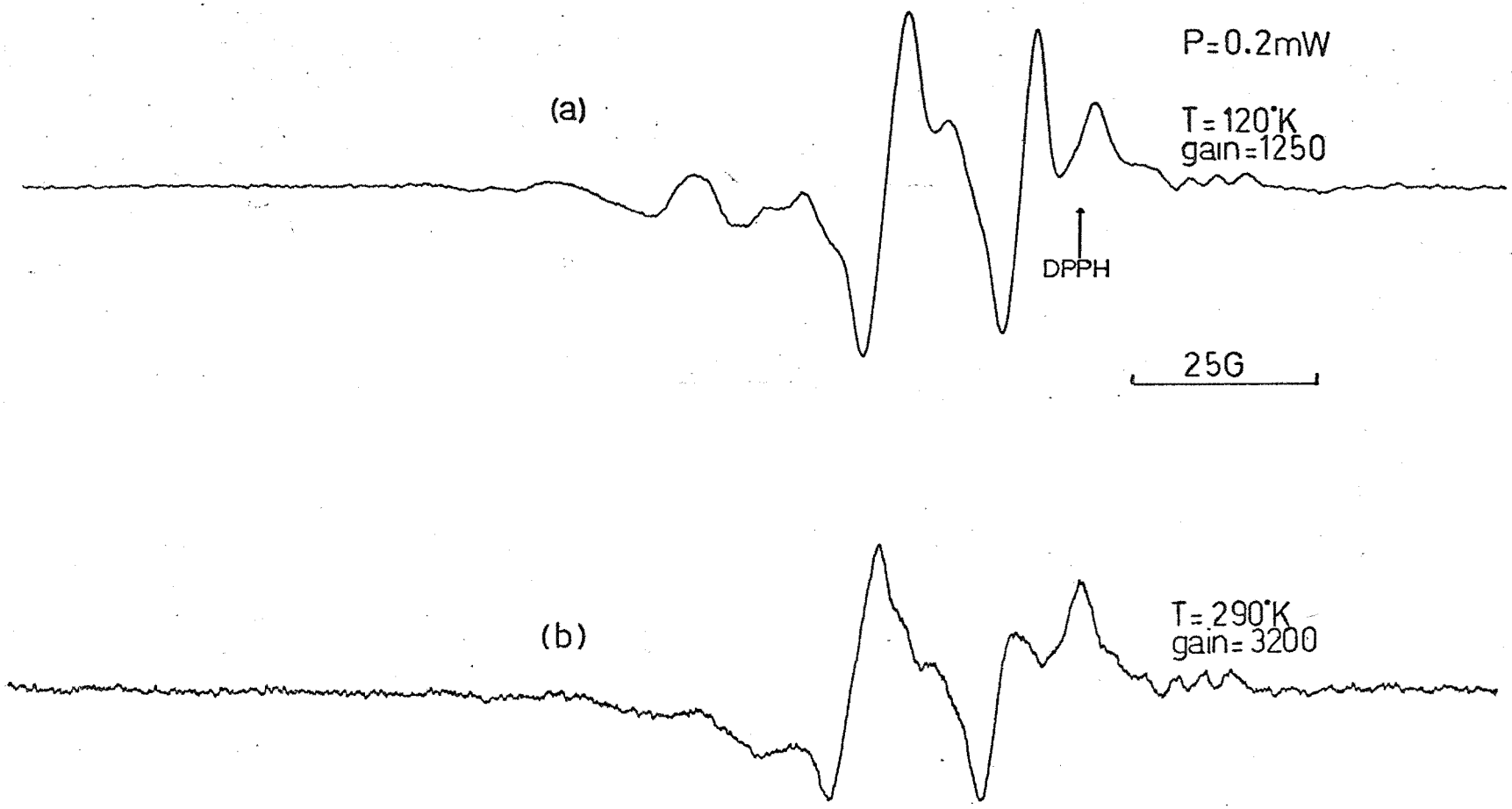

FIG 4.4 Crystal irradiated at 290°K.
Temperature dependence.

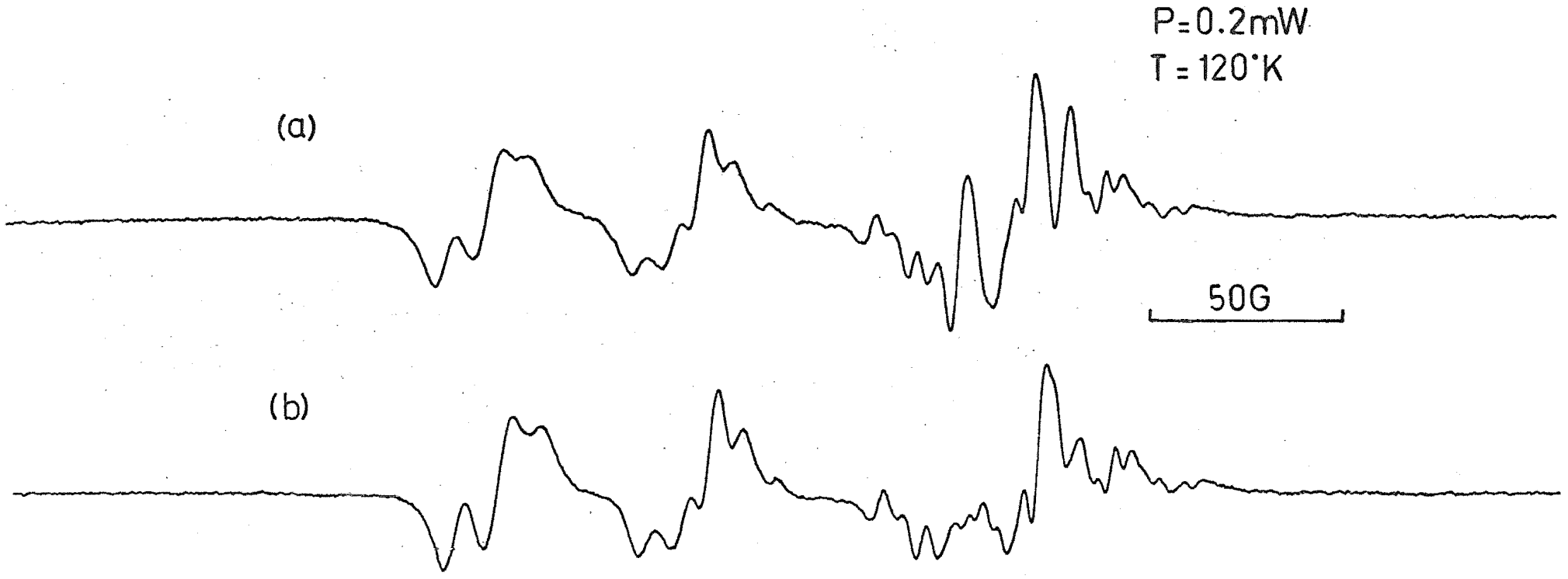

FIG 4.5 Crystal irradiated at 105°K
(a) before, (b) after, momentary
warming to 220°K

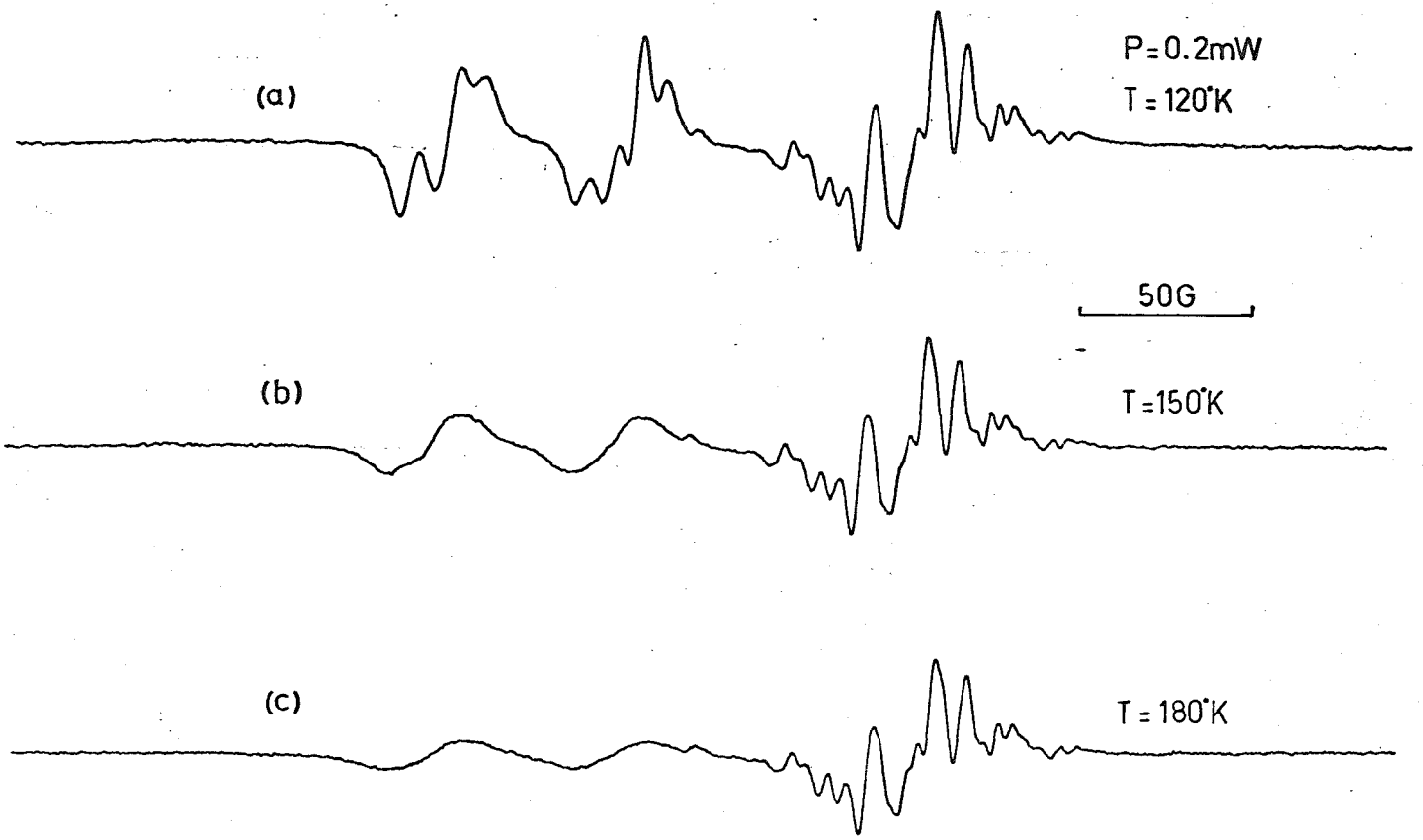

FIG 4.6 Crystal irradiated at 105°K.
Temperature dependence.

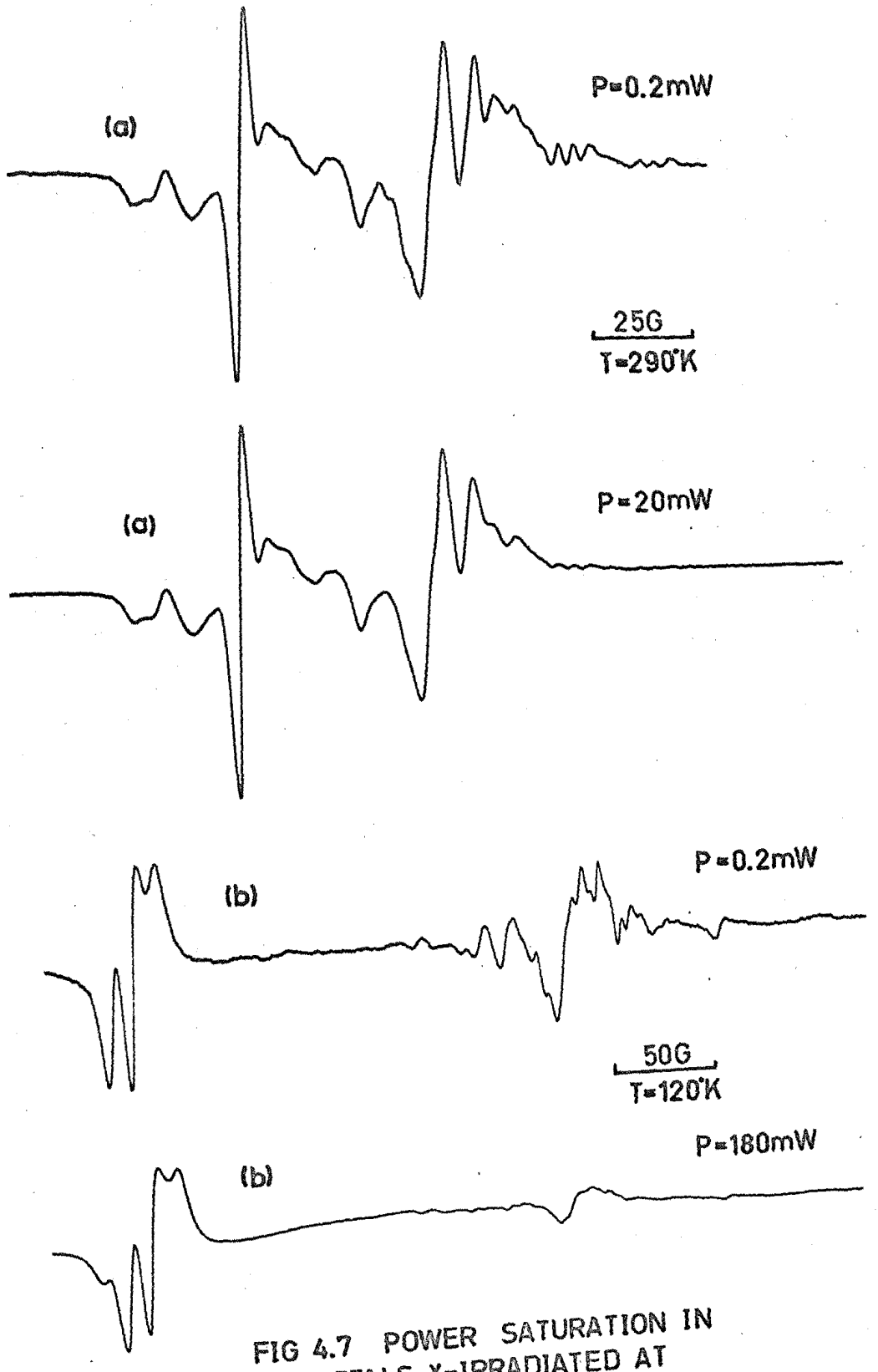

FIG 4.7 POWER SATURATION IN CRYSTALS X-IRRADIATED AT (a) 290°K (b) 105°K

recorded at room temperature although the linewidths of most of the lines decreased as the temperature was lowered (Fig. 4.4) which caused the signal height to increase by a factor of three as the temperature was lowered from 290°K to 120°K.

The esr signals produced in crystals irradiated at 105°K faded irreversibly as the temperature was raised above 150°K although the rate of loss of signal intensity was slow until temperatures near room temperature were reached. Not all lines faded at the same rate (Fig. 4.5). Those signals occurring at lowest field values were very temperature dependent and were barely observable at 200°K (Fig. 4.6), at which temperature there was no resolved hyperfine structure. The marked temperature dependence of these lines is associated with the great variation of linewidth with temperature that is characteristic of radicals which have large spin-orbit coupling and therefore very anisotropic g-values.

4.4 Saturation of ESR Lines

The esr spectra of crystals irradiated at room temperature, obtained at a microwave power level of 200 mW were very similar to spectra obtained at a power level of 0.2 mW except that spectral lines were slightly broader and the signal height was about twenty five times greater at the higher power level. Most of the spectral lines changed in a very similar manner as the microwave power was varied except that a group of weak lines near g = 2.003 saturated more readily than the other lines (Fig. 4.7a).

The lines of the esr spectra of the crystals irradiated at 105°K all saturated as the microwave power was increased beyond 0.2 mW although the low field lines saturated much less readily than the lines nearer g = 2.00 (Fig. 4.7b).

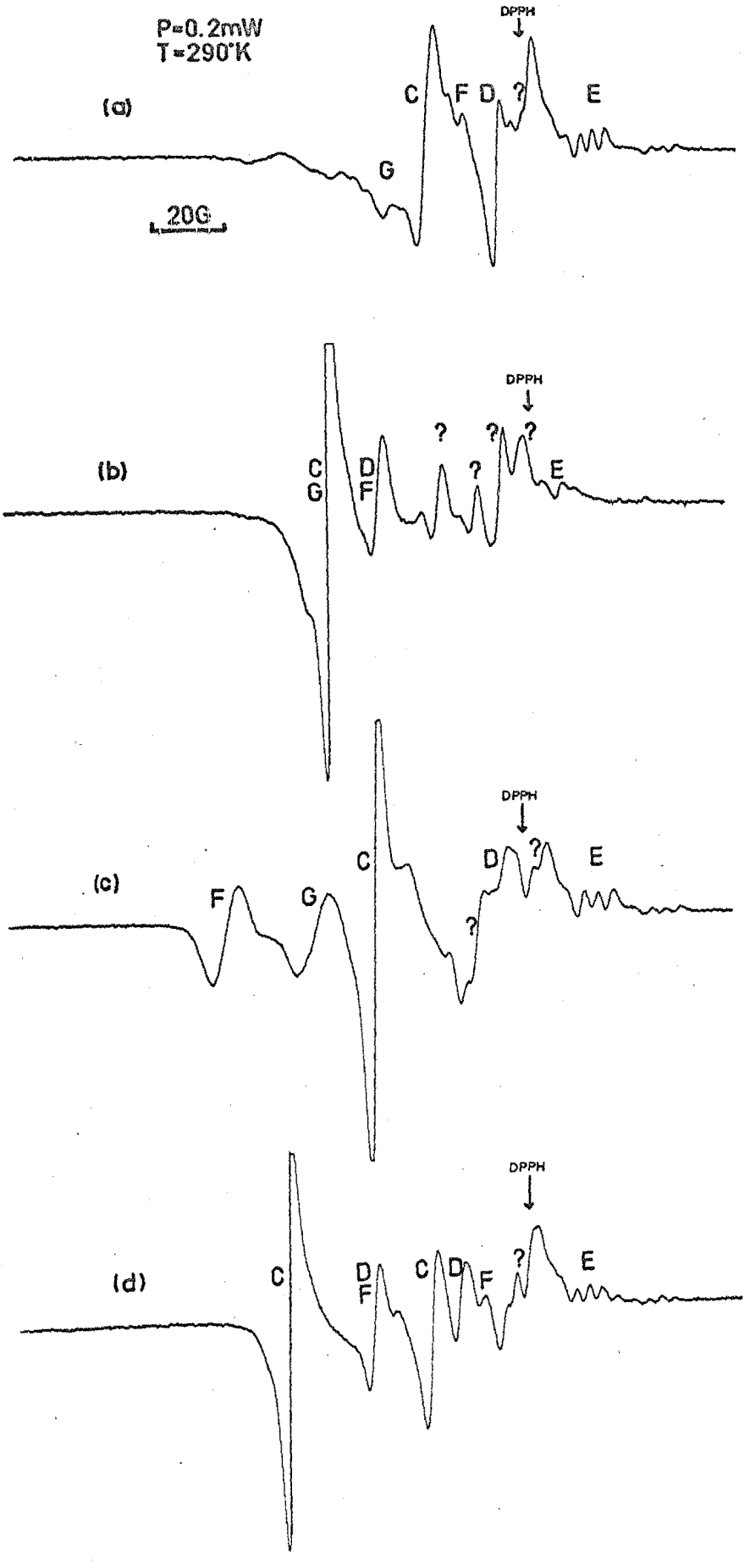

FIG 4.8 ESR spectra of crystal irradiated at 290°K, with the magnetic field along (a) (1,0,0), (b) (0,1,0), (c) (0,0,1), (d)(0.91, 0.39, 0.0)

4.5 Interpretation of ESR Spectra

4.5.1 Irradiation at room temperature

Spectra were generally composed of a complex of unrelated lines (Fig. 4.8) almost all of which showed a marked angular dependence in position and height.

The most intense lines (marked C in Fig. 4.8) were easily seen at all orientations of the crystal in the magnetic field and a g-tensor was readily calculated. There are four magnetically inequivalent C radicals in the general orientation but when the magnetic field is in any plane containing two of the crystal axes only two species are distinguishable and even these become equivalent when the magnetic field is parallel to the crystal axes or in the bc-plane. The g-tensor for radical C is given in Table 4.2. Symmetry related species differ only in the signs of the elements of the tensor, to within experimental error. Principal values calculated from this tensor are given in Table 4.3. The small size of the bc-element makes it impossible to distinguish between the two possible combinations of signs of the off-diagonal elements but the principal values of both combinations agree within experimental error. The linewidth was approximately constant at 3.5G.

The principal axes can not be unambiguously related to the direction cosines of molecular bonds derived from atomic coordinates because it is not possible to be sure which of the symmetry related g-tensors corresponds to the calculated direction cosines of Table 4.1. A comparison of Table 4.1 with Table 4.3 shows that the maximum principal value for radical C is likely to be close to either the C_1N or the S_1S_2 direction and that no principal value lies near to the normal to the molecular plane. The former choice, with g_{max} near C_1N

TABLE 4.2

Sodium Diethyldithiocarbamate

g-tensors

Radical	Tensor[a]		
C[b]	2.0202	± 0.0159	± 0.0145
		2.0357	± 0.0002
			2.0277
D	2.0080	- 0.0089	- 0.0022
		2.0272	- 0.0038
			2.0086
E[d]	2.0047	- 0.0004	- 0.0017
		2.0078	- 0.0001
			2.0027
F[b]	2.0168	± 0.0131	± 0.0001
		2.0248	± 0.0072
			2.0528
G[c]	2.0268	± 0.0156	± 0.0172
		2.0358	± 0.0109
			2.0383

[a]Upper diagonal half of symmetric matrix in crystal axis coordinates, abc.

[b]Sign ambiguity due to small size of one off-diagonal element.

[c]Sign ambiguity

[d]Determined for one site only. Off-diagonal elements may be closer to 0.0000

TABLE 4.3

Sodium Diethyldithiocarbamate
g-tensors

Radical	Principal Value[c]	Direction Cosines[ab]		
C	2.0490	0.588	0.702	0.399
	2.0310	0.176	-0.594	0.783
	2.0036	0.789	-0.390	-0.474
D	2.0310	0.347	0.930	-0.123
	2.0103	0.515	-0.079	0.854
	2.0025	0.784	-0.360	-0.506
E	2.0078	-0.125	0.992	0.023
	2.0056	0.860	0.120	-0.495
	2.0017	0.494	0.042	0.868
F	2.0548	0.096	0.271	0.958
	2.0328	0.608	0.746	-0.272
	2.0067	0.788	-0.608	0.093
G_1	2.051	-0.607	-0.056	0.793
	2.047	+0.372	-0.862	+0.345
	2.003	0.702	-0.504	0.502
G_2	2.061	-0.533	-0.555	+0.638
	2.030	+0.081	-0.785	-0.615
	2.013	0.842	-0.276	+0.464

[a] relative to crystal axes, abc

[b] symmetry related species have direction cosines with one of the axial directions reversed in sign

[c] standard deviation = 0.0006 for C, D, F
= 0.0005 for E
= 0.001 for G.

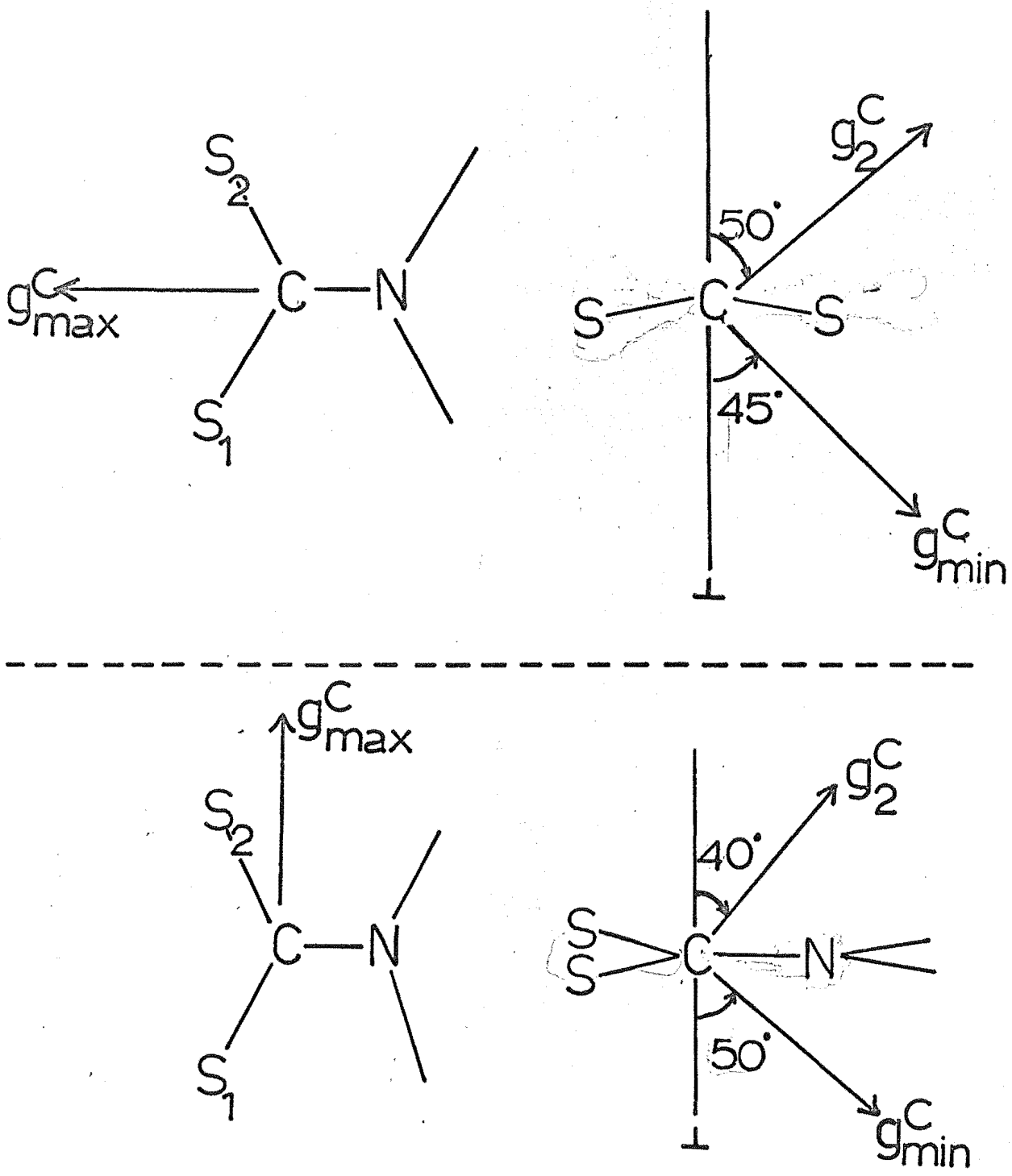

FIG 4.9 Possible orientations of principal axes of radical C.

but 17° above the molecular plane, means that the g_2 and g_{min} principal axes lie at 50° and 45° from the normal to the molecular plane and approximately coplanar with the S_1S_2 direction. The second alternative, with g_{max} 9° from the S_1S_2 direction, places the g_2 and g_{min} principal axes at 40° and 50° from the normal to the molecular plane and approximately coplanar with the C_1N direction (Fig. 4.9).

The lines marked D in Fig. 4.8 have been characterised by a g-tensor (Table 4.2) which has a similar symmetry to the g-tensor of radical C but which is less anisotropic. The height of the lines in the spectrum due to radical D are about one fifth of the height of the lines due to radical C. The line-width is approximately constant at 3.5G.

The minimum principal value lies within 3° of the orientation of the minimum principal value of radical C but the remaining principal axes are rotated 36° from the corresponding axes for radical C and neither lie in the molecular plane. The maximum principal value lies 19° or 32° from the C_1S_1 bond direction depending on which of the symmetry related species is chosen.

At the high field end of each spectrum a series of triplet lines is apparent. The lines of each triplet are equally intense and equally spaced and therefore must be due to the nuclear hyperfine interaction of a single nitrogen atom. Two of these triplets (labelled E in Fig. 4.8) are clear at all orientations but further lines are generally overlapped by larger signals due to other radicals. The peak heights of the two resolved triplets are in the ratio of between 1:3 and 1:4 and the spectrum does not change very markedly with orientation. The spectrum due to radical E is readily saturated and is not

observable at a power level of 200 mW. The spectrum also fades irreversibly upon storage at room temperature for several months. No resolvable site splitting was observed although the widths and heights of the lines did vary as the crystal was rotated in the magnetic field. The distance between the triplets is almost isotropic and varies from 19.5G to 21G. The nitrogen hyperfine splitting is isotropic at 3.0 - 3.5G. This isotropy and the constant intensity ratio of adjacent triplets suggests that a radical containing one nitrogen atom and either three or four equivalent protons is present. It was not possible to determine whether a ratio of 1:3:3:1 or of 1:4:6:4:1 was present, from simulation of spectra but the g value of the 1:3:3:1 set has principal values of 1.9958, 1.9997 and 2.0019 which are all less than g_e. This would be most unusual, implying an absence of low energy filled orbitals. The g-values associated with the 1:4:6:4:1 set are 2.0078, 2.0047, 2.0027 which are more usual for carbon centred radicals. It therefore appears that the radical is due to a species with four equivalent hydrogen atoms. A g-tensor based on this assumption is given in Table 4.2.

The maximum g-value is directed at 10° from the N_1C_2 bond while the other two principal axes are both 45° from the normal to the molecular plane, although these directions are not very accurate since no account was taken of site splitting in the determination of the g-tensor.

In addition to the lines due to these radicals there are at least two other major sets of lines (labelled F and G in Fig. 4.8) which are clearly apparent at the low field end of the spectra. These lines are at least 5G wide and their linewidth appears to vary as the crystal is rotated in the

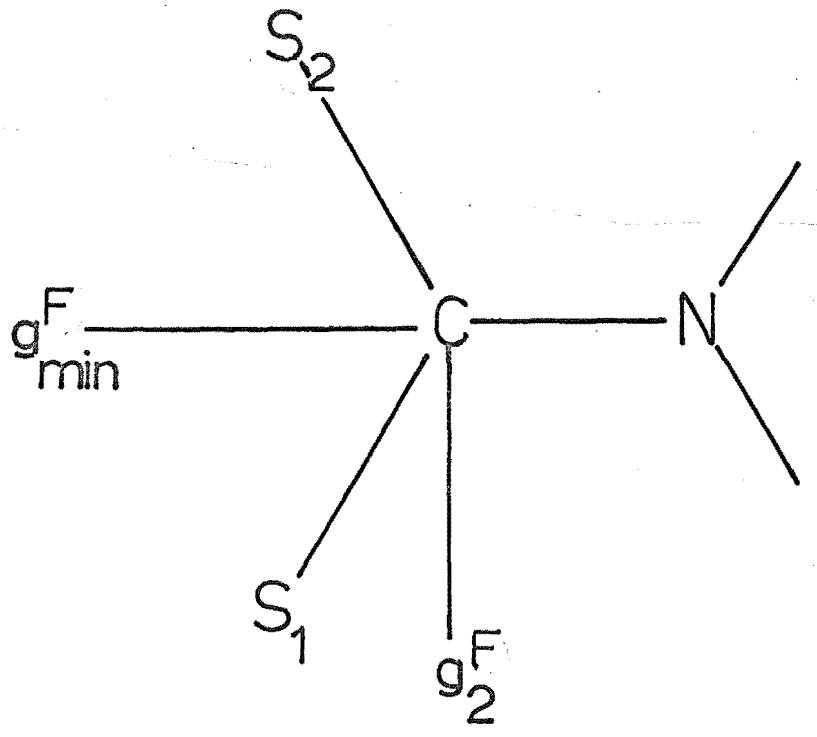

FIG 4.10 Orientation of principal axes of radical F.

magnetic field. Lines due to G are less intense than lines due to F and appear to have partially resolved hyperfine structure at some orientations. As these lines were only about one tenth the height of lines due to radical C it was not possible to determine their positions at all orientations. Sufficient resolved spectra were, however, obtained to enable g-tensors to be calculated for both radicals and these are given in Table 4.2. It was not however possible to be sure which of the two possible combinations of signs of the off-diagonal elements best described the variation of the g-value because of the low intensity and breadth of the signals. The difference is not important for radical F because of the small ac-element of the tensor but for radical G two quite different sets of principal values were obtained (Table 4.3). G_1 is obtained from the G tensor when there is an odd number of off-diagonal elements and is more likely to be correct because no lines at $g > 2.05$ were observed at any orientation. No lines were observed at $g = 2.003$ which could be attributed unambiguously to radical G but this may be because such lines overlap with other species.

The principal axes of F are directed in the manner shown in Fig. 4.10 with g_{max} 14° from the normal to the molecular plane and g_{min} 9° from the C_1N bond direction. No attempt was made to calculate the orientation of radical G although g_{min} appears to be nearer the S_1S_2 direction than any other.

4.5.2 Irradiation at low temperatures

Spectra were generally dominated by two sets of lines, marked A and B in Fig. 4.11. A number of weaker lines were also observed but no attempt was made to analyse them since their position could seldom be followed as the crystal was

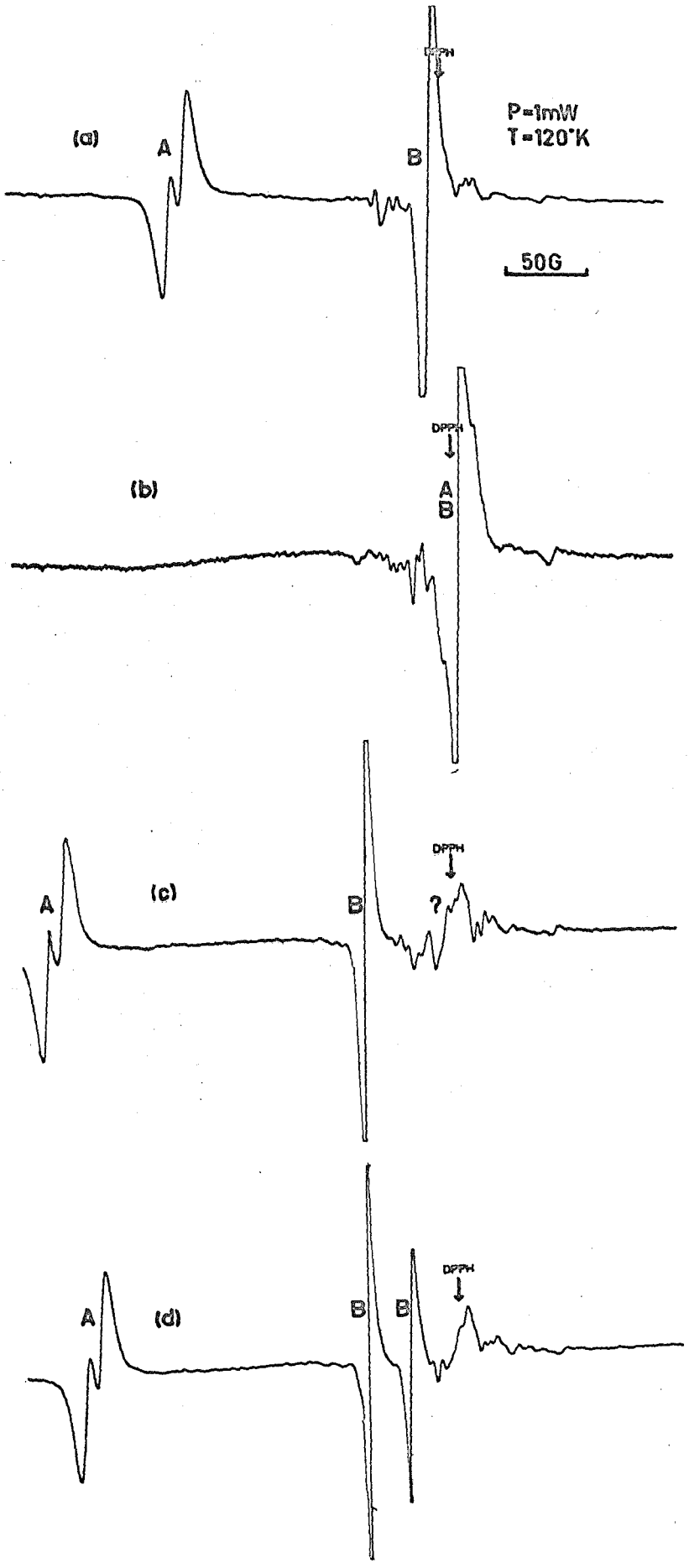

FIG 4.11 ESR spectra of crystal irradiated at 105°K. with the magnetic field along (a) (1,0,0), (b) (0,1,0), (c) (0,0,1), (d) (0.5, 0.0, 0.87).

TABLE 4.4

Sodium Diethyldithiocarbamate

g-tensors

Radical	Tensor[a]		
A	2.1072 ± 0.0139	0.0000	
	1.9974 ± 0.0024		
	2.1613		
B[b]	2.0075 ± 0.0002	± 0.0095	
	1.9997 ± 0.0076		
	2.0362		

Radical	Principal Values[d]	Direction Cosines[c]		
A	2.1613	-0.004	0.015	0.999
	2.1089	0.992	-0.124	0.006
	1.9956	0.124	0.992	-0.014
B	2.0404	0.273	0.177	-0.946
	2.0053	0.932	-0.291	0.215
	1.9977	0.237	0.940	0.244

[a]Upper diagonal half of symmetric matrix in crystal axis coordinates, abc.

[b]Sign ambiguity due to small size of one off-diagonal element

[c]Relative to crystal axes, abc.

[d]Standard deviation = 0.0005.

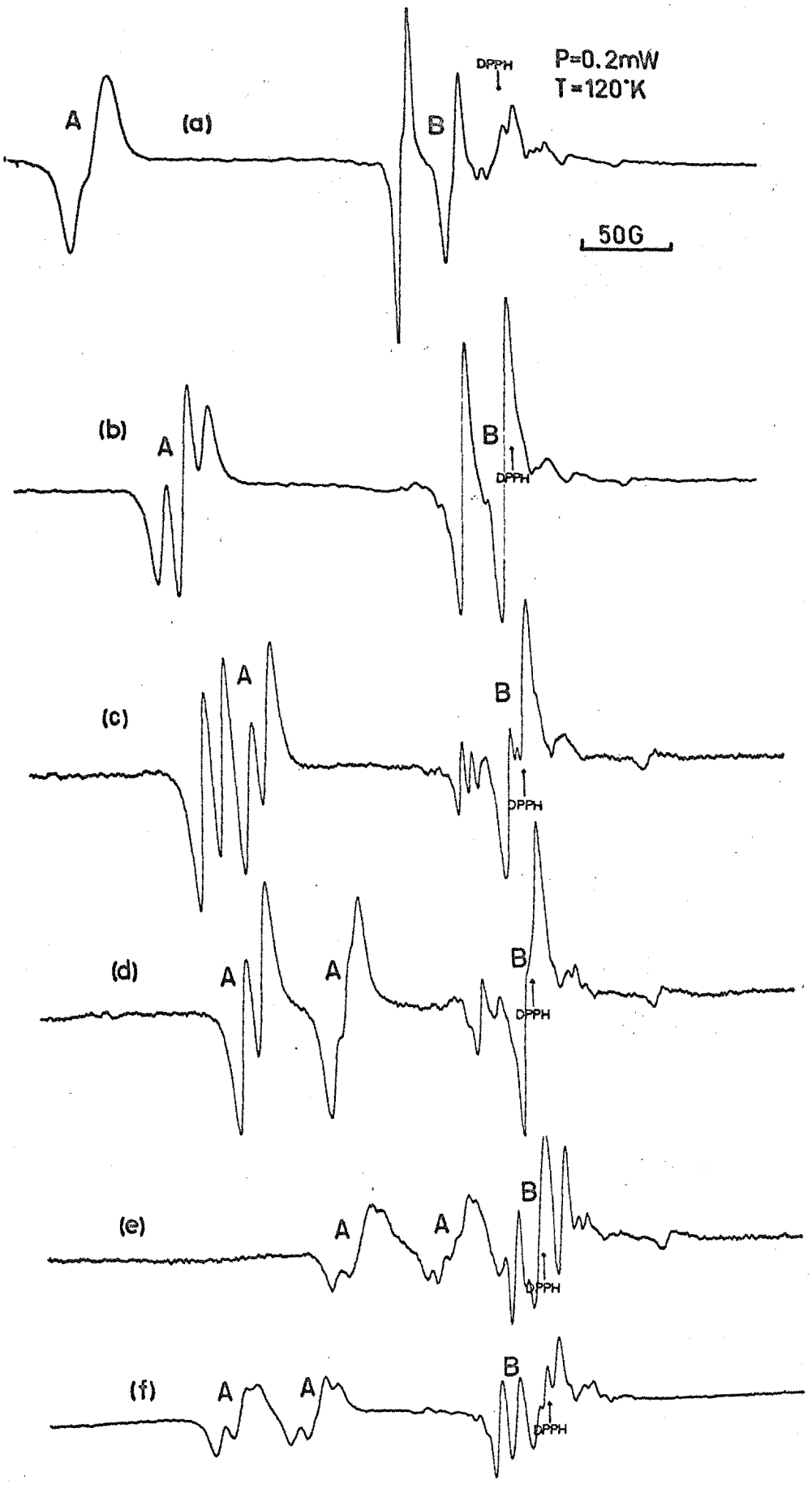

FIG 4.12 ESR spectra of crystal irradiated at 105°K, showing hyperfine structure of A at several orientations.

rotated in the magnetic field.

The lines marked B have no hyperfine structure and arise from four magnetically inequivalent sites although this number reduced to two when the magnetic field was in a plane containing two crystal axes. The g-tensor is given in Table 4.4.

There is also a set of broad lines, marked A in Fig. 4.11, which have a very anisotropic g-value (Table 4.4) and which have some resolved hyperfine splittings. When the magnetic field is in the ac-plane there is only one species and there is a constant doublet splitting of 8.5-11G. When the magnetic field is in the ab- or bc-planes there are two species present and the hyperfine structure varies with orientation from a doublet to a more complex structure (Fig. 4.12) which was not normally symmetric and which contained up to four resolved lines. This additional complexity could be due to an additional site splitting caused by imperfect alignment of the crystal in the magnetic field. Such poor alignment could arise because of the great anisotropy of the g-value and because of the difficulty of accurately aligning the crystals while keeping them cold. When the magnetic field is along the b-axis the spectrum reduces to a broad line 16G wide, although this may also be two doublets incompletely superimposed through imperfect alignment of the crystal. The lines due to radical A broadened considerably as the temperature was raised above 110^{o}K, and were less readily saturated than the other lines in the spectra.

The maximum principal value for B is 4.4^{o} from the normal to the molecular plane and the intermediate principal value is only 5.0^{o} from the C_1S_2 bond direction, as shown in Fig. 4.13. The anisotropy of the g-value indicates that there is considerable

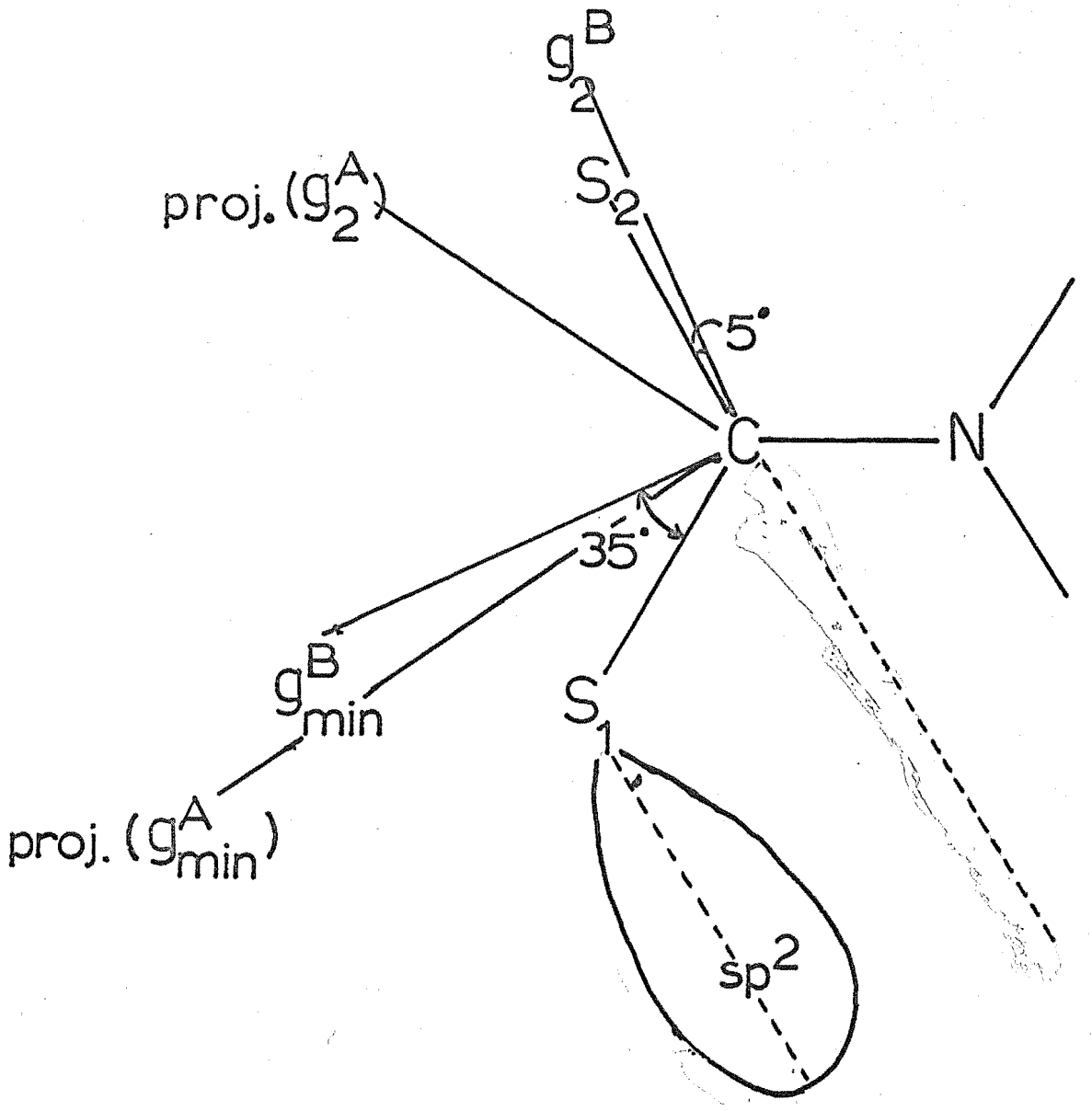

FIG 4.13 Orientation of principal axes of radicals A and B.

spin density upon a sulphur atom, and the orientation of the principal axes suggests that the unpaired electron is localised mainly on one of the sulphur atoms either in a p-orbital on S_2 or in a sp^2-orbital on S_1.

The principal axes of A are not as close to the molecular plane, the normal to which is 17° from the axis associated with the maximum principal value. The intermediate and minimum principal values lie 29° and 22° from the C_1S_2 and C_1S_1 directions respectively, and 16° and 5° from the molecular plane. The g-value of radical A is extremely anisotropic and only one principal value is near the free spin g-value. There is a hyperfine interaction with at least one nucleus which has a nuclear spin of ½ and which is probably hydrogen. This hyperfine interaction is approximately isotropic.

4.5.3 Discussion of structures

The lack of hyperfine structure and the anisotropic g-values suggest that several different radicals with their unpaired electrons in orbitals centred upon sulphur atoms are formed. It had been anticipated that radicals would be formed with their unpaired electron in orbitals encompassing the SCS functional group. For such radicals some hyperfine coupling from the nitrogen atom might be expected since the carbon-nitrogen bond in the parent molecule has considerable double bond character (135,141). Furthermore, the principal axes should be oriented normal to the molecular plane, along the C_1N_1 bond direction and along the S_1S_2 direction. Of the radicals observed, only radical F comes close to this orientation, and this radical does not have the unpaired electron in a Π orbital normal to the molecular plane because if such were the case, the principal value oriented parallel to the symmetry

axis of the Π-orbital would be close to g = 2.003 as has been observed for radicals of similar symmetry. If the orbital of the unpaired electron is in the molecular plane the relationships:

$$g_{zz} = 2.0023 - 2 \sum_{n} \sum_{kj} \frac{\langle \psi_0 | \zeta_k L_{zk} \delta_k | \psi_n \rangle \langle \psi_n | L_{zj} \delta_j | \psi_0 \rangle}{E_n - E_0}$$

$$L_z|P_z\rangle = 0 \qquad L_z|P_x\rangle = P_y \qquad L_z|P_y\rangle = P_z$$

may be used in an analogous manner to their use in the CS_2^- molecule (140) which has a similar group symmetry, to deduce that the maximum g-value will probably be oriented normal to the molecular plane, as is observed for radical F. It appears likely that radical F has been formed by loss or gain of an electron by an orbital which is in the plane of the molecule and which is delocalised over the CSS group. According to ultraviolet spectroscopic results (141) the strongest electronic transitions involve orbitals located mainly on the CSS group.

The major radical, C, has its maximum principal value in a direction either near the S_1S_2 direction or near the C_1N direction, but the other two principal axes indicate that considerable rearrangement of the molecular structure has occurred and it seems that the arrangement about the central carbon atom may have changed, possibly by rotation of the CSS group although the coordination of S_1 to the sodium ion makes this seem unlikely. The minimum principal value of radical D is directed in a similar manner to that in radical C which suggests that the two radicals have the unpaired electron in the same orbital but that the molecule has undergone rotation by 36° about the axis of the orbital containing the unpaired

electron. The principal values of the two radicals C and D are however markedly different.

The fact that all radicals are formed with radiation doses of about 1 Mrad and are stable at room temperature for months, and the observation that the crystal is not mechanically damaged upon irradiation suggest that they are formed without gross rearrangement of the molecular structure, as products of the radiation mechanism and not as radicals formed from further irradiation of products as appears to be the case in thioacetamide. The principal values of all of the radicals, except E, are similar in magnitude to those observed for radicals containing an unpaired electron in a p orbital of the sulphur (Table 3.2) and it appears likely that radicals C, D and G are of this type. Because S_1 is within the coordination sphere of the sodium ion the unpaired electron is likely to be in an orbital on S_2 and it seems probable that the C_1S_2 bond has moved from its orientation in the parent molecule.

Radical E appears to have been formed by loss of a hydrogen atom. The small magnitude of the nitrogen hyperfine splitting discounts the possibility that the unpaired electron is located mainly on the nitrogen atom. The isotropic hydrogen hyperfine splitting of about 20G and the orientation of g_{max} indicates that the unpaired electron is in an orbital on C_2. The radical is probably

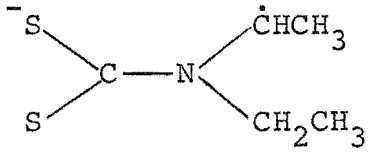

although the equivalence of the alpha and beta protons is unexpected.

The radicals produced upon low temperature irradiation have principal axes oriented as shown in Fig. 4.13. The observation that the maximum g-value is directed close to the normal to the molecular plane suggests that the unpaired electron occupies an orbital in the molecular plane, as previously discussed for radical U. Radical B has the symmetry expected for an unpaired electron in a sp^2 orbital of the S_1 atom directed at 120^o to the C_1S_1 bond in the molecular plane, and it appears probable that little reorientation of the parent molecule has occurred. This assignment aligns g_2 along the axis of the orbital containing the unpaired electron which is also the case in CS_2^- (140). Since the sp^2 orbitals are filled in the parent molecule, the radical is likely to be the neutral $S_2CN(C_2H_5)_2$ species formed by loss of an electron from the parent anion.

The direction cosines of radical A are not exactly in the molecular plane which indicates that some atomic rearrangement has occurred. The hydrogen hyperfine splitting must be due to a hydrogen atom which has transferred to the SCS group from either a water molecule or from the ethyl groups of neighbouring molecules, or possibly by intramolecular transfer from the same molecule. Carbon or hydroxyl radicals could give rise to some of the lines near g = 2.00 but no attempt was made to identify them. The g-value of radical A is extremely large for a sulphur radical and only in L-Cysteine Hydrochloride has a larger g-value been observed (26), this being attributed to the $HOOCCH(NH_3Cl)CH_2S\cdot$ radical. Isotropic hyperfine couplings to two hydrogen atoms were also observed for this radical. Such a large g-value can only occur if there are filled molecular orbitals close in energy to the orbital of the unpaired

electron. The broadening of the spectrum as the temperature is raised is consistent with such a large spin-orbit coupling (139).

If a hydrogen atom were to attach to the central carbon atom a change from sp^2 to sp^3 hybridisation about the carbon atom would occur and this would be accompanied by a great change in atomic positions. The deviation of the principal axes of the g-tensor from the molecular plane is less than 20° so it appears unlikely that such a change has occurred. A more probable structure is the attachment of a hydrogen atom to one of the sulphur atoms,which would be accompanied by a slight reorientation about the other sulphur atom upon which the unpaired electron would be located. The principal axes of A and B are approximately colinear and it seems probable that the symmetry of the orbital of the unpaired electron is similar in the two radicals. Considerable differences between the highest energy filled orbitals must however exist between the two to account for the great differences in g-value, and this suggests that one of the species has two more electrons than the other.

The irradiation of crystals of sodium diethyldithiocarbamate produces several radicals which have no resolved hyperfine structure and which are mostly oriented in a manner that suggests considerable rearrangement of the parent molecule in the course of the irradiation. These factors mean that structures must be assigned largely on the basis of the g-tensors and only for radicals B and F do the principal axes agree with the symmetry of the undamaged molecule.

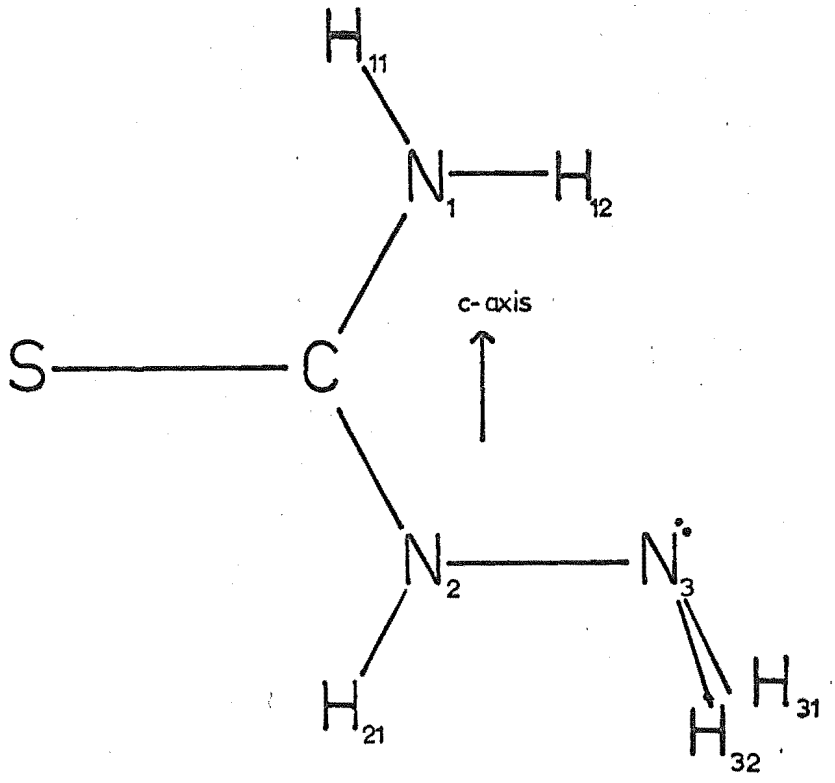

FIG 5.1 THIOSEMICARBAZIDE

CHAPTER 5

RESULTS FOR THIOSEMICARBAZIDE

5.1 Crystal Structure

Crystals were colourless elongated plates with ill defined edges so that it was not possible to identify the crystal axes, with the exception of the axis of elongation which was identified as the c-axis from single crystal x-ray diffraction photographs.

The crystal structure has previously been determined (142,143) by x-ray diffraction methods. The crystals are triclinic, space group $P\bar{1}$, with two molecules in a unit cell of dimensions: a = 4.934Å, b = 7.330Å, c = 9.396Å, $\alpha = 44.39^{\circ}$, $\beta = 83.23^{\circ}$, $\gamma = 76.99^{\circ}$. The axis of elongation is the c-axis and is almost parallel to the N_1N_2 direction (Fig. 5.1). The molecule is planar, except for the two hydrogen atoms bonded to N_3, and the two C-N bonds are of equal length which indicates delocalisation of the double bond over the SCN_1N_2 group. Since the unit cell has a centre of symmetry both molecules are magnetically indistinguishable.

5.2 Irradiation

Crystals became green upon x- or γ-irradiation at room temperature. Exposures were for 8-12 hours for an estimated dose of 2-3 Mrad. ESR spectra of crystals irradiated for 25 hours were identical to those of crystals irradiated for shorter periods as were the spectra of crystals γ-irradiated in a sealed evacuated quartz tube. Crystals were also x-irradiated at about $105^{\circ}K$ and transferred to the cavity of

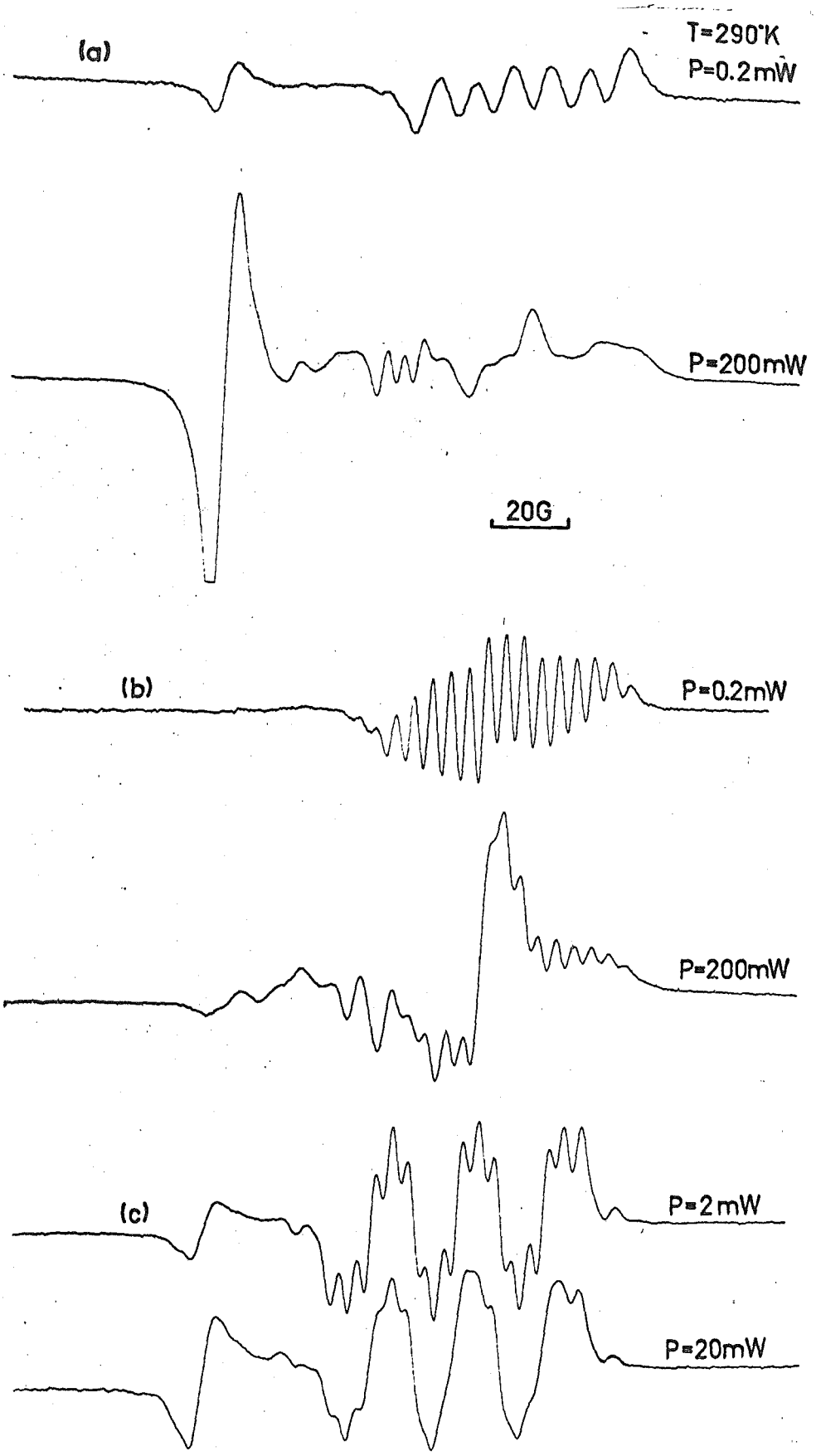

FIG 5.2 Unidentified lines in (a,b) normal, (c) deuterated, Thiosemicarbazide.
(irradiated 4 months previously)

the esr spectrometer which was at 120°K. The spectra of these crystals were identical to those of crystals irradiated at room temperature.

5.3 Saturation

The main spectrum showed strong power saturation effects even at power levels as low as 0.01 mW although this was observed primarily in the line intensities, there being only a small degree of line broadening at power levels below 50 mW.

In addition to the main spectrum there was a group of weak lines occurring at the low field end of the spectrum (Fig. 5.2) which became of comparable intensity to the lines of the main spectrum when the latter were strongly saturated. Since these lines were very weak at power levels of 0.2 mW they did not interfere with the analysis of the main spectrum. The additional lines became more intense relative to the major signals after the irradiated crystals had been kept at room temperature for several months but were still clearly observable only at high power levels. Such signals were not analysed because they overlapped the main signals and because the lines were frequently broad and their positions difficult to determine very accurately. The centre of such signals was displaced to the low field side of $g = 2.00$ and averaged about $g = 2.03$ although the complexity of the spectra was such that there appeared to be at least two unrelated paramagnetic species contributing to the signals.

5.4 Temperature Dependence

ESR spectra obtained at 120°K for both deuterated and undeuterated samples were very similar to those obtained at room temperature, there being a slight increase in intensity

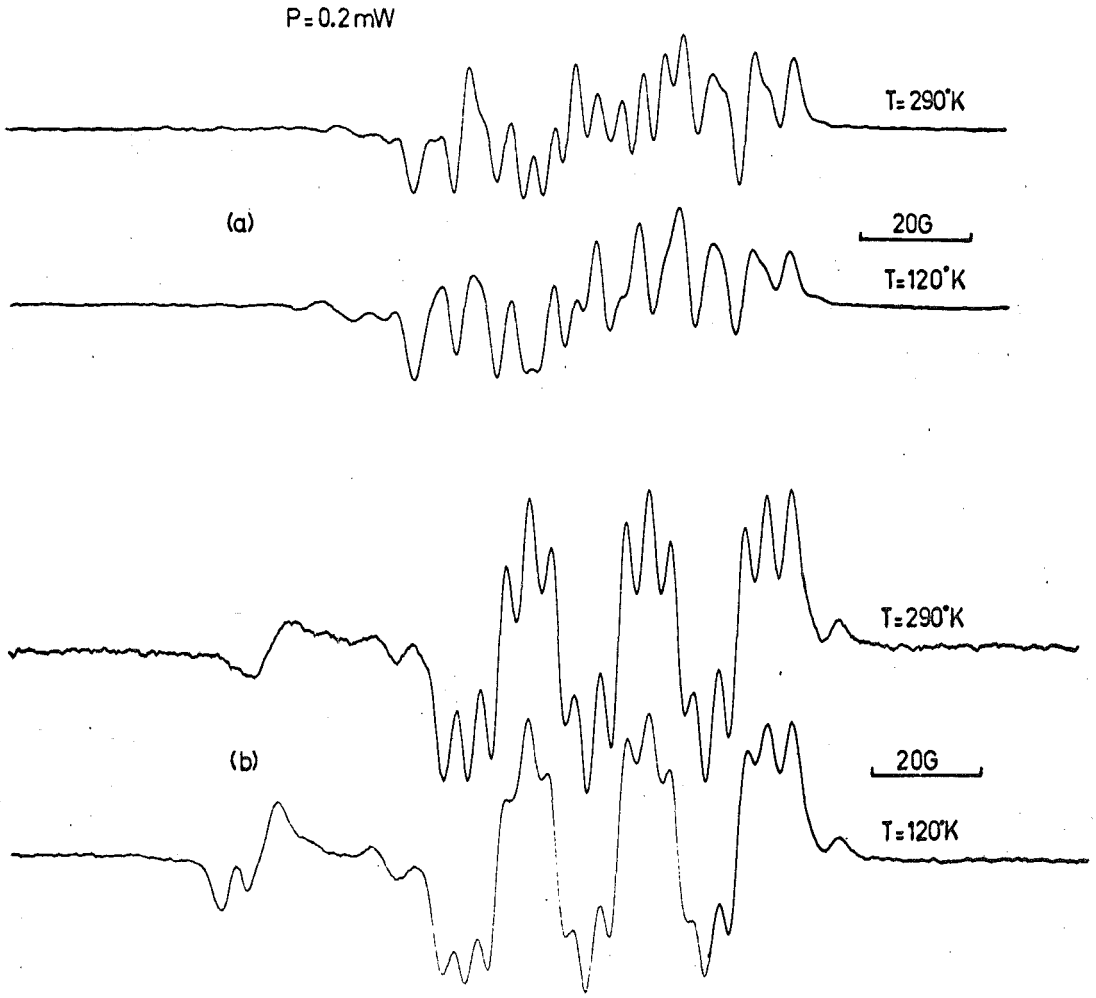

FIG 5.3 Temperature dependence of esr spectra of (a) normal, (b) deuterated Thiosemicarbazide

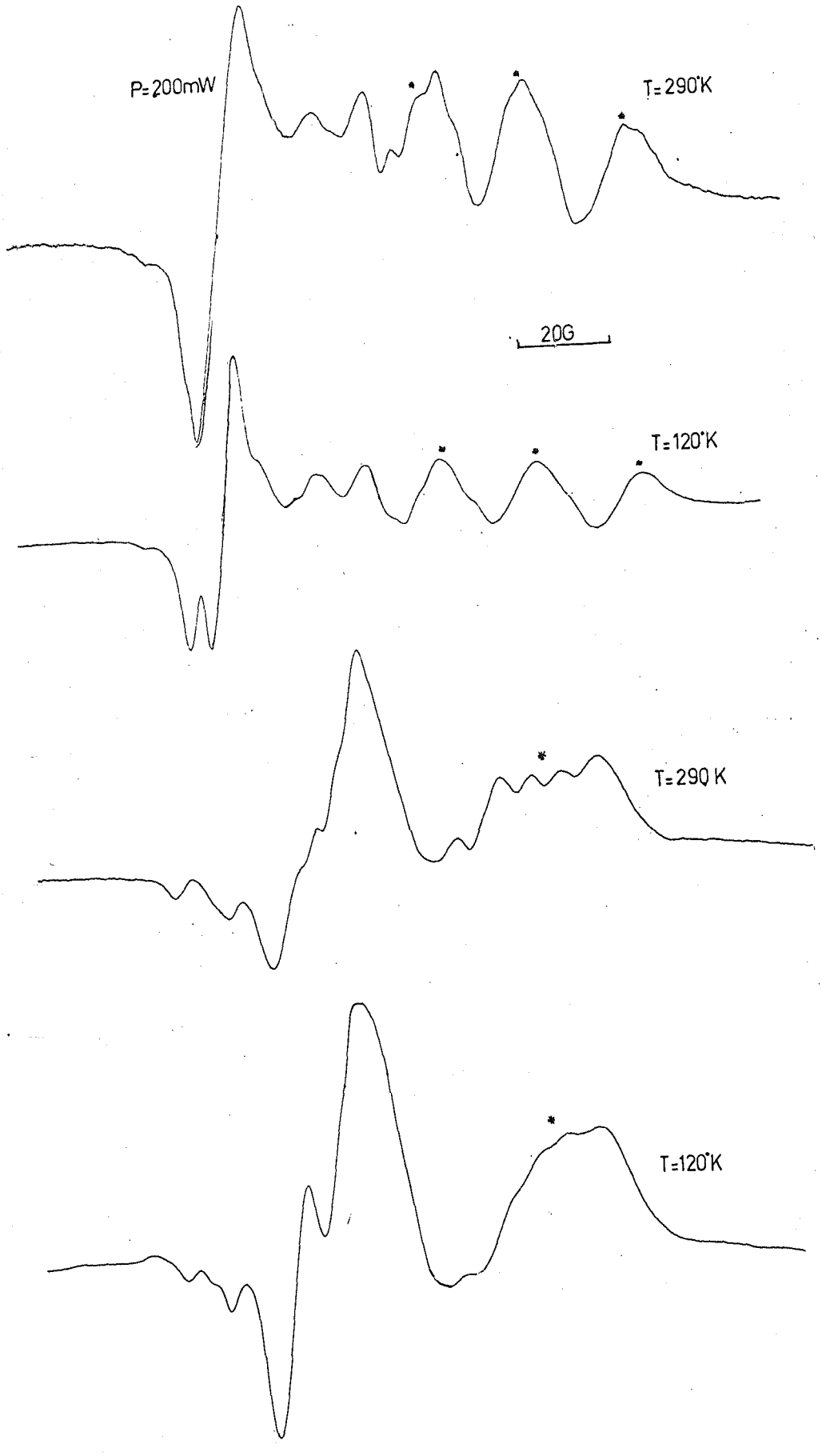

FIG 5.4 Temperature dependence of unidentified lines in Thiosemicarbazide.
(* identified species)

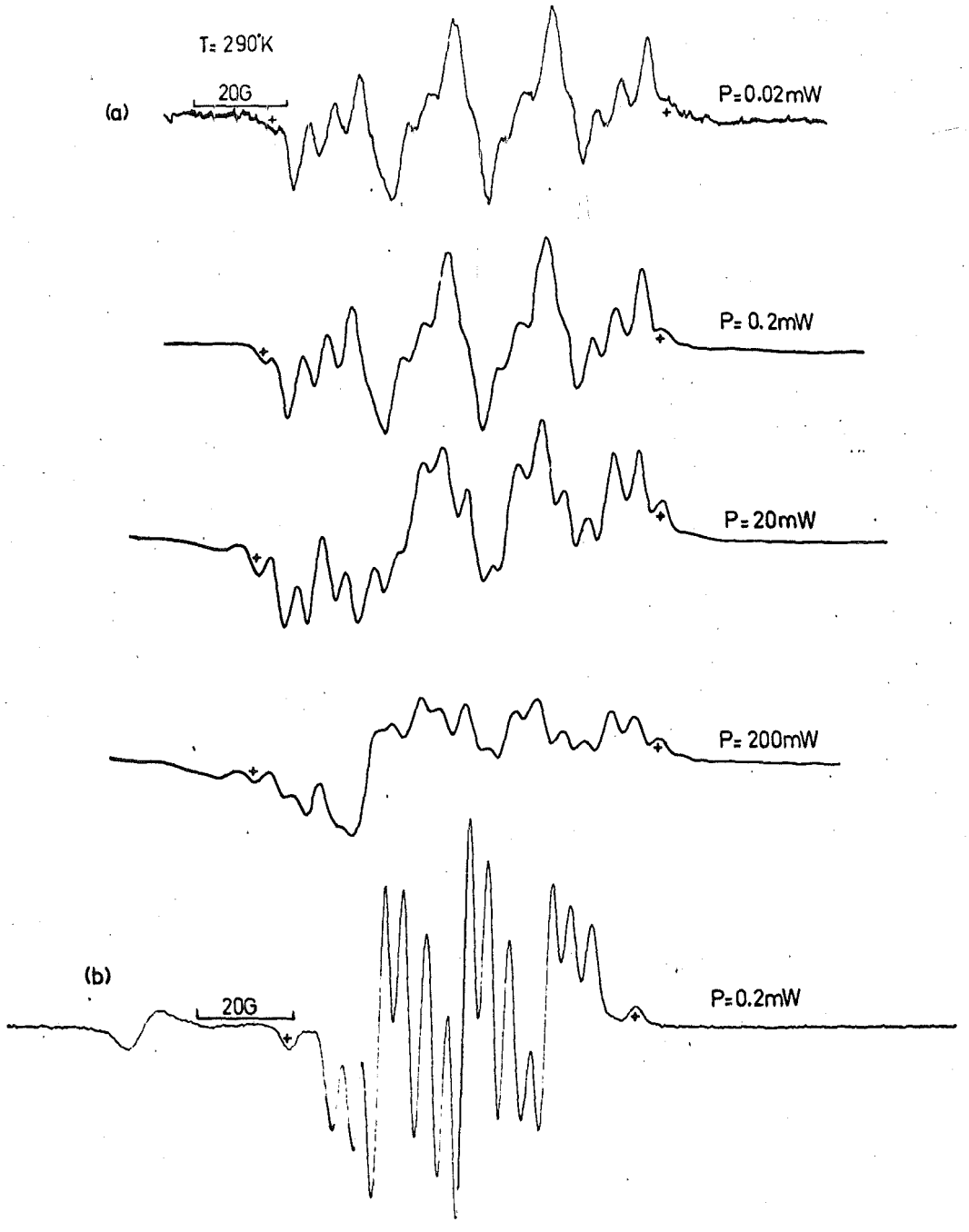

FIG 5.5 Second order lines (+) in (a) normal, (b) deuterated, Thiosemicarbazide

and a small decrease in resolution as the temperature was decreased (Fig. 5.3). The decrease in resolution was apparently the result of a small increase in linewidth, which was observable only when the spectra had many lines resolved. The increase in intensity may be attributed to the effect of temperature on the distribution of spin states described by the Boltzmann Distribution. The increase in linewidth is uncommon and may be due to a change in the interaction of nuclei whose hyperfine couplings are not resolved but which contribute to the linewidth.

The radicals were stable in air at room temperature for several months although an irreversible loss occurred when the temperature was raised above 60°C. At such elevated temperatures all the spectral lines disappeared at the same rate.

The weak signals which are observed mainly under saturating conditions, increased in height more than the main signals as the temperature was lowered, and resolution improved, as expected for line-broadening due to spin-lattice relaxation (Fig. 5.4).

5.5 Interpretation of ESR Spectra

5.5.1 Undeuterated Thiosemicarbazide

The ESR spectra were symmetrical about the centre at all orientations at room temperature and low microwave power levels, indicating a single radical per unit cell which is consistent with the symmetry of the parent crystal.

In a few orientations a weak line was observed at each end of the spectrum (Fig. 5.5). The intensity of these lines increased slightly relative to the other lines as the microwave power level was increased (152). Such lines arise from the

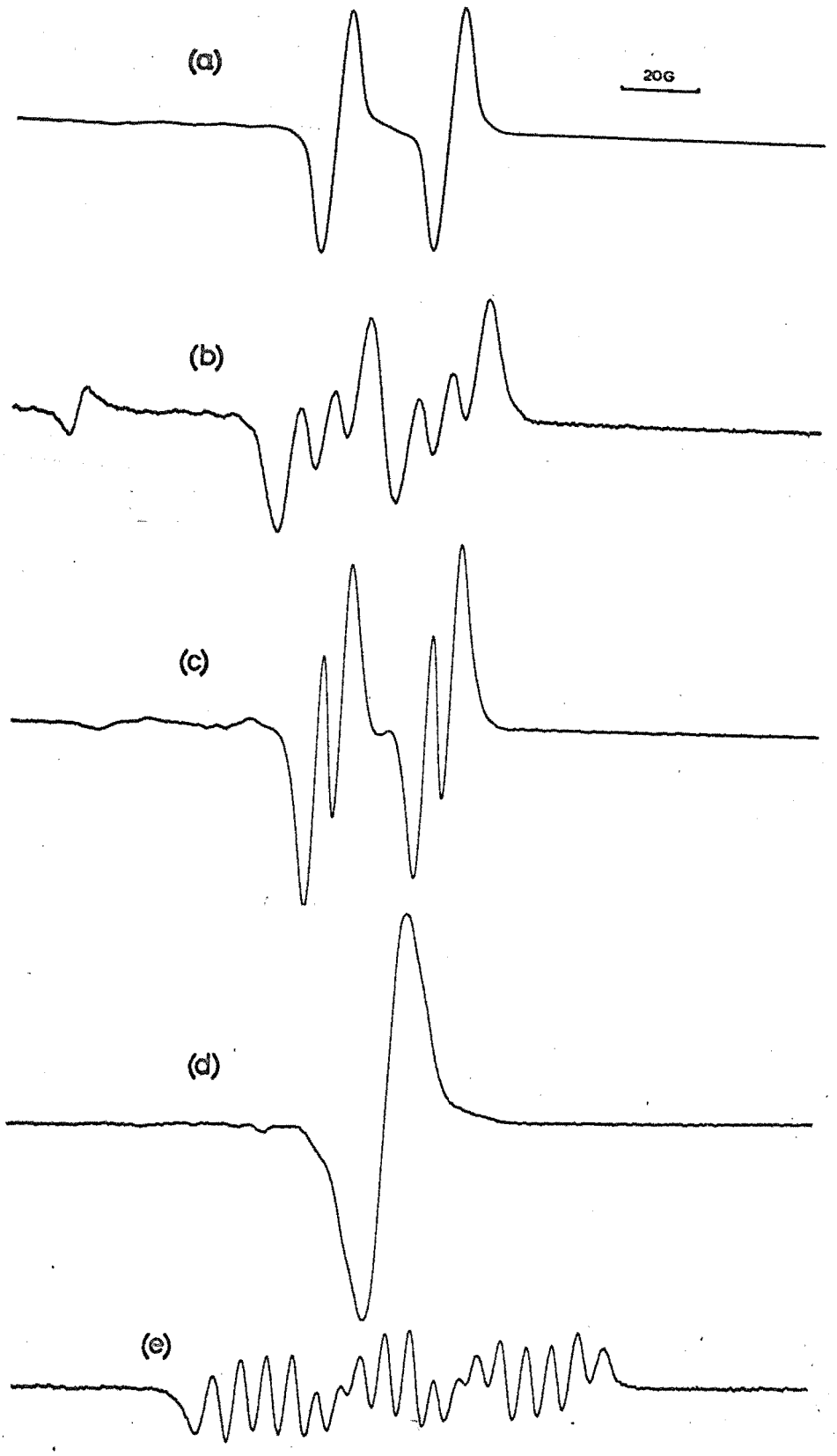

FIG 5.6 Thiosemicarbazide with the magnetic field along:
(a) (0.74, 0.67, 0.0), (b) (0.94, 0.34, 0.0),
(c) (0.90, 0.0, 0.44), (d) (0.0, 0.79, 0.62),
(e) (0.0, 0.28, 0.96), in the $a_1b_1c_1$-axis system

second order effects discussed in Chapter 1.2 and were not analysed further.

The spectra changed markedly as the orientation of the crystal in the magnetic field was varied, with as many as eighteen distinct lines being observed. In a number of orientations the pattern of lines reduced to easily identifiable groups shown in Fig. 5.6.

The doublet (Fig. 5.6a) can only be due to the interaction of a single nucleus with a nuclear spin of one half which, from the structure of the molecule must be a hydrogen nucleus, henceforth labelled H_α. This doublet is split further by three lines of equal intensity (Fig. 5.6b) which indicates interaction of a single nitrogen nucleus, $N_\alpha (I = 1)$.

In one orientation (Fig. 5.6c) the doublet is split by another hydrogen nucleus, H_β, producing four lines of equal intensity.

Near the crystal c-axis the spectrum collapses to a single line about 20G wide at which point the major nitrogen and hydrogen hyperfine splittings are close to their minima (Fig. 5.6d).

Such sets of simple patterns show that there are interactions with two hydrogen atoms and one nitrogen atom. These are not sufficient to account for all of the lines observed at a general orientation (Fig. 5.6e) and it is found that a further nitrogen nucleus, N_β, is interacting with the unpaired electron.

Spectra were taken at 2° intervals in three arbitrary orthogonal planes which enabled most of the lines to be followed as their positions varied. The tensors calculated for the undeuterated material are given in Table 5.1 and the

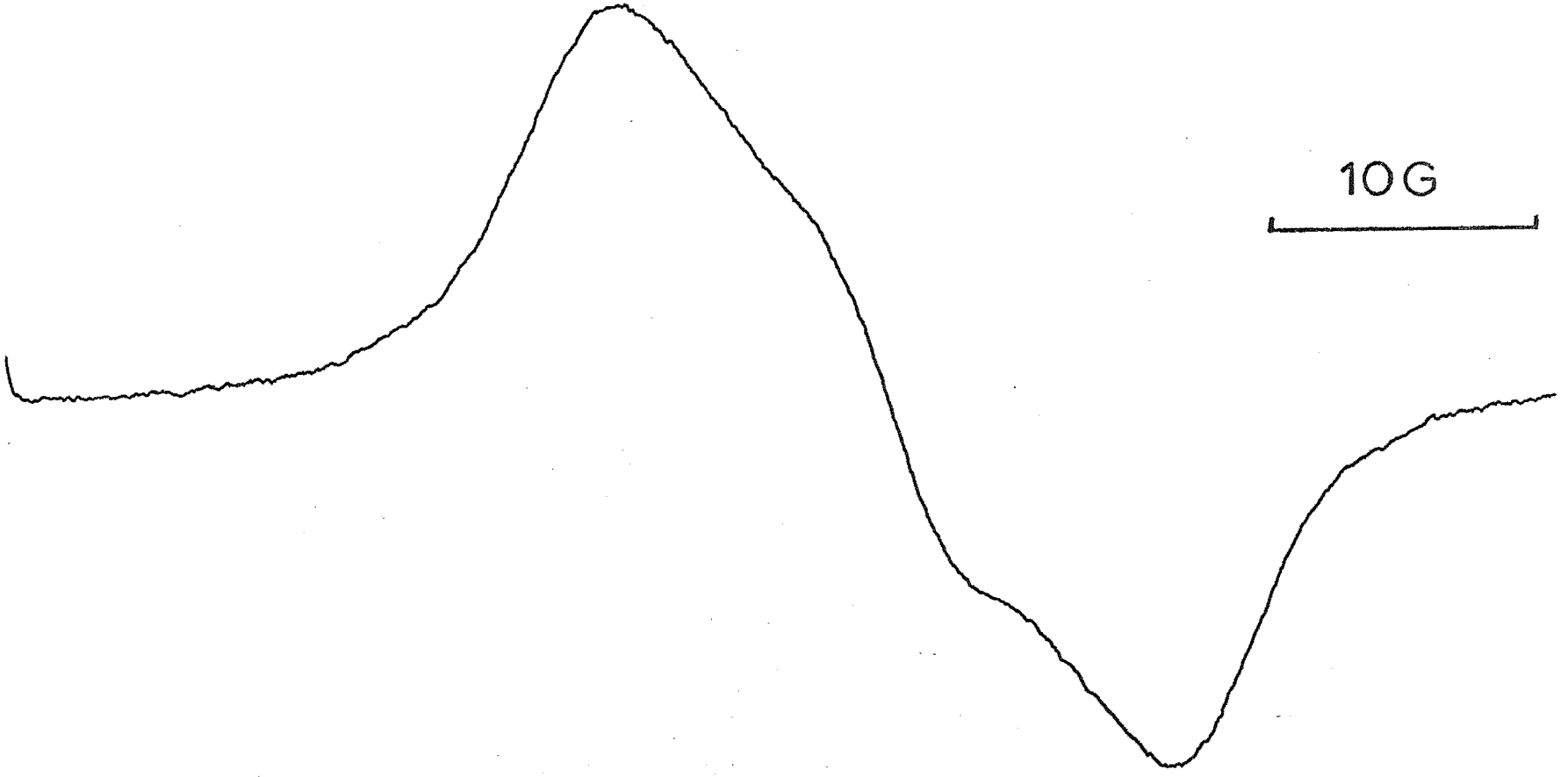

FIG 5.7 Thiosemicarbazide: magnetic field along c-axis

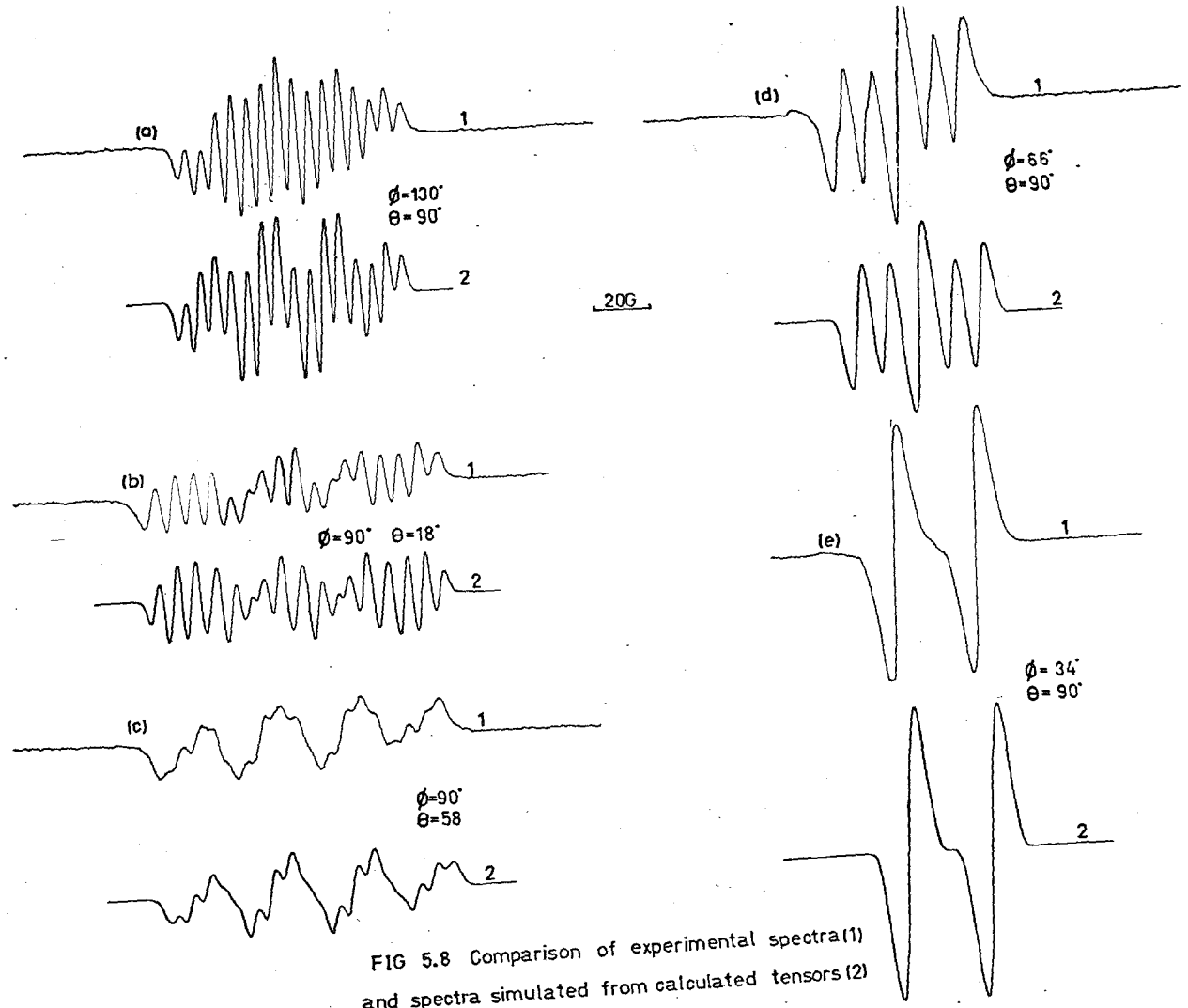

FIG 5.8 Comparison of experimental spectra (1) and spectra simulated from calculated tensors (2) for Thiosemicarbazide.

principal values and their associated direction cosines in Table 5.2. The sign of the H_α coupling has been given in accordance with theoretical predictions (144,145).

In addition to these rotations, the crystal was oriented with the magnetic field along the axis of elongation (Fig. 5.7). Since the axis was poorly defined the error in alignment was estimated as $\pm 6^\circ$. Along this axis both nitrogen hyperfine splittings are close to their minima, the H_α hyperfine splitting is about 8.5G and the H_β hyperfine splitting is about 4.5G. The direction cosines of the crystal c-axis were estimated as (0.0, 0.9, -0.44) in laboratory coordinates.

Because the linewidths were as large as 3.0G it was not possible to determine the minimum principal values with very great accuracy. The tensors listed in Table 5.1 lead to simulated spectra that agree well with the experimental spectra for those orientations of the crystal where the H_α and N_α hyperfine splittings are large; but sometimes do not agree very well when the hyperfine splittings are small. Some examples of simulated spectra are given in Fig. 5.8. Because the orientation of the minimum principal value is constrained by the accurate determination of one or two of the other principal axes, the direction cosines of all three principal axes have similar errors, except in the case of N_α where two of the principal axes were less accurately determined than the unique axis.

The hyperfine tensors describing the interaction of the hydrogen atoms with the unpaired electron were determined with the use of second order equations but the difference between the elements of tensors determined by first and second order methods was only of the magnitude of the experimental error.

TABLE 5.1

Undeuterated Thiosemicarbazide

Experimental Tensors[a]

H_α	26.7	7.5	0.4
		9.7	7.3
			16.3
N_α	7.8	-6.6	-9.6
		9.9	12.0
			20.4
H_β	4.1	-2.1	1.0
		2.7	1.8
			5.9
N_β	2.3	-1.6	-2.6
		3.1	0.8
			5.0
g	2.0061	-0.0000	0.0022
		2.0039	-0.0012
			2.0037

[a]Expressed in laboratory axis system $a_1b_1c_1$.

TABLE 5.2

Undeuterated Thiosemicarbazide

	Principal Value[a]	Direction Cosines[b]		
H_α	-30.2 ± 0.4G	0.883	0.405	0.237
	-19.1 ± 0.5G	-0.390	0.352	0.851
	- 3.4 ± 2.0G	-0.261	0.844	-0.469
N_α	33.6 ± 0.3G	-0.413	0.502	0.760
	2.7 ± 1.0G	0.831	-0.134	0.540
	2.0 ± 1.0G	0.373	0.855	-0.362
H_β	6.7 ± 0.5G	0.06	0.38	0.92
	5.6 ± 0.7G	0.84	-0.52	0.16
	0.4 ± 0.9G	0.54	0.76	-0.35
$\lvert N_\beta \rvert$	7.2 ± 0.4G	-0.528	0.372	0.764
	2.9 ± 0.6G	-0.141	0.848	-0.511
	0.3 ± 0.9G	0.838	0.378	0.395
g[c]	2.0074	0.823	-0.192	0.535
	2.0043	0.400	0.864	-0.306
	2.0018	-0.403	0.466	0.788
c-axis		0.0	0.9	-0.44

[a] Errors are estimated to give a measure of twice the standard deviation at any orientation.

[b] With respect to arbitrary orthogonal axes, $a_1 b_1 c_1$.

[c] Standard deviation = 0.0003.

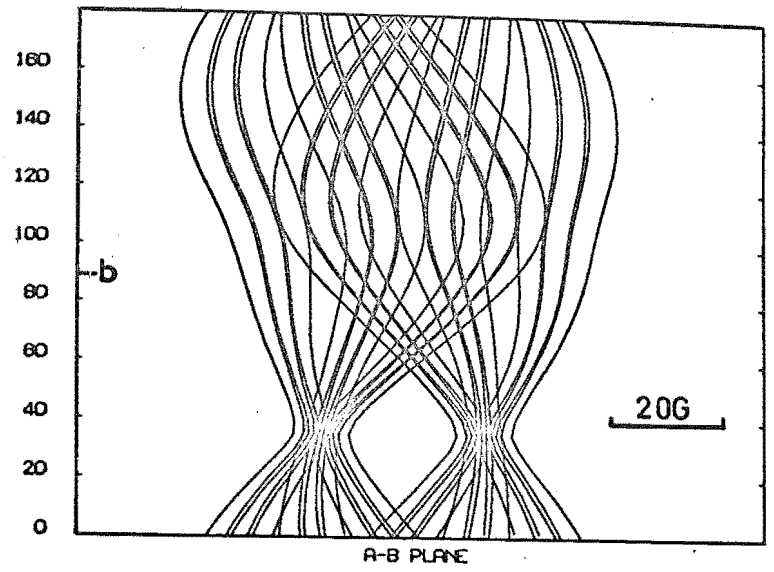

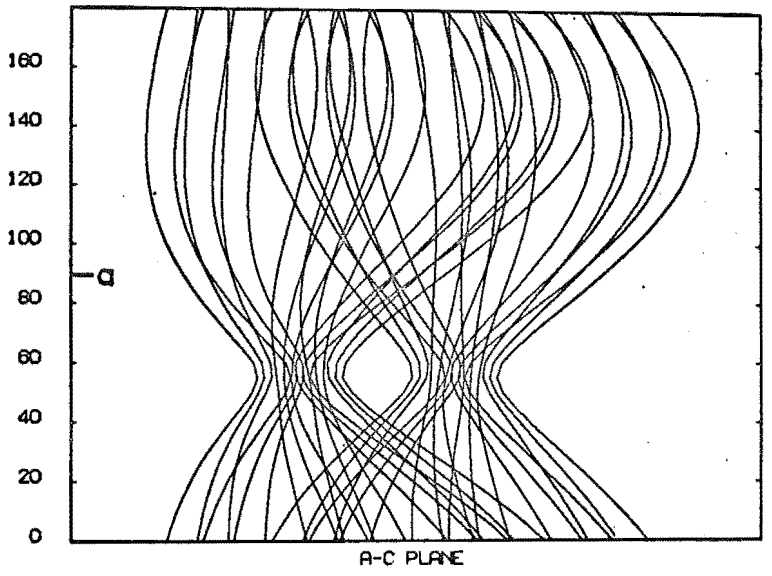

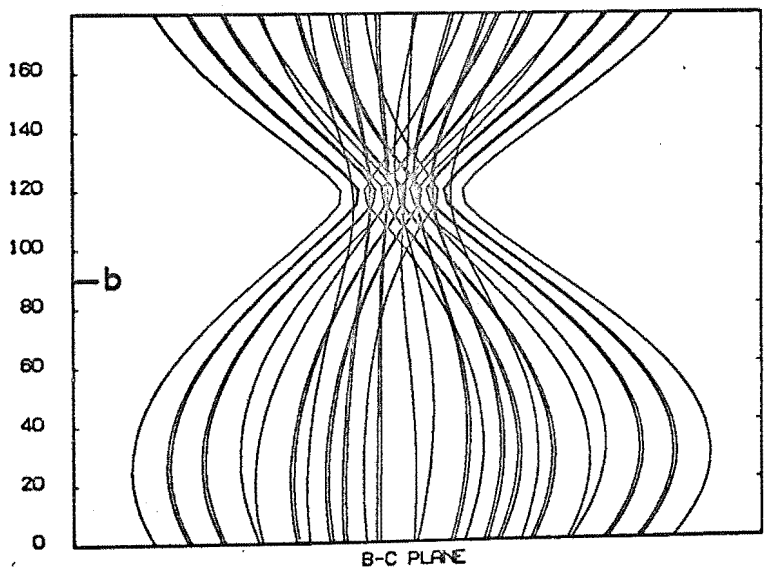

FIG 5.9 Thiosemicarbazide

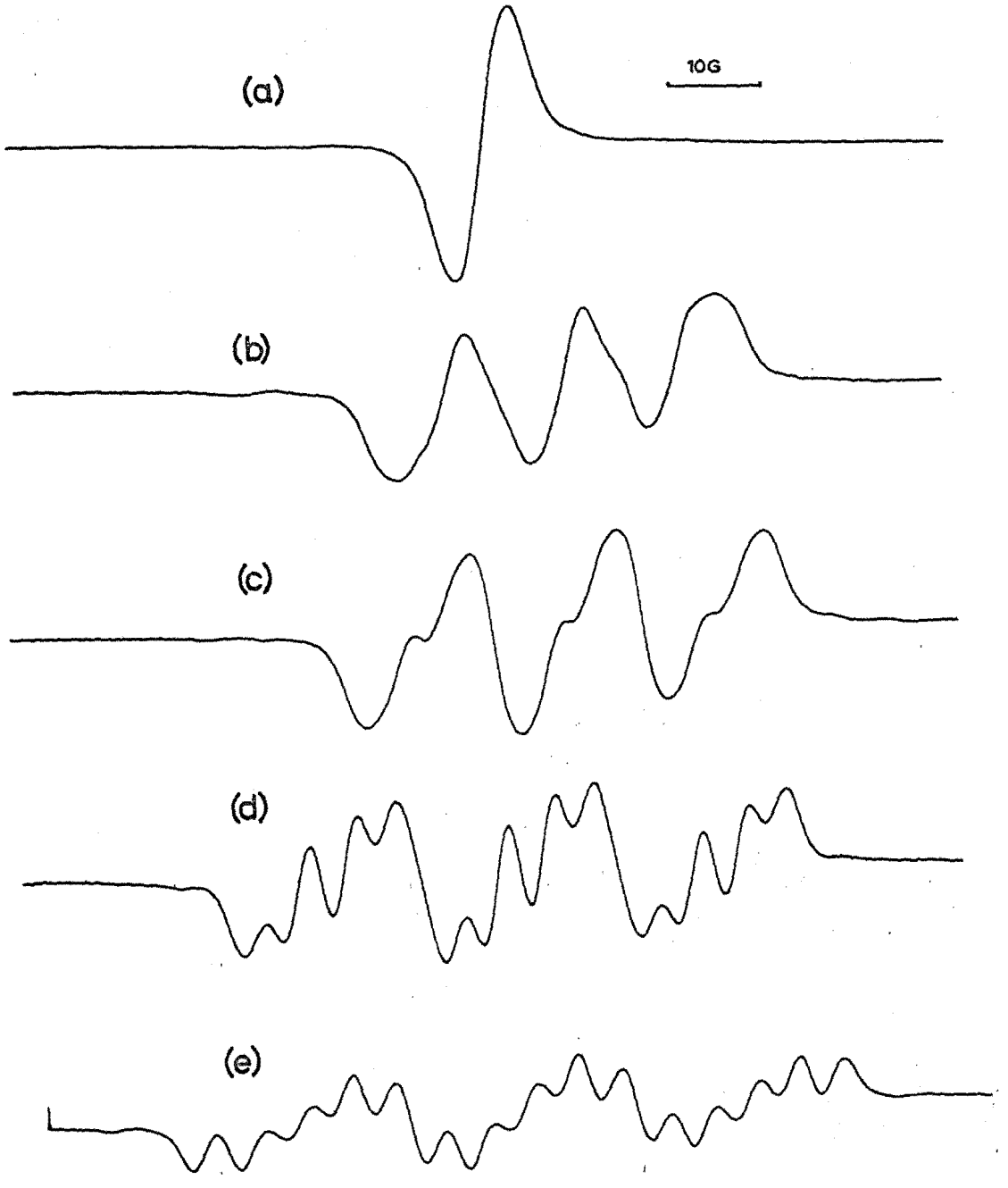

FIG 5.10 Deuterated Thiosemicarbazide with the magnetic field along (a) (0.81, 0.0, 0.59), (b) (0.70,-0.72, 0.0), (c) (0.85,-0.53, 0.0), (d) (0.24, 0.0, 0.97), (e) (0.0, 0.59, 0.81), in the $a_2 b_2 c_2$-axis system.

The variation of each of the hyperfine coupling constants and of the g-value as the crystal is rotated about the three orthogonal axes in which the tensors are expressed are combined in Fig. 5.9 to show the variation of the complete spectrum with orientation.

5.5.2 Deuterated thiosemicarbazide

The deuterated crystal gives rather different combinations of lines and the maximum width of the spectrum is 85G instead of 100G as observed for the undeuterated material. For this orientation of the undeuterated crystal A_{N_α} = 30.0G, A_{H_α} = 21.0G, A_{N_β} = 6.5G, and A_{H_β} = 6.5G. If H_α and H_β were replaced by deuterium the width of the spectrum would reduce to 82G whereas if only H_α were replaced the width of the spectrum would be 86G.

There are no groupings comparable to Figs 5.6(a)-5.6(c). The spectrum does collapse to a single line of width 6G (Fig. 5.10a) and also into three broad lines of equal intensity (Fig. 5.10b) due to the hyperfine coupling of either a nitrogen or a deuterium nucleus. These three lines are each split into three, four or five further lines (Figs 5.10c-e) which are attributed to the combination of a doublet and a triplet. The doublet can only arise from interaction of a hydrogen nucleus which has a hyperfine coupling constant of about six gauss. Since this splitting never exceeds 10G it must be due to H_β.

The large triplet splittings are similar to the N_α splittings in the undeuterated material, and the small triplet splittings have a similar magnitude to the N_β splittings. The relative orientations of the principal axes of the tensors calculated for these triplets are similar to those of the nitrogen hyperfine tensors calculated for the undeuterated

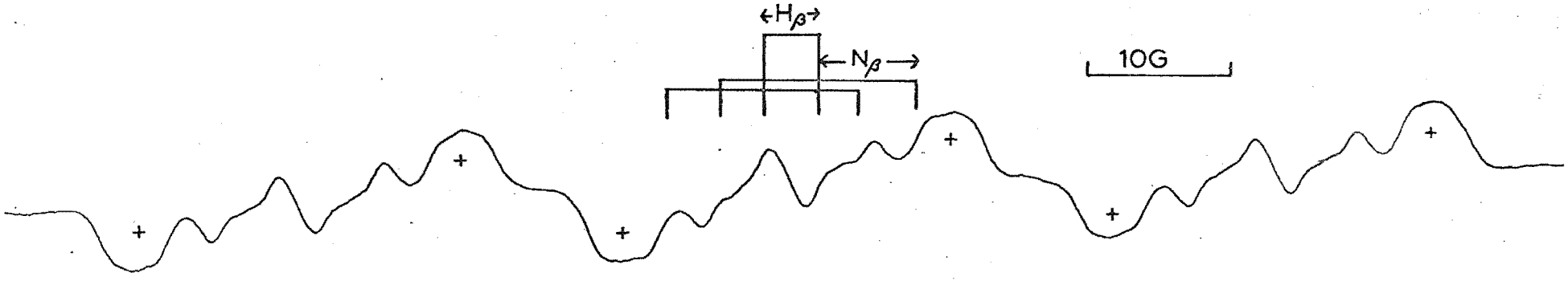

FIG 5.11 Deuterated Thiosemicarbazide showing unresolved hyperfine structure(+)

material and the tensors have therefore been attributed to N_α and N_β respectively.

There appears to be no resolved splitting due to D_α which must therefore be less than the linewidth at all orientations. The linewidth was only calculated at a few crystal orientations, because the hyperfine splitting parameters were not determined to sufficient accuracy to make it possible to calculate the linewidth at orientations where lines overlapped a great deal. In the undeuterated crystals a minimum linewidth of 3.0G was observed whereas the minimum linewidth in the deuterated crystals was 2.0G.

For some orientations of the deuterated crystal in the magnetic field individual lines became partly resolved to reveal further structure (Fig. 5.11) but this was indistinct and was not fully analysed. Such additional line splitting was always less than 2.5G.

The difference between the minimum linewidths in the two compounds suggests that there could be interactions with further protons and this is also suggested by the unusual variation of the linewidth as the temperature was varied.

The parameters calculated for the deuterated crystals are given in Tables 5.3 and 5.4. The anisotropy of the g-tensor and each of the hyperfine interaction tensors are combined in Fig. 5.12 to show the variation of the complete spectrum with orientation of the crystal in the magnetic field.

5.5.3 Interpretation

The magnitude of the hyperfine couplings of the most strongly interacting hydrogen and nitrogen atoms leaves no doubt that the radical is of the type ·NHR.

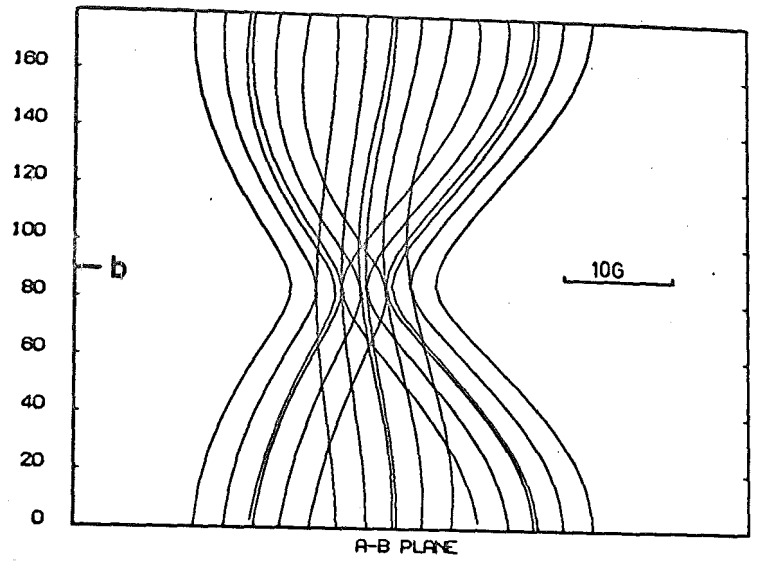

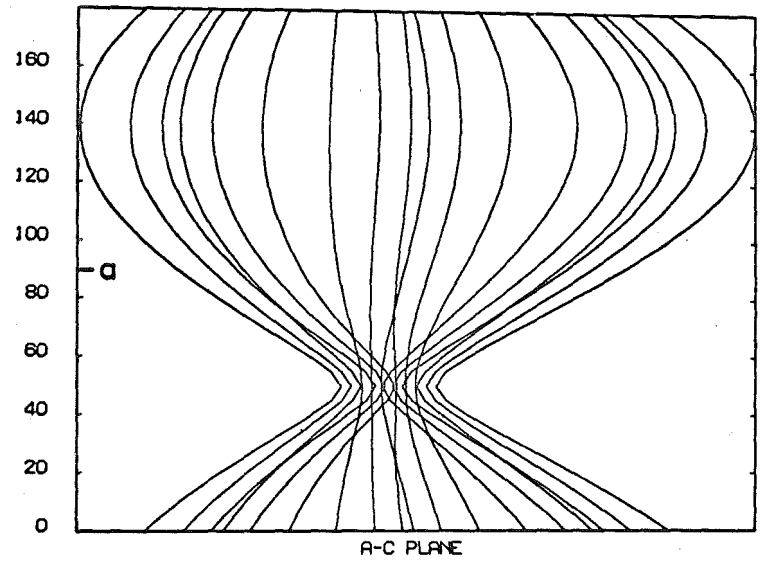

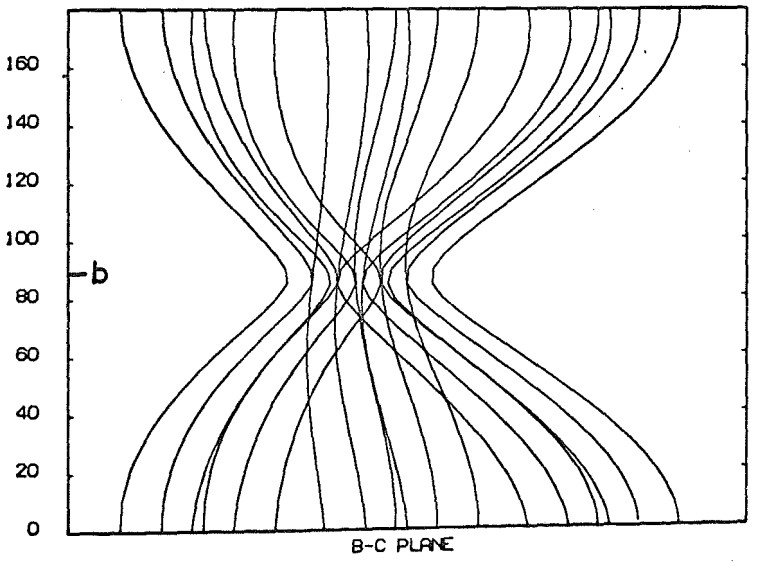

FIG 5.12 deuterated Thiosemicarbazide

TABLE 5.3

Deuterated Thiosemicarbazide

Experimental Tensors[a]

N_α	13.1	0.5	-14.9
		3.3	1.0
			23.8
H_β	5.8	2.5	- 4.0
		4.7	2.9
			8.2
N_β	3.0	0.6	- 2.7
		3.4	0.4
			5.0
g	2.0041	-0.0005	0.0012
		2.0066	0.0000
			2.0030

[a]Expressed in laboratory axis system $a_2b_2c_2$.

TABLE 5.4

Deuterated Thiosemicarbazide

	Principal Value[a]	Direction Cosines[b]		
N_α	34.2 ± 0.5G	-0.58	0.03	0.82
	3 ± 3G	0.4	0.8	0.3
	2 ± 3G	0.7	-0.5	0.5
H_β	11.3 ± 0.6G	-0.53	0.17	0.83
	7.5 ± 1.0G	0.60	0.77	0.22
	0.0 ± 2G	0.60	-0.62	0.51
$\|N_\beta\|$	6.9 ± 0.4G	-0.57	-0.00	0.82
	3.6 ± 0.6G	0.23	0.96	0.16
	0.9 ± 1.6G	0.79	-0.28	0.55
D_α	< 2.5G			
g^c	2.0067	-0.211	0.975	-0.064
	2.0048	0.806	0.211	0.553
	2.0022	-0.553	-0.065	0.831

[a] Errors are estimated to give a measure of twice the standard deviation at any orientation.

[b] With respect to arbitrary orthogonal axes, $a_2 b_2 c_2$.

[c] Standard deviation = 0.0003

The radical ·NHR which has the unpaired electron in a p orbital on the sp^2 hybridized nitrogen atom is expected (146) to be comparable to the $R_2\dot{C}H$ radical (12,164), and the theory describing the g- and hyperfine tensors of this species (70, 144,145) has been successfully used to account for several nitrogen-centred radicals such as $\cdot NH(SO_3^-)$ (146), $\cdot NH_2^+SO_3^-$ (147), and $\cdot NHNH_3^+$ (108). This theory predicts that minimum g-value and the intermediate principal value of the H_α hyperfine tensor will be directed along the symmetry axis of the p orbital. It is also expected (148) that the maximum principal value of the nitrogen hyperfine splitting will be in this direction. The smallest value of the H_α hyperfine splitting is predicted to coincide with the direction of the N-H bond. The nitrogen hyperfine tensor is expected to be axially symmetric although deviations are often observed (108,147). The experimentally observed directions of the principal axes g_{min}, N_α^{max} and H_α^2 are as predicted for both deuterated and undeuterated samples, so that the unpaired electron is deduced to be in a π orbital perpendicular to the molecular plane. It is also observed that the maximum principal value of the N_β hyperfine splitting is oriented in this direction which indicates some delocalisation of the unpaired electron over the two nitrogen atoms.

The coplanarity of the remaining principal axes is entirely consistent with the crystallographic data which show that the molecule is planar.

Since the splitting due to H_α is not observed in the deuterated crystal it must arise from a hydrogen atom on one of the terminal atoms, and the presence of a doublet splitting in the spectra of the deuterated material indicates that the H_β

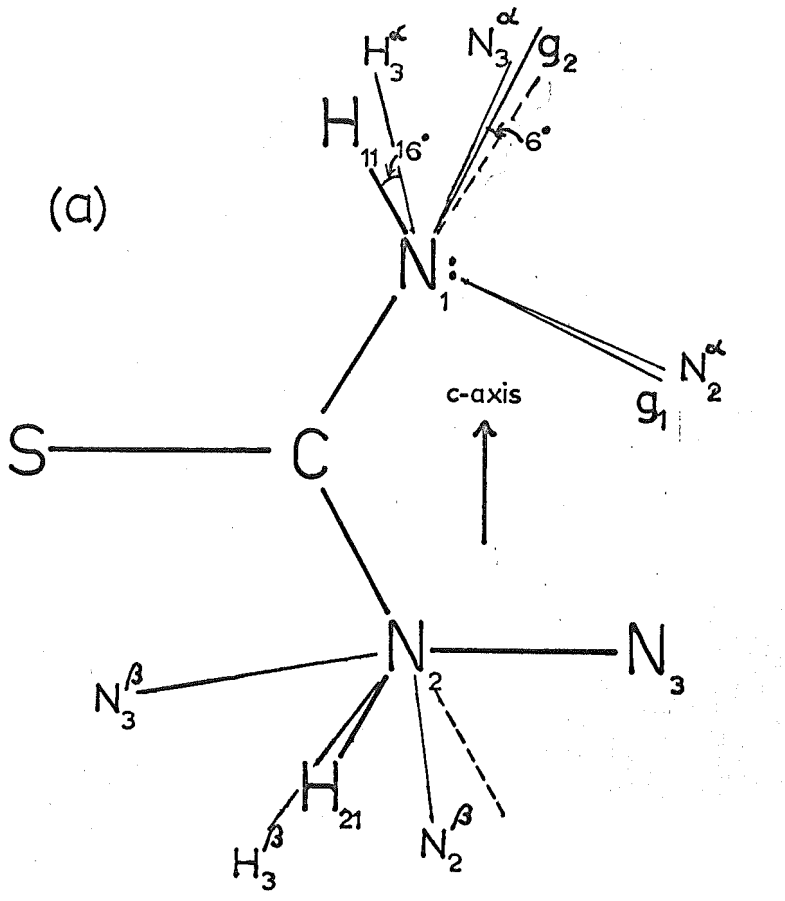

RADICAL I

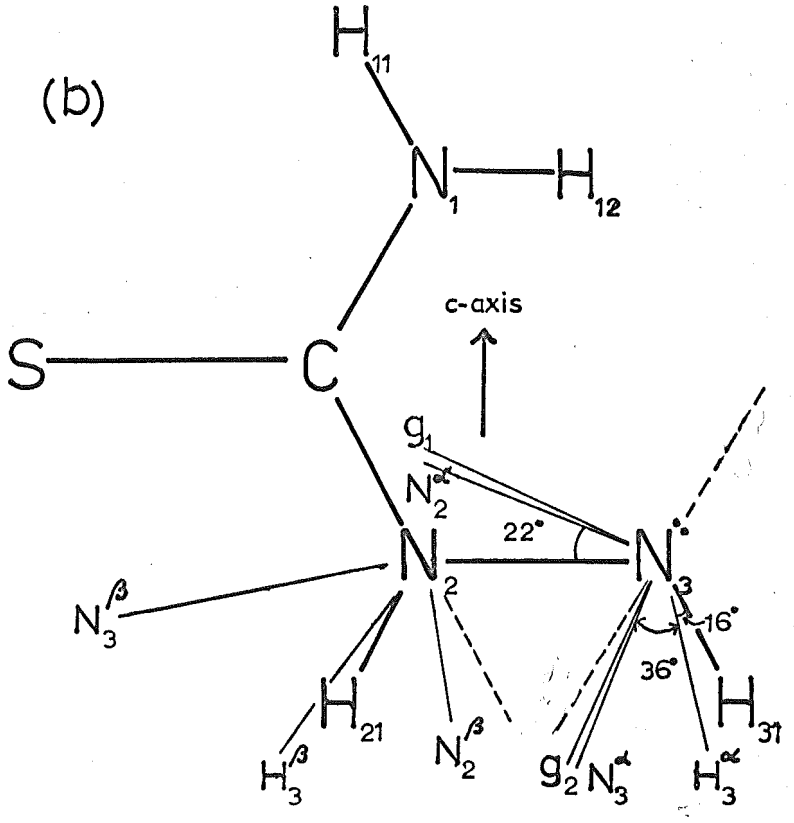

RADICAL II

FIG 5.13

hyperfine coupling arises from H_{21}, in which case the small nitrogen coupling is likely to be of N_2 (Fig. 5.13).

There are only two possible radicals that can account for all of these observations, and these are not easily distinguished.

(II) (I)

However, the observation that both nitrogen hyperfine couplings and the larger hydrogen hyperfine coupling are close to their minima when the magnetic field is along the c-axis provides a means of distinguishing them, since the minimum alpha hydrogen hyperfine coupling is expected to be directed along the NH bond (70).

From the crystal structure determination it is known that the angle between the c-axis and the N_1H_{11} direction is 31.6°, whereas the N_3H_{31} and N_3H_{32} directions are not close to the c-axis and do not lie in the SN_1N_2 plane. If it is assumed that there is no major reorientation of the parent molecule upon irradiation then the N_3H bond of radical II is not close to the observed direction of the minimum principal value of the H_α hyperfine coupling which is about 15° from the c-axis.

The possibility remains that a radical of type II is formed by reorientation of the terminal N_3H group, so that the unpaired electron lies in a p orbital normal to the molecular plane and that the N_3H_{31} bond lies in the plane at 120° to the N_3N_2 bond, as expected for trigonal hybridisation (Fig. 5.13b)

From observations along the c-axis it was found that this axis is 15° and 22° from the directions of the minimum principal values of the H_α and N_α hyperfine tensors respectively, to

within about 8°. Thus if the radical is of Type I (Fig. 5.15a), the minimum principal value of the N_α hyperfine coupling and the intermediate principal value of the g-tensor lie very close to the direction of the CN_1 bond and the minimum principal value of the H_α hyperfine coupling is about 16° from the N_1H_{11} bond direction. Of the principal axes of the H_β hyperfine coupling only the minimum principal value lies in the molecular plane, near the N_2H_{21} bond direction.

If the radical is of type II but reoriented in the manner explained above, the principal axes would still be directed approximately in this manner with respect to the bond directions except that the intermediate principal value of the N_α coupling, and the minimum principal value of the g-tensor would be 22° and 24° respectively from the N_2N_3 bond direction (Fig. 5.13b).

The average g-value is 2.0044 which is similar to that observed for the $NH_2CONH\cdot$ radical in urea (105) and for $\cdot NH_2$ radicals (165), although greater than for the $\cdot NHNH_3^+$ radical (108). Some controversy has existed over the orientation of the g-tensor in analogous radicals. The maximum g-value has been found to almost coincide with the H_α^{min} value in $\cdot NHNH_3^+$ but to be 45° from this direction in $\cdot NHSO_3^-$ (146) and to coincide with H_α^{max} in $\cdot CH(CO_2H)_2$ (166). Other workers have found the principal axes to be in orientations not related to the radical symmetry as determined by crystallographic data or from the hyperfine interactions. Such ambiguity is partly due to experimental inaccuracies in determining an almost isotropic quantity. The principal axis of the maximum g-value is largely determined by the symmetry of the completely filled orbital nearest in energy to the orbital containing the

unpaired electron. In most nitrogen radicals this will be the sp^2 non-bonding orbital containing the lone pair.

The close similarity of the orientations of the principal axes for the N_α and g-tensors indicates that they reflect the symmetry of the radical. For radical I the g_2 and N_3^α principal axes lie near the NH bond whereas in radical II they lie near the symmetry axis of the lone pair. Since the g-tensor is more likely to reflect the symmetry of the lone pair orbital which is almost certainly involved in the lowest energy electronic transition, radical II seems to be a more probable structure for the species. An unpaired electron in a π-orbital on N_1 would probably be delocalised over the SCN_1 group and a greater g-value might be expected than has been observed. On the other hand formation of such a radical involves no reorientation of the terminal amino group.

In the undeuterated sample additional hyperfine interactions with the hydrogen atoms attached to N_1 could account for the greater linewidth when compared with spectra of the deuterated sample.

The D_α hyperfine splitting in the deuterated sample appears to be only one half of the magnitude predicted by the H_α hyperfine splitting of the undeuterated sample, and the H_β splitting is considerably greater in the deuterated sample than in the undeuterated sample. The N_α and N_β splittings do not alter. These differences indicate that the orientation of the hydrogen atoms may be slightly different in the two radicals, but it is clear that the differences between the deuterated and undeuterated radicals are restricted to the hydrogen and deuterium atoms and may be accounted for by slight differences in bond lengths and angles and in the strength of hydrogen

bonding. Such differences have been observed to occur in other compounds upon deuteration (149,150,151) and in some cases different species are formed upon irradiation (71,72).

The principal values of the hyperfine coupling constants may be used to determine the distribution of the unpaired spin density throughout the radical. The theory of the nuclear hyperfine coupling is discussed in section 1.2.1.

From the isotropic hyperfine coupling an estimate of the s character of the orbitals may be deduced. The isotropic alpha hydrogen coupling is 17.6G which is slightly smaller than is usual for π-radicals (16) but similar to that observed for $\cdot NHNH_3^+$ (108). Theoretical calculations of the hyperfine coupling constants using equations 1-11 and 1-13 and values of $|\psi(0)|^2$ and $\langle r^{-3} \rangle$ calculated by self-consistent field methods as tabulated by Morton (52), give A^N_{2s} = 550G, A^N_{2p} = 17.2G, A^H_{1s} = 507G. Using these figures, the spin density in the alpha hydrogen 1s orbital is 0.035 and in the beta hydrogen 1s orbital is 0.008. The isotropic couplings of the nitrogen atoms are consistent with a spin density in the nitrogen 2s orbital of 0.023 for the alpha nitrogen atom and of 0.006 for the beta nitrogen atom. To a good approximation the alpha nitrogen coupling is cylindrically symmetrical with a_n = 12.7G and b_n = 10.4G. This value of b_n implies a spin density of 0.63 in the nitrogen 2p orbital. The beta nitrogen coupling is not cylindrically symmetrical but can be decomposed into an isotropic and two anisotropic parts, the smaller representing the deviation from axial symmetry.

$$\begin{vmatrix} 3.5 & & \\ & 3.5 & \\ & & 3.5 \end{vmatrix} + \begin{vmatrix} 4.6 & & \\ & -2.3 & \\ & & -2.3 \end{vmatrix} + \begin{vmatrix} -0.9 & & \\ & 1.8 & \\ & & -0.9 \end{vmatrix}$$

$$a_n \qquad\qquad b'_n \qquad\qquad b''_n$$

Associated with b_n' is a spin density of 0.12 in the nitrogen 2p orbital. The deviation from axial symmetry indicates that there is additional spin density in the beta nitrogen sp^2-orbitals.

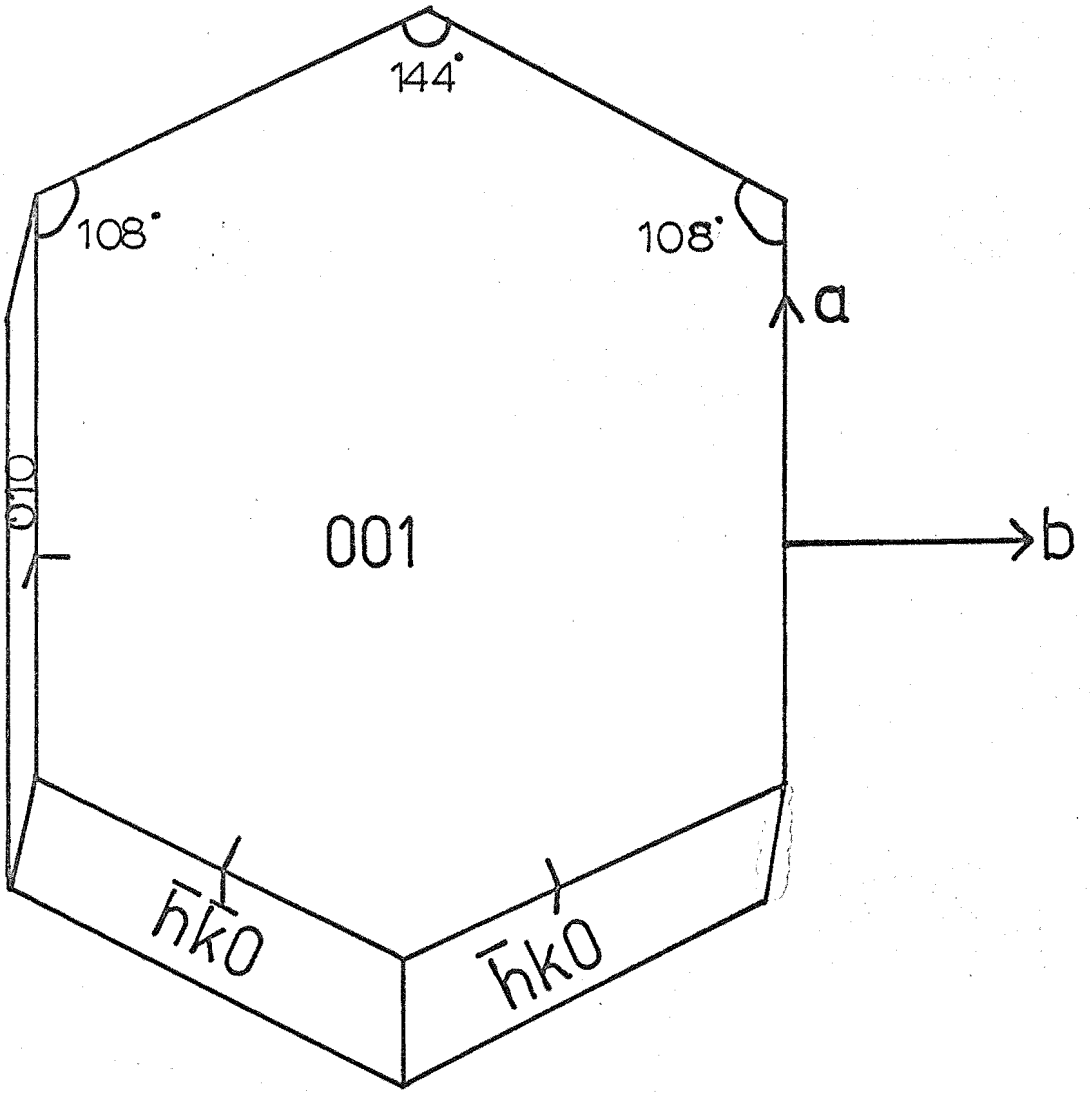

FIG 6.1 Crystal habit of Thiosemicarbazide . HCl.

CHAPTER 6

RESULTS FOR SEMICARBAZIDE DERIVATIVES

A THIOSEMICARBAZIDE HYDROCHLORIDE

6A.1 Crystal Structure

As far as could be ascertained, the crystal structure of thiosemicarbazide hydrochloride has not been elucidated. Crystals of the oxygen analogue, semicarbazide hydrochloride (153), are orthorhombic, space group $P2_12_12_1(D_2^4)$, with four molecules in the unit cell. Although replacing sulphur for oxygen will affect the hydrogen bonding in the crystal, comparison with similar compounds (109) suggests that the structure is orthorhombic. The x-ray powder photographs of the two compounds are however quite different, which shows that the unit cell parameters are not similar.

The crystal habit is shown in Fig. 6.1 together with the axial system used to determine the tensors. Crystals grown from deuterium oxide were indistinguishable from crystals grown from water.

6A.2 ESR Spectra

Crystals became brown upon irradiation at room temperature both in air and in vacuo. Crystals irradiated at 105°K and studied at 120°K gave the same results as crystals irradiated at room temperature, and there were only minor differences between the esr spectra of deuterated and undeuterated compounds.

The esr spectra were generally complex,consisting of a large number of lines arising from at least four chemically different radicals and spread over 600G. The line positions were all very dependent upon the orientation of the crystal

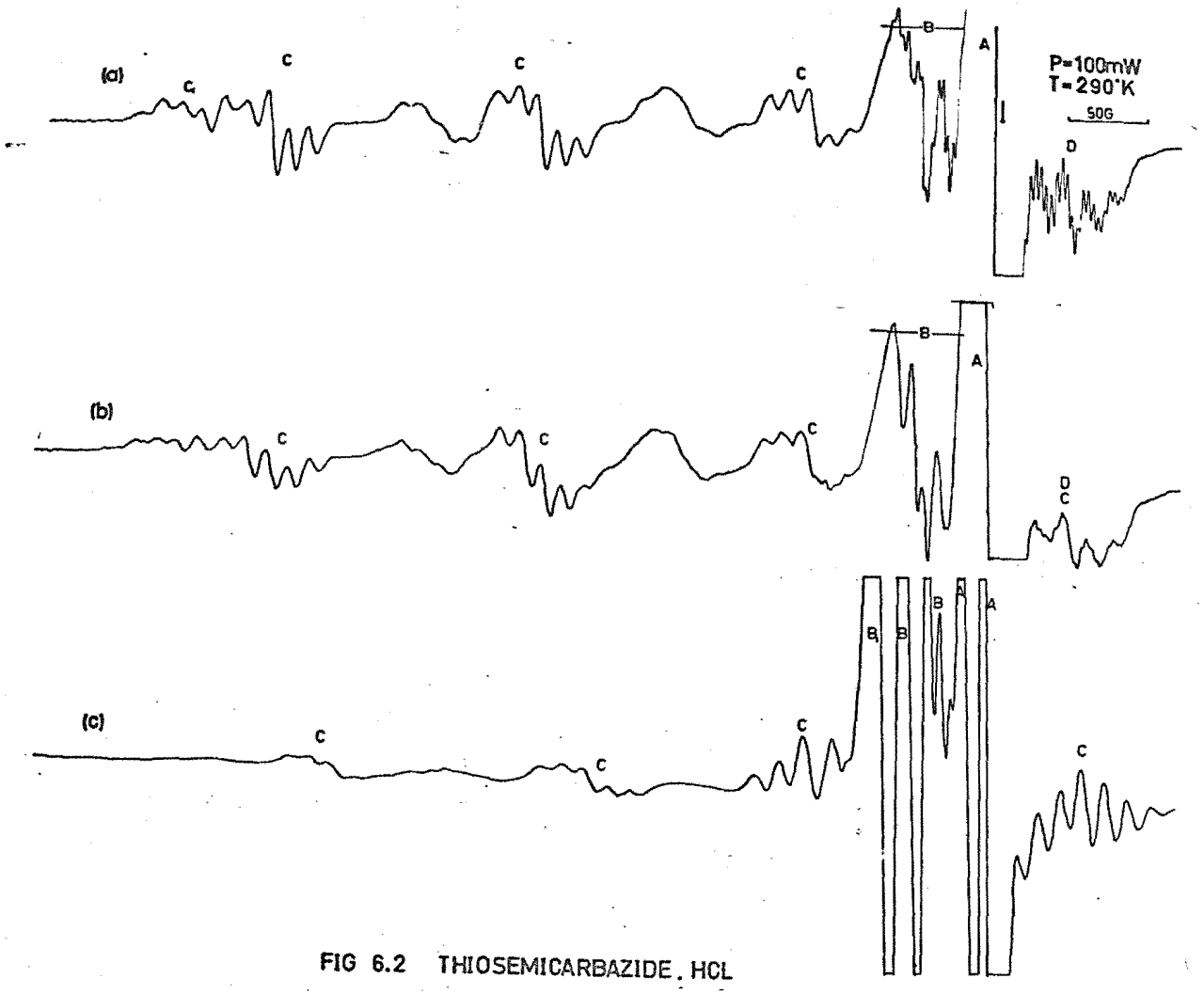

FIG 6.2 THIOSEMICARBAZIDE. HCL

in the magnetic field and it was necessary to record spectra at one degree intervals in three planes to determine the nuclear hyperfine tensors.

Figure 6.2 shows clearly three types of radical. At the magnetic field corresponding to the free spin g-value there is a single intense line, henceforth designated as arising from radical A. Centred about this point are a large number of narrow, closely spaced lines arising from radical D. These lines fade rapidly at room temperature and are clear at only a few orientations. This is shown in Fig. 6.2 where (a) and (b) were obtained at crystal orientations which differed by only six degrees. Most of the remaining lines arise from a stable species, designated C, although there are several further lines in the area labelled B that arise from other species. These are seen more clearly in Fig. 6.2c where the lines due to C are less intense. Because lines arising from different radicals overlap so much, some difficulty was experienced in calculating the parameters of the Hamiltonian from the spectra.

Radical D could be observed in only a few crystals and because of its lability no tensors could be calculated. It was not observed in crystals γ-irradiated in vacuo, although several days elapsed before the spectra of such crystals could be obtained, or in crystals x-irradiated at $105^{\circ}K$. Radical C is characterised by a very broad spectrum of many lines and although some of these lines were always obscured by lines due to radicals A and B, at most orientations there remained enough well resolved lines for tensors to be calculated.

Attempts were made to anneal the crystals by heating them in a stream of nitrogen and also by irradiating them with

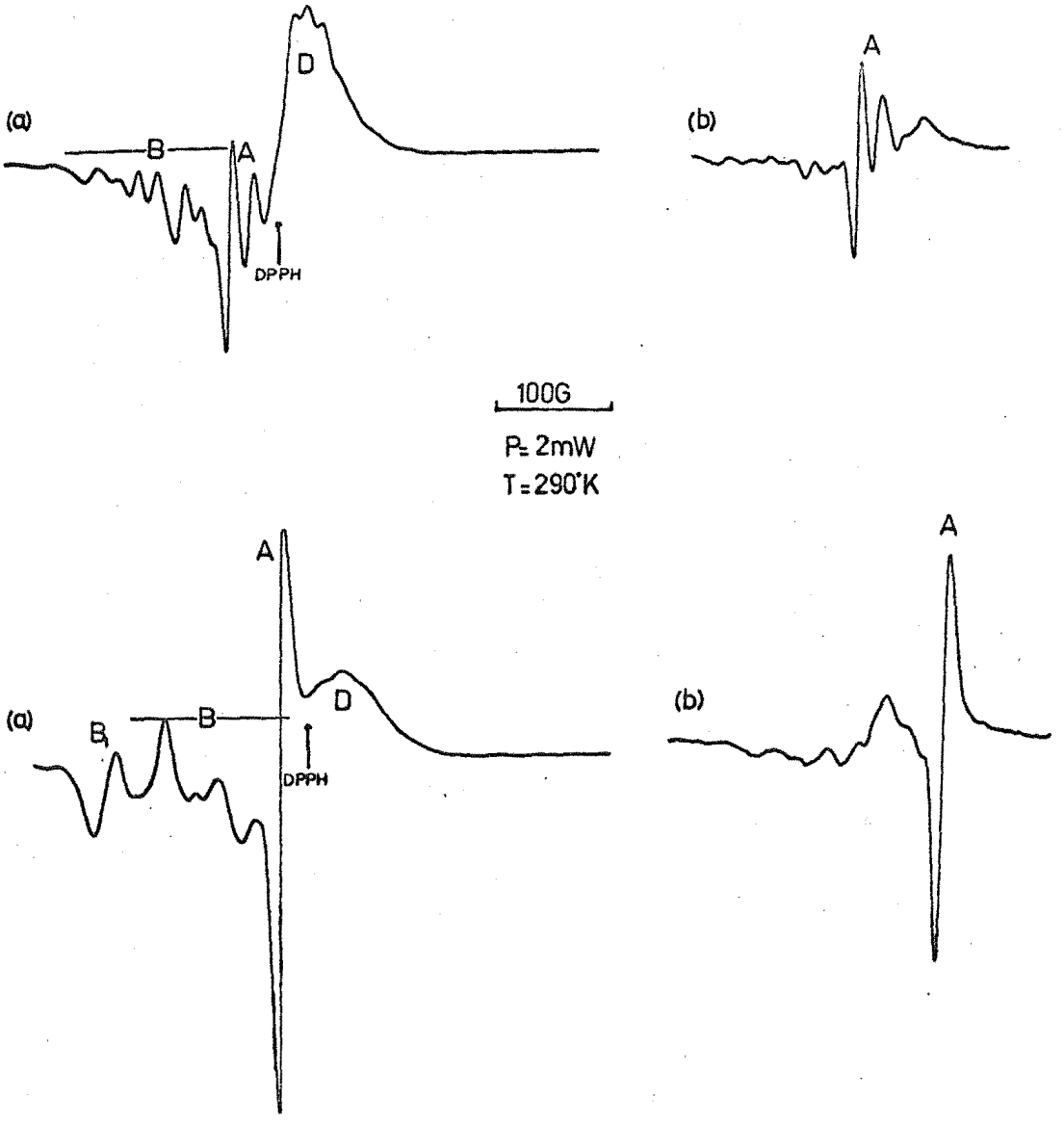

FIG 6.3 Deuterated Thiosemicarbazide. HCl
(a) before, (b) after annealing with uv-light

uv light from a mercury lamp, and by this means lines due to radicals B and D were reduced in intensity relative to the other lines (Fig. 6.3). A similar effect was noted when irradiated crystals were stored at room temperature for some months. The annealing process was accompanied by a fading of the brown colour. It was noticeable that uv-irradiation was a much more efficient means of preferentially removing radical B than thermal annealing although very slow thermal annealing, achieved by keeping crystals at room temperature in the dark, was equally as effective. At higher temperatures all esr signals decreased irreversibly in intensity.

The esr spectra changed markedly as the microwave power was varied (Fig. 6.4). At power levels of 0.2 mW where little saturation occurs, the spectra are dominated by the lines of A and B. The lines arising from species C only become clear when the microwave power is increased which affords a greater signal to noise ratio. Such lines do not alter significantly as the power level is raised whereas some of the central lines do broaden, as do the lines due to D.

6A.3 Interpretation of ESR Spectra

6A.3.1 Radical A

The most intense line of the esr spectrum in both deuterated and undeuterated crystals arises from a species that has no observable nuclear hyperfine splitting and which has a g-tensor with principal values of 2.002, 2.007, 2.018 (Table 6.1). This line dominated all spectra at all microwave power levels from 0.2 mW to 200 mW and at all temperatures from 120^{o}K to 430^{o}K, and could not be removed by annealing except at temperatures above 320^{o}K when the whole esr spectrum gradually disappeared. The linewidth is about 7-8G which is very broad

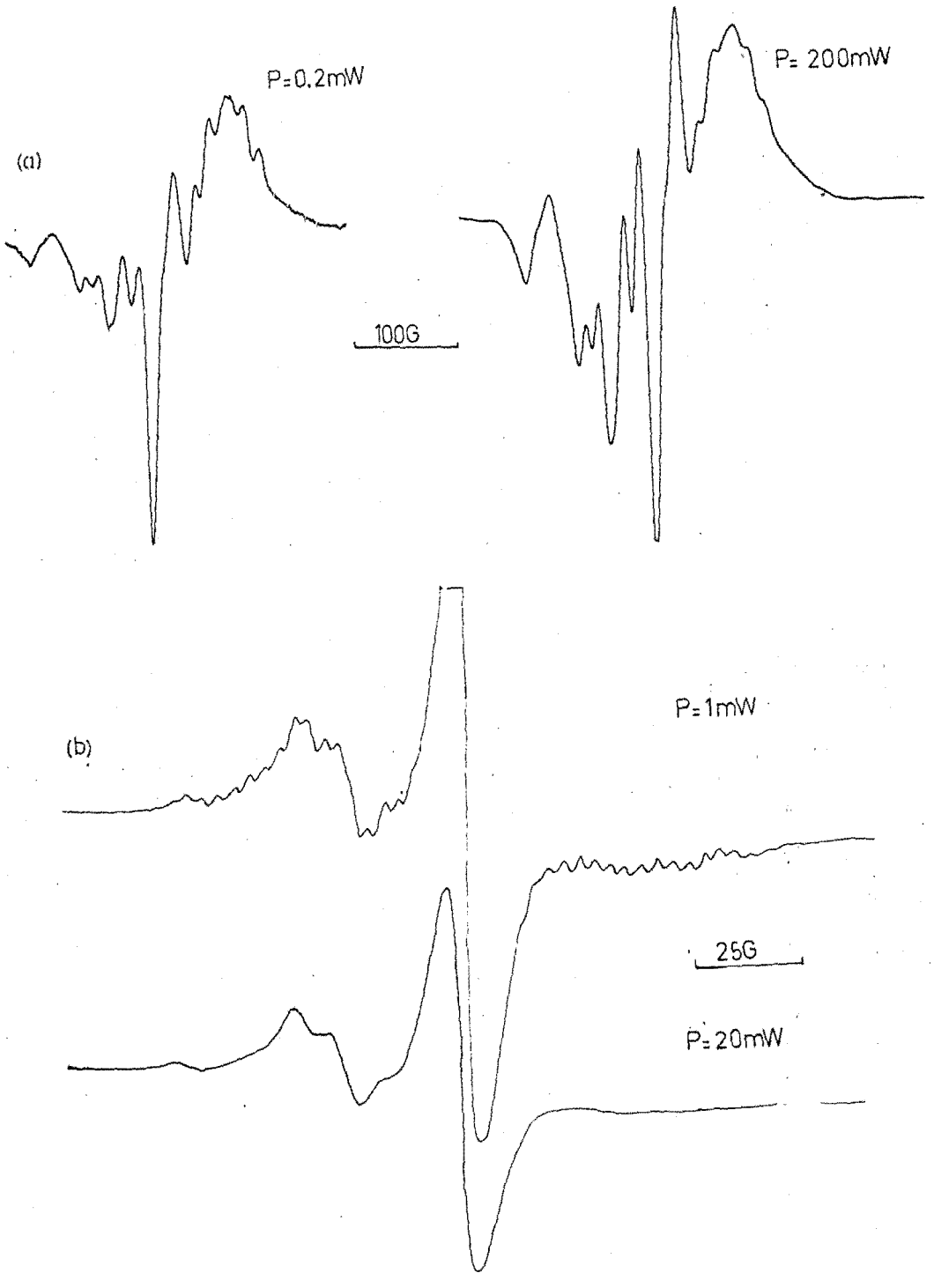

FIG 6.4 Power saturation in
(a) deuterated, (b) undeuterated
Thiosemicarbazide HCl

TABLE 6.1

Thiosemicarbazide Hydrochloride

Radical A

Principal Value[b]	Direction Cosines[a]		
2.0019	0.941	-0.334	-0.040
2.0067	0.290	0.866	-0.408
2.0178	0.171	0.373	0.912

g-Tensor in laboratory coordinates

2.0028	0.0022	0.0019
	2.0077	0.0037
		2.0159

[a]With respect to laboratory axes, abc

[b]Standard deviation = 0.0006.

for radicals with fairly isotropic g-values and this indicates that there may be unresolved nuclear hyperfine interactions. The linewidth does not vary significantly with orientation.

Recent CNDO/2 calculations for the $S\dot{C}NH_2$ radical, which take into account the sulphur d-orbitals, predict the unpaired electron to be in a σ orbital (154) with small anisotropic nuclear hyperfine splittings and a doublet splitting of about 13G. Neither ^{33}S nor ^{13}C hyperfine splittings were detected but the average g-value for radical A is 2.008, which is reasonable for a radical in which the unpaired electron is in a σ orbital on a carbon atom adjacent to a sulphur atom. Any nuclear hyperfine splitting must be less than 5G.

6A.3.2 Radical B

The lines labelled B in Fig. 6.2 are present in both deuterated and undeuterated crystals but are always weaker in the deuterated compound when compared with the intensity of radical A. Several lines are present in this region and only in the a-b plane was it possible tofollow their position as the orientation of the crystal was varied and even in this plane the relationship of the lines to one another was not clear. The g-value of the major lines, B_1, ranges from 2.003 ± 0.002 to 2.044 ± 0.004 when the magnetic field is in the ab-plane and it seems probable that the species has a high unpaired spin density upon the sulphur atom. None of the lines appears to have resolved hyperfine splitting and when crystals were annealed by irradiating them with light from a mercury lamp the lines labelled B in Fig. 6.3 disappeared much more rapidly than the lines due to radical A.

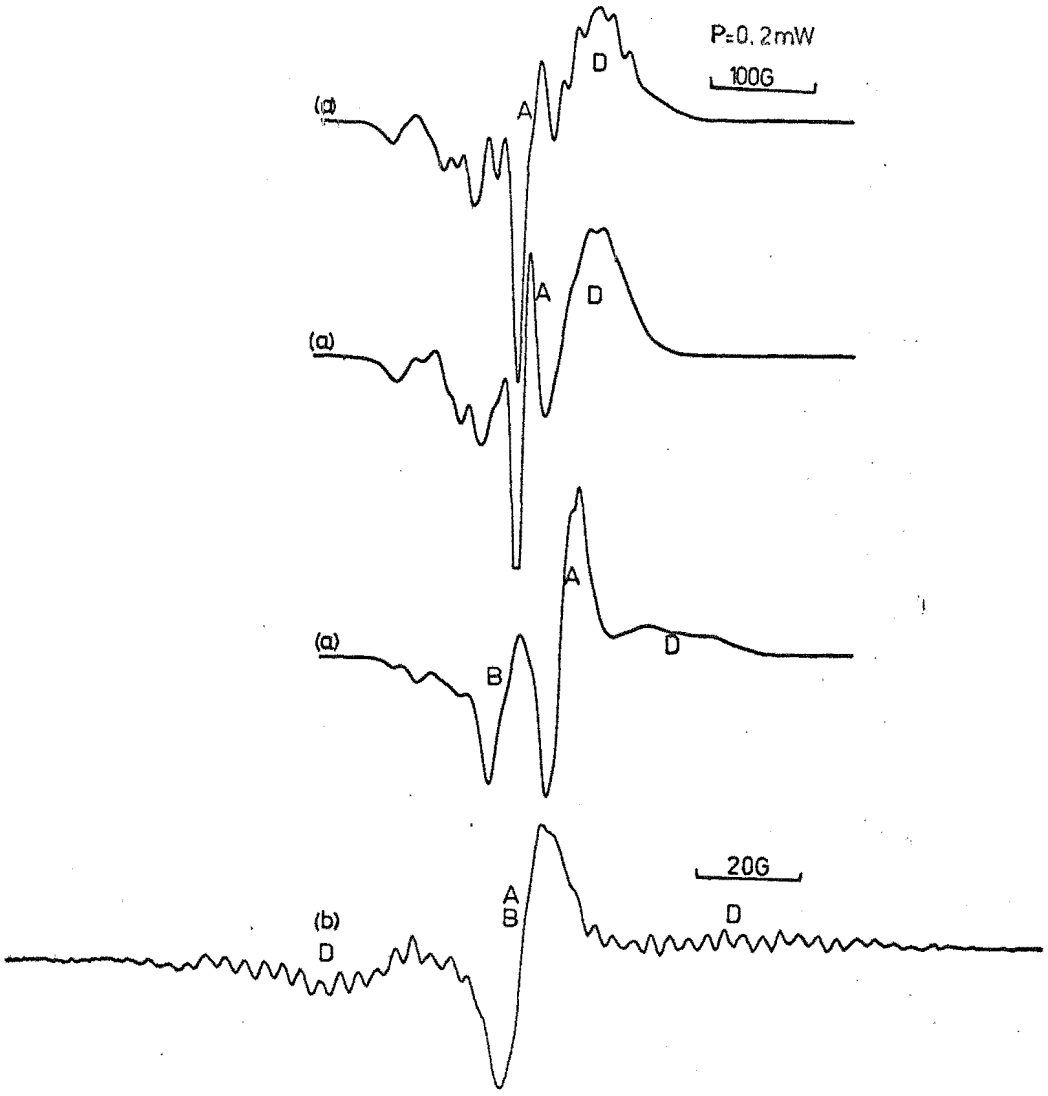

FIG 6.5 THIOSEMICARBAZIDE.HCL
(a) deuterated, (b) undeuterated

6A.3.3 Radical D

The esr spectrum assigned as arising from radical D was observed only in spectra taken within a few hours of x-irradiation at room temperature, and only at some orientations of the crystal in the magnetic field, namely when the magnetic field was along or near to the a-axis. No similar spectra were observed in deuterated crystals but a short lived species with fewer hyperfine lines and a similar g-value was observed (Fig. 6.5).

In the undeuterated crystals the esr spectrum of radical D was composed of at least 48 resolved lines approximately equally spaced, 1.8G wide, and 3.0G-4.0G apart. Because these spectra were always superimposed on spectra due to other species it was not possible to accurately determine the relative intensities of such lines. The fact that the spectra were observable only at a few orientations indicates that lines overlap considerably. The observation that lines are approximately equally spaced with the same spacing at all orientations is not regarded as significant in view of the few orientations at which resolved lines were observed. It was not possible to determine the number of magnetically inequivalent D radicals in the unit cell but the overlap of lines at most orientations indicates that there were more than one and it is probable that there are four inequivalent sites in the general orientation as expected for the crystal symmetry. The g-value appeared to be reasonably isotropic at $g = 2.003 \pm 0.002$.

In crystals of deuterium substituted thiosemicarbazide deuterochloride no such species was observed, but a radical with an isotropic g-value of 2.003 ± 0.002 and a hyperfine structure which varied markedly with orientation was observed. The equality of the g-tensors and the similarity in stability

of the radical to radical D leaves little doubt that it is the deuterated equivalent of radical D. The maximum width of this spectrum is 100G compared with about 170G for the undeuterated species. This width is greater than that observed for the radical produced in thiosemicarbazide but compares qhite well with the total width of the spectrum of $\cdot NHNH_3^+$ observed in semicarbazide hydrochloride (108). Radical D may be attributed to a species containing nitrogen and hydrogen nuclei which interact with an unpaired electron which probably resides primarily on a nitrogen atom. The isotropic g-factor shows that there is very little spin density on sulphur or chlorine atoms which have large spin-orbit coupling constants. If radical A is indeed $S\dot{C}NH_2$, then radical D is likely to be the $\cdot NHNH_3^+$ radical, similar to that observed in semicarbazide hydrochloride, although much less stable.

6A.3.4 Radical C

The lines labelled C clearly arise from a species which interacts with a single nucleus with $I = \frac{3}{2}$ since there are four equally intense, widely spaced groups of lines. Each of these lines is further split into five lines with relative intensities 1:2:3:2:1 which arises from a hyperfine interaction with two equivalent nuclei of nuclear spin, I = 1.

It was originally thought that this spectrum arose from a species containing one chlorine and two equivalent nitrogen nuclei but all attempts to find lines due to ^{37}Cl which has a natural abundance of 24.6% and which has a nuclear magnetic moment of 0.68330 nuclear magnetons, compared with 0.82091 nuclear magnetons for the ^{35}Cl nucleus were unsuccessful. The expected weaker lines falling within the ^{35}Cl spectrum were not present. The high g-value and the presence of weak lines just

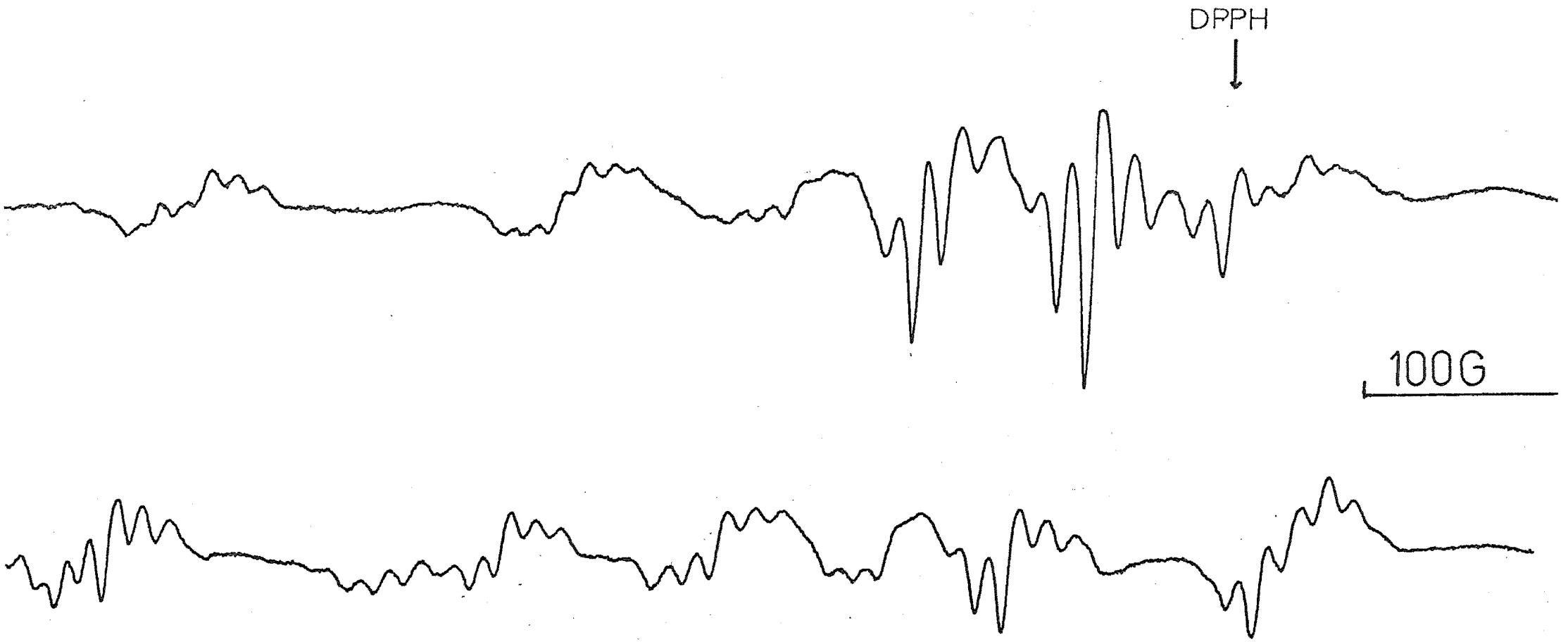

FIG. 6.6 Unirradiated crystal of Thiosemicarbazide. HCl.

outside the main spectrum (Fig. 6.2) suggested that the $I = \frac{3}{2}$ nucleus was copper and the subsequent observation of this species in unirradiated crystals (Fig. 6.6) confirmed that it is indeed a paramagnetic impurity. Copper has two naturally occurring isotopes with $I = \frac{3}{2}$, ^{63}Cu (μ = 2.2206 nuclear magnetons, 69.09% abundant) and ^{65}Cu (μ = 2.3790 nuclear magnetons, 30.91% abundant), which explains the weaker lines frequently observed at the low field end of the $M_I = -\frac{3}{2}$ nuclear hyperfine line. The copper impurity is apparently introduced from the hydrochloric acid, and the ambiguity arose because preliminary checks showed no such signals in unirradiated crystals. Crystals prepared from one source of hydrochloric acid always showed the copper spectrum. The signals of species A, B and D were not changed by the presence of the copper impurity.

The quadrupole interaction was neglected in the analysis of the spectrum of C because although weak 'forbidden' transitions were observed at some orientations and although the hyperfine splitting was slightly different for different lines, the great sensitivity of the spectrum to orientation meant that further refinement was not justified. The nuclear Zeeman interaction is negligible, and tensors calculated with this term included in the Hamiltonian were not significantly different from tensors that were obtained by neglecting it.

The calculated g- and nuclear hyperfine parameters are given in Table 6.2. There are four magnetically inequivalent species in the general orientation but this number reduces to one when the magnetic field is along the crystal axes and to two in any plane containing two of the crystal axes. This symmetry indicates that the crystal is orthorhombic and that

TABLE 6.2

bis(Thiosemicarbazide) Copper (II) Chloride

	Principal Value[b]	Direction Cosine[a]		
g	2.1561	0.852	0.455	0.254
	2.0545	-0.498	0.563	0.659
	2.0256	0.156	-0.688	0.707
A_{63Cu}	181.1	0.881	0.435	0.184
	56.5	-0.374	0.402	0.834
	32.2	0.288	-0.804	0.518

[a]Relative to laboratory axes, abc.

[b]Standard deviation = 0.003 for g-tensor

2.5G for A-tensor

the crystal axes are identical to the axes used to determine the tensors. The spectra obtained when the magnetic field was in the bc-plane were less accurately analysed as the lines of the spectrum overlapped a great deal. This caused quite large errors in the direction cosines corresponding to the two smaller principal values of the g-tensor. For this reason the standard deviation of the calculated g-value is as high as 0.003.

The results are in substantial agreement with those of Suntsov et al. (155) for powdered crystals of bis(thiosemicarbazide)nickel(II) chloride doped with cupric ions. They obtained values of

$g_{\parallel} = 2.129$ $\quad$ $g_{\perp} = 2.027$

$A_{\parallel}^{Cu} = 180G$ $\quad$ $A_{\perp}^{Cu} = 45G$

$A_{iso}^{N} = 12G$

from powder spectra, assuming axial symmetry. The tensors of Table 6.2 are not cylindrically symmetrical but in all other respects the results agree with the powder analysis to within experimental error. There is therefore no doubt that the spectrum is due to bis(thiosemicarbazide)copper(II) chloride.

The parallel components of the g-tensor and the copper hyperfine tensor are in the same direction but the perpendicular components of the two tensors are in slightly different directions, with an angle between g_{min} and A_{min}^{Cu} of 15^{o}. This difference is not regarded as highly significant in view of the experimental errors. Most studies of copper complexes with organic ligands have either assumed coincident principal axes of the g- and copper hyperfine tensors or have found them to be coincident (156,157). An exception is Copper(II) bis(n-butyldiselenocarbamate) (158,159) where the principal

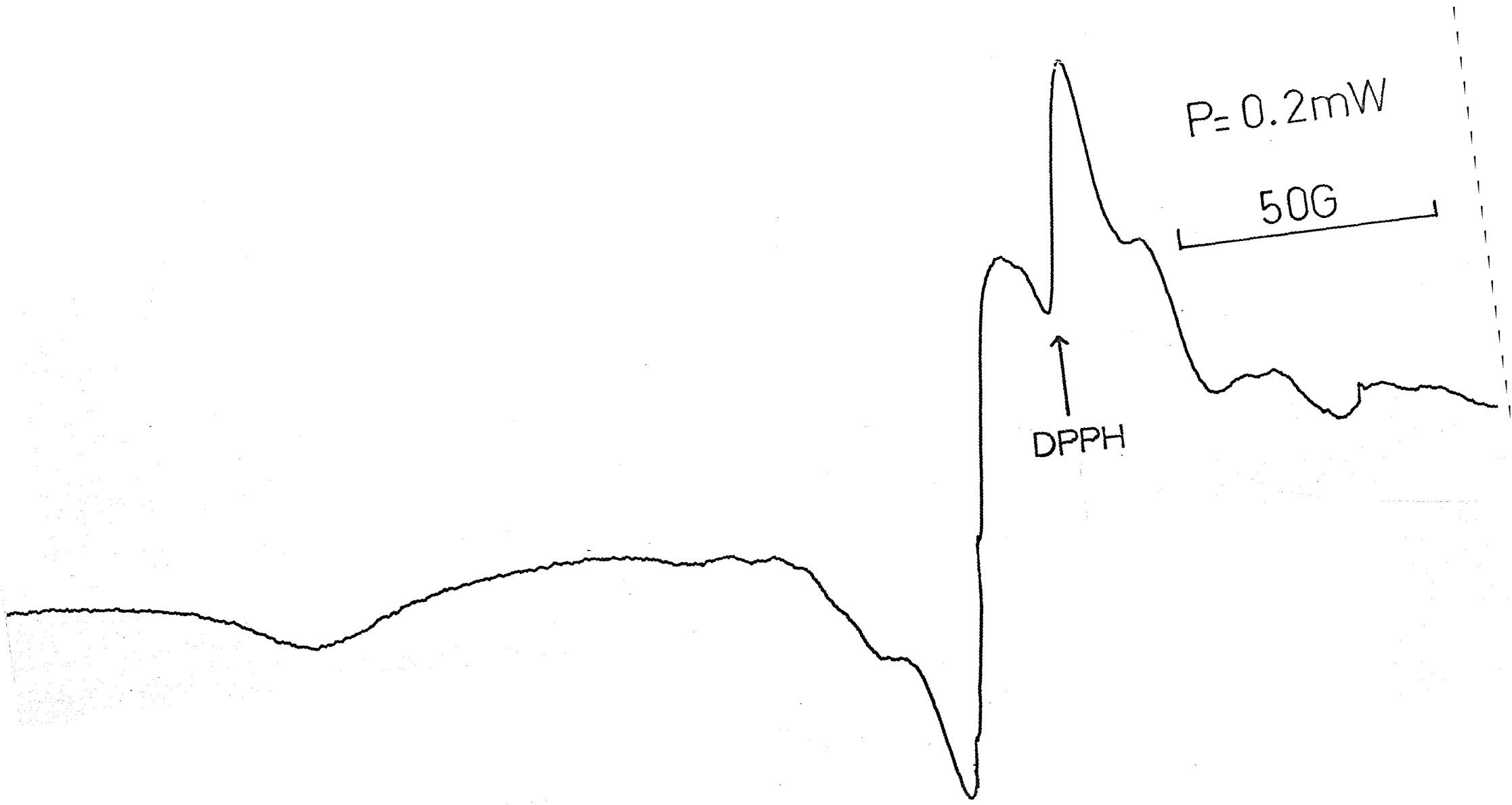

FIG 6.7 Thiosemicarbazide HBr.

axes of the parallel components were coincident but where the other principal axes of the g- and copper hyperfine tensors differed by an angle of 45°. No satisfactory explanation of this difference was advanced. Since the g-tensor reflects the symmetry of the excited electronic states as well as the ground state while the hyperfine interaction is dependent upon the dipolar interaction of the electron spin with the nuclear spin of the central copper atom, this difference in orientation may indicate a difference between the symmetries of the ground and excited electronic states. The lifting of the axial symmetry of the tensors is indicative of a difference in the copper-nitrogen and copper-sulphur bonds.

B THIOSEMICARBAZIDE HYDROBROMIDE

Crystals of thiosemicarbazide hydrobromide were very similar to crystals of the hydrochloride as were x-ray powder photographs of the two, although the separation of the powder lines was slightly greater in the hydrochloride indicating that the crystal axes were slightly shorter. This is consistent with results obtained for similar systems (160,161,162) where axes of the bromine analogue are normally about 2% longer than axes of the chlorine analogue.

Upon x-irradiation at room temperature, crystals became brown, but the esr spectrum consisted of several weak, broad and poorly resolved lines (Fig. 6.7) centred at g ~ 2.00 which could not be satisfactorily analysed but which did not appear to be the same as the lines observed in the hydrochloride.

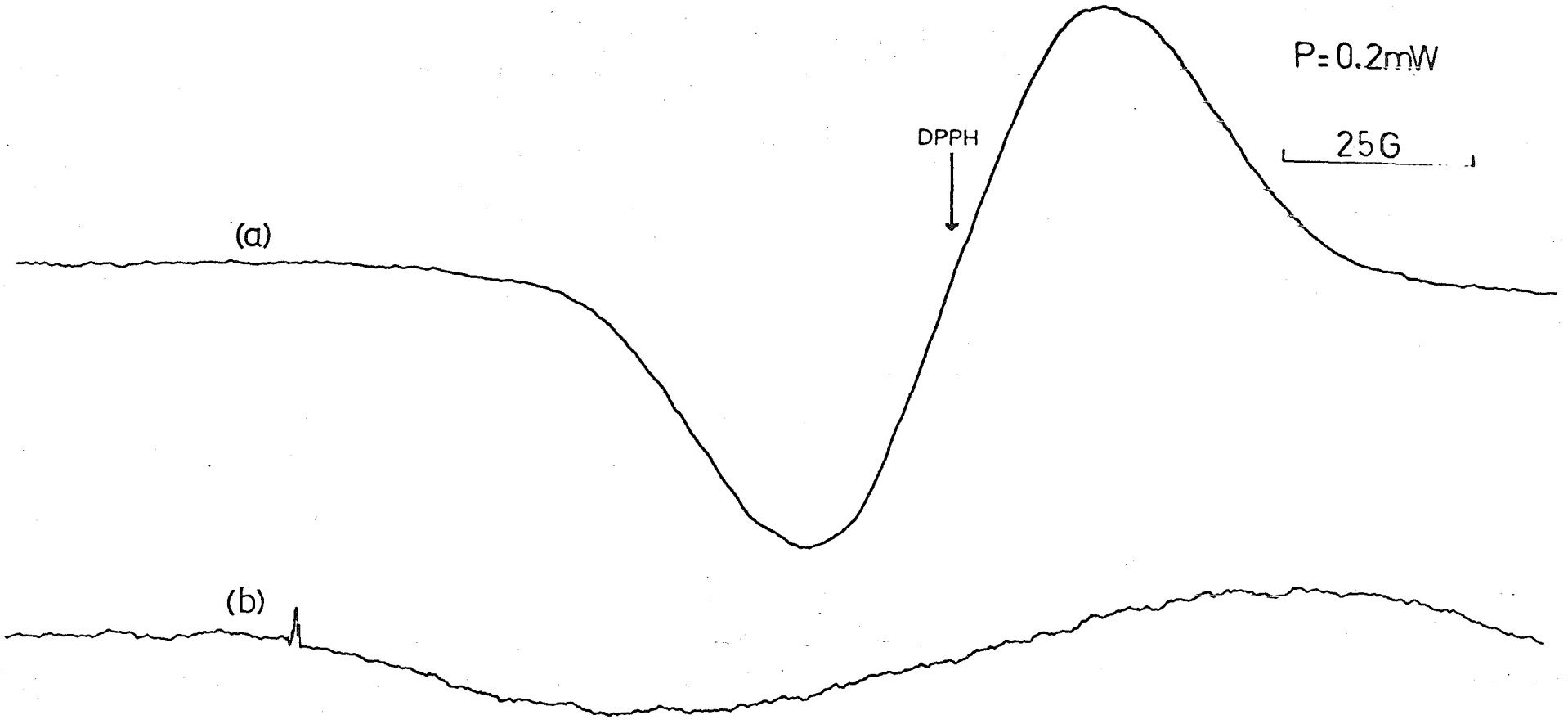

FIG 6.8 Semicarbazide HBr.

C SEMICARBAZIDE HYDROBROMIDE

Crystals of semicarbazide hydrobromide are long and needle-like whereas those of the hydrochloride are broader and well suited to esr studies. Semicarbazide hydrobromide is orthorhombic (167) and isomorphous with the hydrochloride so that two magnetically inequivalent radicals are expected when the magnetic field is in a plane containing two of the crystal axes.

Upon x-irradiation at room temperature crystals gave an esr spectrum which consisted of a single broad line centred at $g \sim 2.004 \pm 0.002$. The width of this line varied from 50G to at least 160G as the orientation of the crystal in the magnetic field was altered, but no resolved structure was observed at any orientation (Fig. 6.8), even at 120°K. The great variation in linewidth, which is similar to the variation of the total width of the spectrum observed for semicarbazide hydrochloride, indicates that there are several anisotropic nuclear hyperfine interactions. It is probable that the radical is similar to that produced in the hydrochloride although individual lines of the spectrum appear to be broader in the hydrobromide which suggests that the halide ion may be involved in the spin-relaxation mechanism.

D 3-PHENYL THIOSEMICARBAZIDE

Crystals of 3-phenyl thiosemicarbazide upon x-irradiation at room temperature gave esr spectra (Fig. 6.9) that were symmetrical about their centres at most orientations. In some orientations well resolved lines were observed but it was not possible to follow the variation in line positions over a

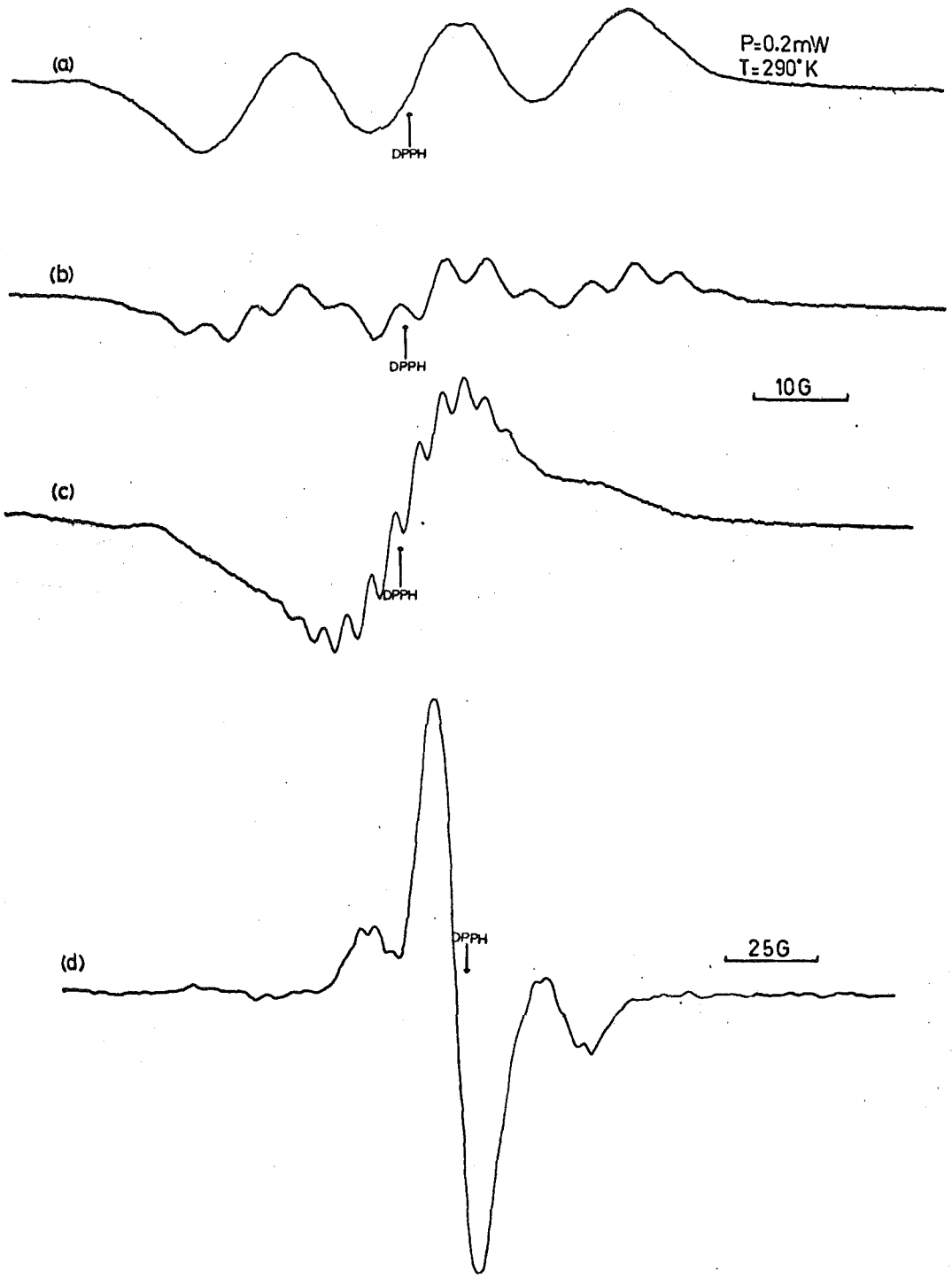

FIG 6.9 3-PHENYL THIOSEMICARBAZIDE

complete rotation of the crystal about an axis. Crystals were thin plates shaped similarly to crystals of thiosemicarbazide hydrochloride (Fig. 6.1). Axes were assigned in a similar manner.

The g-value is approximately isotropic and near g ~ 2.003. In several orientations three broad lines of equal intensity are observed with a maximum spacing of about 28G. The spectrum also reduces to a single broad line which shows that this triplet spacing is very anisotropic. It appears probable that the triplet arises from a nitrogen atom upon which the unpaired electron is located as in the radical observed in thiosemicarbazide. The triplet splitting is the only large hyperfine splitting observed at any orientation and although in many orientations further splittings are observed, these are always less than 14G. This clearly indicates that the radical has no alpha hydrogen since this would have a maximum hyperfine splitting of at least 20G and probably nearer 30G. It seems from these results that the radical is

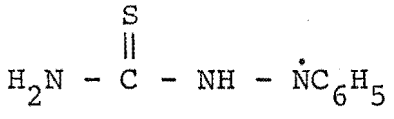

with the unpaired electron in a π-orbital on the nitrogen atom, N_3. This radical is similar to the radical observed in thiosemicarbazide. The spectrum is complicated by the presence of two magnetically inequivalent radicals at most orientations. These are clearly shown in Fig. 6.9d. No significant gain in resolution was apparent when spectra were obtained at 120°K.

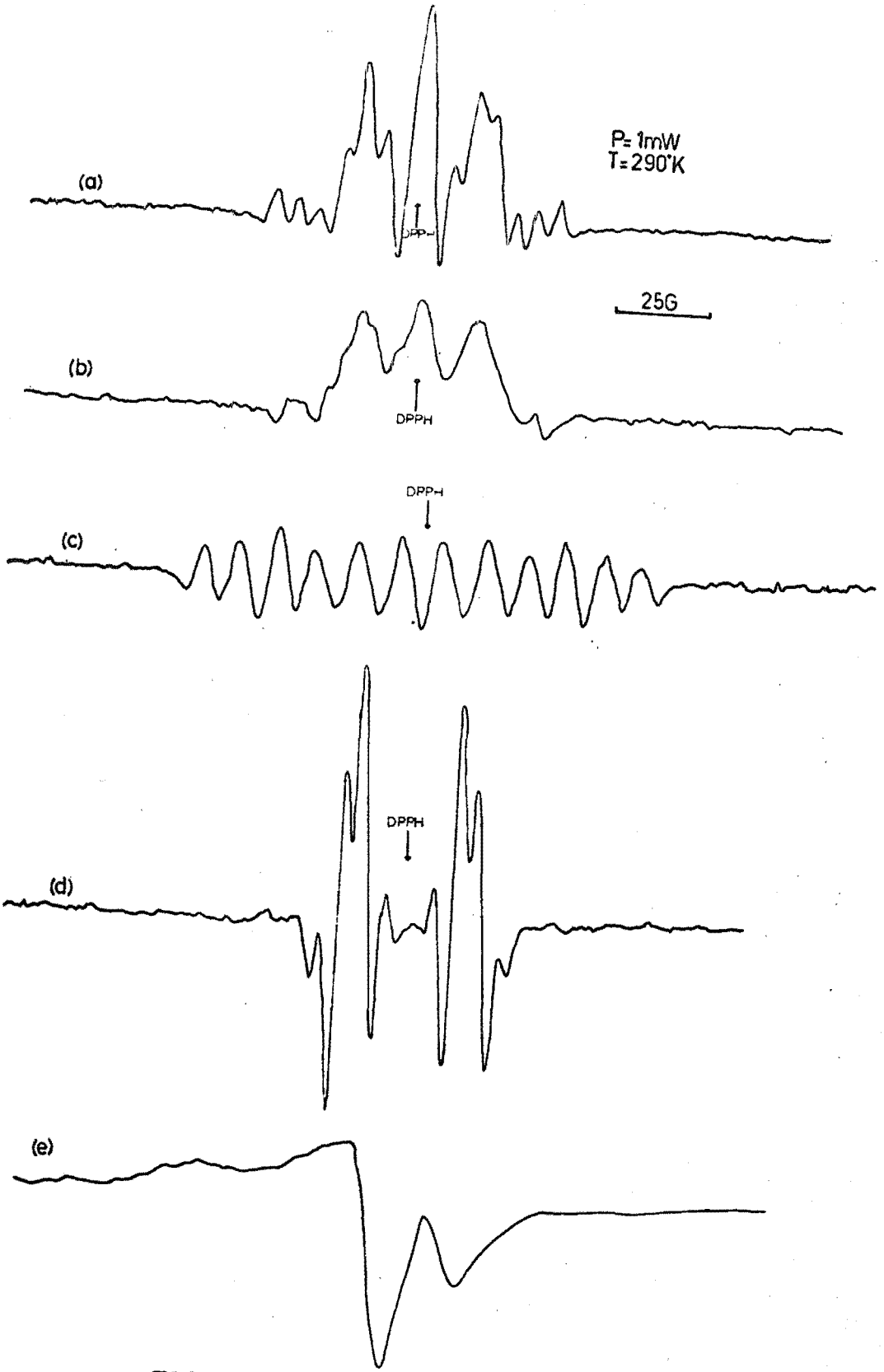

FIG 6.10 CARBAZIDE
a-d: second derivative
e : first derivative

E CARBAZIDE

Crystals of carbazide became white and opaque upon x-irradiation at room temperature and gave orientation dependent esr signals, which were not very stable. It seems likely that crystals are mechanically damaged by irradiation. In many cases there were no esr signals in freshly irradiated crystals and in others the signals were suddenly lost, sometimes being replaced by weak powderlike isotropic signals (Fig. 6.10e). It is concluded that the irradiated crystals are susceptible to mechanical shock which causes loss of the crystalline order. In spite of this peculiarity many normal spectra were obtained. These were generally complex and often symmetric about the centre of the spectrum which was at g ~ 2.003 ± 0.003. Two doublets were clear at some orientations (Fig. 6.10d), one with a hyperfine spacing of about 27G and one about 7G. A triplet of equally intense lines about 12G apart was sometimes observed (Fig. 6.10b) and in other orientations three equally intense lines about 5G apart were to be seen at the ends of the spectrum (Fig. 6.10a).

During the course of this project, results were published describing the formation of triplet species in carbazide irradiated at 77°K (109). A singlet species was observed which is apparently the same as that observed upon room temperature irradiation, although the spectrum could not be fully analysed. These published results and the results obtained here both indicate the formation of $NH_2NHCONHNH\cdot$ radicals which have the unpaired electron in a π-orbital on a terminal nitrogen atom.

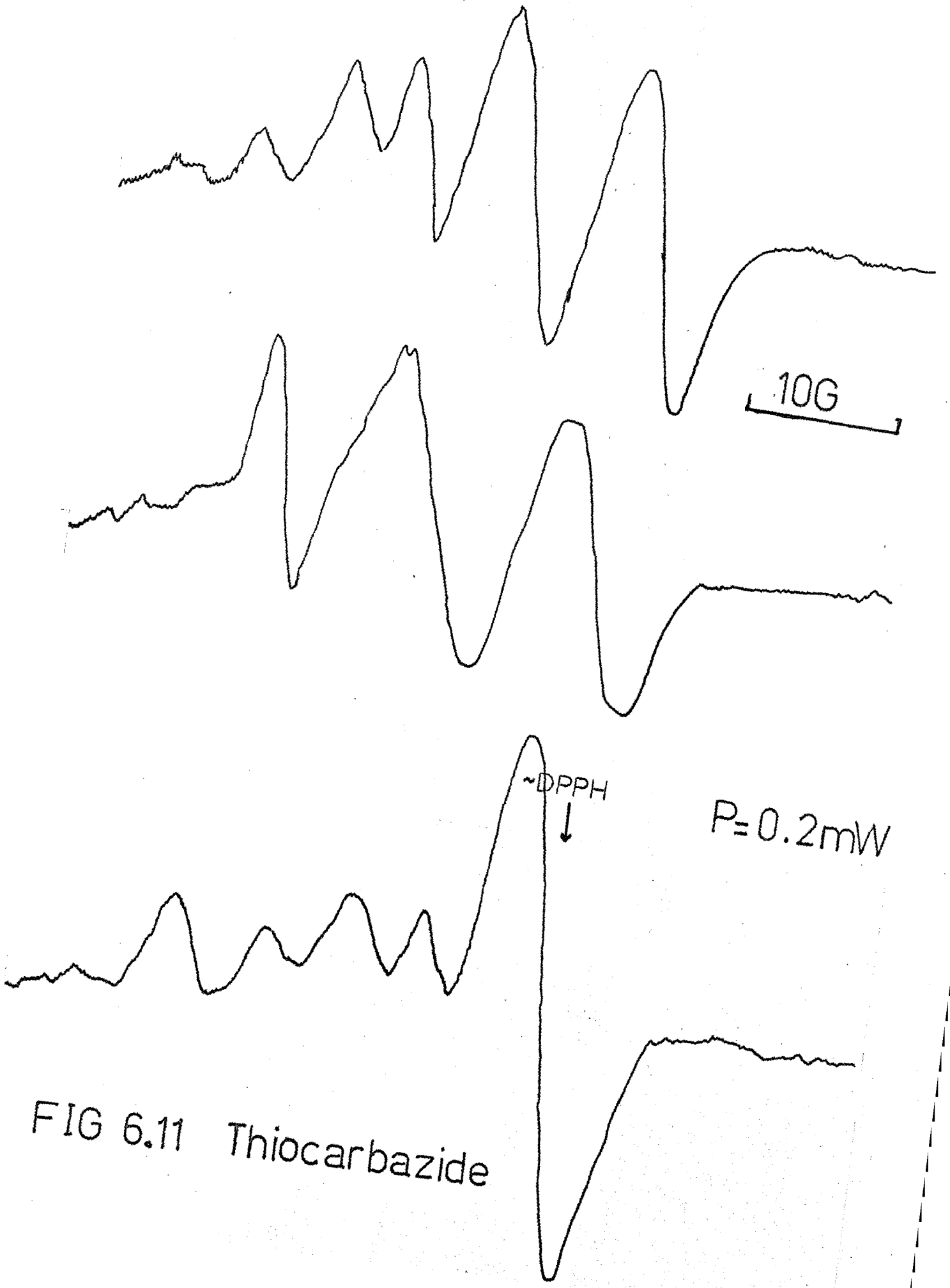

FIG 6.11 Thiocarbazide

The maximum width of the spectrum is 114G and there are at least twelve distinct lines apparent although these are not of equal intensity. Simulation of these lines gave an approximate intensity ratio of 1:2:3:3:4:5:5:4:3:3:2:1 which is consistent with interactions of two nitrogen and two hydrogen nuclei. The maximum width is consistent with that expected for the assigned radical.

F THIOCARBAZIDE

Large crystals of thiocarbazide could not be grown but x-irradiation of small crystals showed the presence of orientation dependent esr signals (Fig. 6.11) that must arise from at least two species, neither of which seems to be a nitrogen radical. The most intense signal is a singlet near $g \sim 2.00$ although two sites are apparent as predicted for the space group $P2_1/c$ (122). Crystals become green upon irradiation.

G THIOCARBAZIDE HYDROCHLORIDE

Large crystals of this compound (168) showed no evidence of damage upon x-irradiation at room temperature. The presence of molecules of water of crystallisation is likely to lead to rapid decay of radicals by intermolecular transfer of hydrogen.

CHAPTER 7

SUMMARY OF RESULTS AND CONCLUSIONS

As was discussed in section 1.4, the intention of this project was to study the effect of ionising radiation upon unsaturated carbon-sulphur bonds with a view to determining the structure of radicals produced and the reaction sequence leading to their formation, and also to clarify the structures of nitrogen centred radicals.

From the general sequence of events in irradiated organic compounds (section 1.1) it is known that the primary products of irradiation will be cations and anions formed by loss or gain of an electron by the irradiated molecule. Both of these species have been observed in irradiated thioureas (7) but were found to decay at temperatures below 77°K. The analogous species were therefore not expected to be observed at the temperatures available for this project, except perhaps in the case of sodium diethyldithiocarbamate where the unpaired electron might be delocalised over the SSCN group, which would stabilise the radicals. Indeed no such species were observed in thioacetamide or thiosemicarbazide crystals or in any of their derivatives. Reiss and Gordy (109) found no evidence of ionic species in carbazide crystals γ-irradiated and observed at 77°K, although they did observe radical pairs. Signals attributed to ionic species have been observed in O-methyl-isouronium chloride, $[CH_3OC(NH_2)_2]Cl$ (107), at 77°K but not in urea (105). The acetamide anion, formed in irradiated glasses, was found to be stable at temperatures as high as 180°K (85). This has an unpaired spin density of 0.23 on the oxygen atom

and of 0.69 on the central carbon atom and there are well resolved hyperfine interactions with the methyl protons. In general sulphur compounds have more delocalised molecular orbitals than do the comparable oxygen compounds (163, page 406) and for this reason ionic species are expected to be more stable. It appears however that they decay at temperatures below 110°K even in compounds with molecular orbitals extending over four atoms, as in thiosemicarbazide.

In irradiated organic sulphur compounds where ionic radicals have been observed, the relative stabilities of the cation and the anion vary, depending upon the orbital in which the unpaired electron is located. In disulphides the anion is generally stabler (3, 8, 29) whereas only the cation was observed in DL-methionine (132).

The results for sodium diethyldithiocarbamate irradiated at 105°K suggest that a radical is formed by loss of an electron from a non-bonding sp^2-hybridised orbital on one of the sulphur atoms. This species, labelled B in Table 4.4, has no observable nuclear hyperfine structure and the principal values of the g-tensor are in accord with those anticipated for such a structure. Another, slightly stabler species is formed at the same time. The very great anisotropy of the g-value for this species, labelled A in Table 4.4, indicates that the nearest excited electronic level is unusually close to the ground state electronic level, but the lack of axial symmetry shows that the two levels are not degenerate.

The electronic spectrum of the parent molecule shows that the lowest energy electronic transition is $n \rightarrow \Pi^*$ at 29000 cm^{-1}, and that there are two $\Pi \rightarrow \Pi^*$ transitions corresponding to absorptions at about 35000 cm^{-1} and 40000 cm^{-1}. These latter

transitions are located mainly on the CSS group, (141,169). These assignments indicate that the unpaired electron will be in a non-bonding orbital for the electron deficient radical and in a Π^* orbital for the radical containing an additional electron.

The hyperfine interaction of radical A can only be accounted for by assuming that a hydrogen atom has attached to one of the sulphur atoms. Attachment to the carbon atom would result in a greater distortion from the symmetry of the undamaged molecule than is observed. The isotropy of the hyperfine coupling indicates that the unpaired electron is located in an orbital centred on the other sulphur atom and not close to the hydrogen atom. It is possible that this species is formed by transfer of a hydrogen ion from a water molecule to the primary anion. If this is the case then irradiation at lower temperatures should result in observation of the primary anion. These processes are described by the reaction sequence:

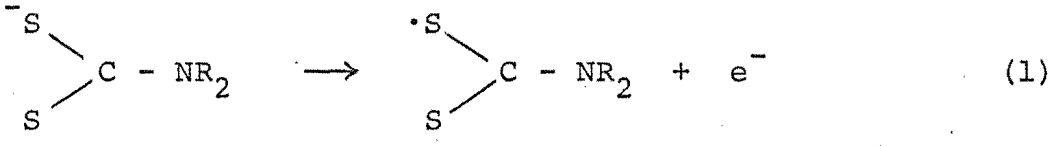

(1)

[radical B]

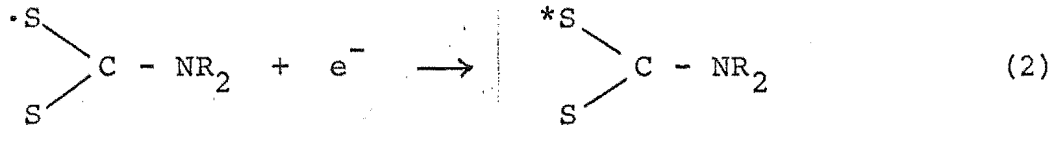

(2)

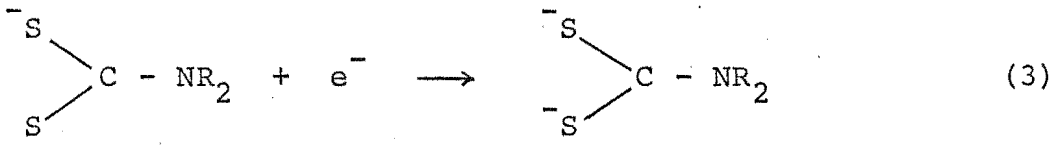

(3)

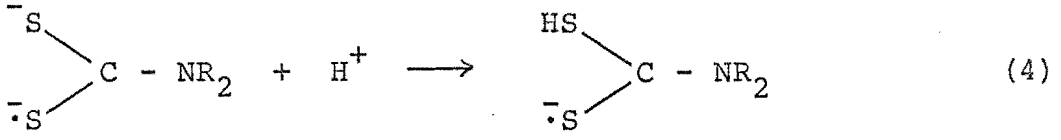

(4)

[radical A?]

The species formed upon low temperature irradiation must decay by recombination, since no new species were observed as the temperature was raised.

A radical has been observed in chloroform solutions of Cr(II) and Ag(II) diethyldithiocarbamate complexes (170,171). Both cations are unstable and apparently reduce the ligand. The radical has a g-value of 2.040 and there is a hyperfine splitting of 12.5G, or 11.6G depending upon which cation is present, due to one nitrogen atom. The radical has been assigned as $(CH_3)_2NCSS\cdot$ although it is more likely to be $(C_2H_5)_2NCSS^{\overline{\cdot}}$, formed by addition of an electron to the anion. This must be formed in analogous manner to reaction (3) above.

The radicals formed upon room temperature irradiation all appear to have the unpaired electron on a sulphur atom, except for radical E which is probably

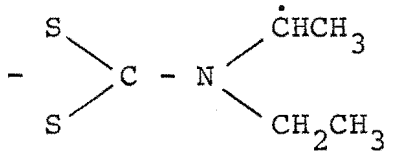

In studies of irradiated amines it has been observed that a hydrogen is generally lost from a carbon atom adjacent to the nitrogen atom (45,106), and the small nitrogen hyperfine coupling supports this assignment. The isotropic hyperfine coupling of the alpha hydrogen is unexplained. Possible modes of formation are:

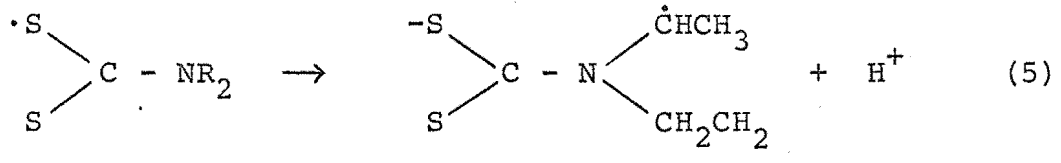

(5)

or

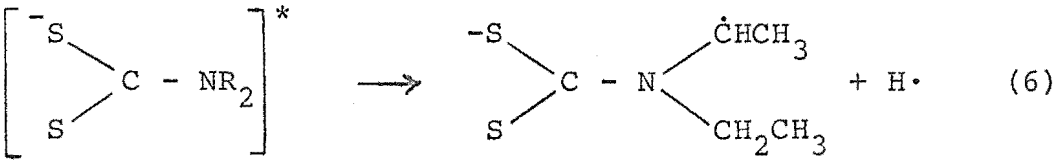

(6)

Formation of CS_2^- and $\cdot N(CH_2CH_3)_2$ is not expected because of the high double bond character of the carbon-nitrogen bond, and these species were not observed.

The other radicals are not satisfactorily explained and it is difficult to account for the orientations of the principal axes of the g-tensor. Many of the weak lines could have a similar origin to those observed by Hahn and Rexroad (25) in irradiated crystals of mercaptosuccinic acid. These appeared to follow the lines due to the thiol radical and to be about one quarter to one sixth as intense as these lines, but no explanation could be found for them. Radical C, the major radical, (Table 4.3), is probably a thiol radical with the unpaired electron in a sulphur p-orbital. It appears that at least one carbon-sulphur bond direction has changed orientation considerably and it is likely that the carbon atom has assumed a tetrahedral configuration following attachment of another species, to form a radical like:

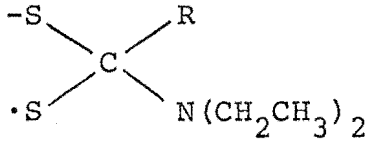

Irradiation of thiosemicarbazide results in the formation of an RNH· π-radical of which few examples have been observed in single crystals, although several have been hypothesised. Normally such radicals, if formed in the presence of carbon-hydrogen bonds, rapidly abstract a hydrogen atom from the carbon atom, with the production of an alkyl radical (71). In such systems low temperatures are required to stabilise the

TABLE 7.1

Crystallographic Bond Lengths (Å)

	C-O	C-S	C-N_1[a]	C-N_2[a]	N_2-N_3[a]	ref.
Urea	1.262		1.335			177
Thiourea		1.713	1.329			175
Thiosemicarbazide		1.707	1.316	1.326	1.411	143
Semicarbazide.HCl	1.238		1.311	1.382	1.411	153
Thiocarbazide		1.724		1.315,1.335	1.405	122
Carbazide	1.242			1.349	1.416	176
Thiocarbazide.2HCl		1.645		1.363	1.418	168
Acetamide	1.250,1.271		1.351,1.317			174
Thioacetamide		1.710	1.324			134
Single bond	1.42	1.81	1.48		1.46	163
Double bond	1.20	1.60	1.24			163

[a]Numbering System: $N_1CSN_2N_3$

nitrogen radicals (172). The semicarbazide series of compounds have no carbon-hydrogen bonds and are therefore ideal for stabilising nitrogen radicals of this type.

There is, however, a remarkable lack of uniformity in the products of irradiated semicarbazides. Semicarbazide hydrochloride (108) forms the $\cdot NHNH_3^+$ radical as apparently does the hydrobromide. Thiosemicarbazide hydrochloride appears to form a similar radical which is however, less stable. Thiosemicarbazide loses a hydrogen atom, as does carbazide, to produce a RNHNH· radical and 3-phenyl thiosemicarbazide forms a similar radical. Thiocarbazide forms no such stable radical, although the $NH_2\dot{N}HCS$ σ-radical may be formed, and thiocarbazide hydrochloride forms no stable radicals at all. Nitrogen radicals have been observed in urea (105) at 77°K and possibly in thiourea (154).

Such differences can however by explained in terms of differences in bond strengths. Crystal structures have been determined for many of these compounds. Some of the bond lengths are tabulated in Table 7.1.

Comparison of the bond lengths in thiocarbazide and in thiocarbazide hydrochloride shows that the cation has a shorter carbon-sulphur bond and longer carbon-nitrogen bonds, indicating less delocalisation of the double bond. The $C-N_2$ bond in semicarbazide hydrochloride is much longer than the comparable bond for other compounds. The weakness of this bond is consistent with its cleavage upon irradiation. The equivalent bond in thiosemicarbazide hydrochloride is similarly expected to be much weaker than in thiosemicarbazide. This conclusion is in agreement with the assignment of the species formed upon irradiation of the hydrochloride, to the radicals

formed by cleavage of the C-N_2 bond. Cleavage of the C-N_1 bond in these compounds is unlikely to occur because of its greater bond strength, when compared with that of the C-N_2 bond. Thus the esr and crystallographic results are entirely consistent with one another.

It is only in recent years that hydrogen atoms have been located by x-ray crystallographic methods and some of the published results may not be very accurate. Published nitrogen-hydrogen bond lengths range from 0.83Å to well over 1.0Å. For thiosemicarbazide (143) the NH bond lengths are given below.

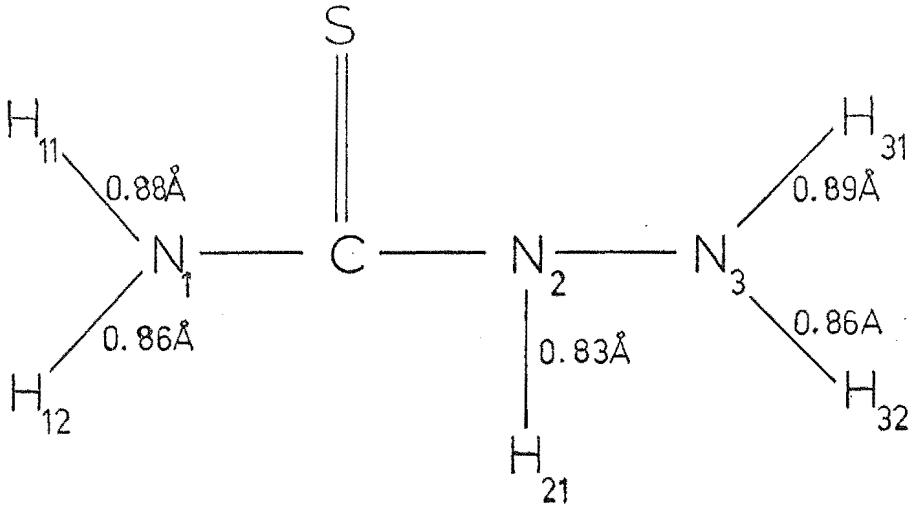

The relative bond lengths are quite accurate although the absolute values may be in error by as much as 0.08Å. It is seen that the N_2H_{21} bond is strongest and that there is a slight difference between the bond lengths of the terminal nitrogen-hydrogen bonds. These results indicate the radical formed upon irradiation is determined by the bond strengths in the molecule. Although accurate bond dissociation energies are known for only a few organic nitrogen compounds (47,48) it is generally

observed that the nitrogen-hydrogen single bond dissociation energy is higher than that of the carbon-nitrogen single bond which is in turn higher than the bond dissociation energy of the nitrogen-nitrogen single bond. Thus the energetically favoured irradiation process is expected to be cleavage of the nitrogen-nitrogen bond. No examples of this have been reported and even in hydrazine, where the bond dissociation energies differ by 5 $kJ.mole^{-1}$, the $NH_2NH\cdot$ radical is produced (173) rather than $\cdot NH_2$ radicals. It is likely that $\cdot NH_2$ radicals and $NH_2CONH\cdot$ radicals would rapidly abstract hydrogen from a terminal nitrogen of the parent molecule to produce the observed products. On the other hand cleavage of a carbon-nitrogen bond is likely to produce two reasonably stable species: $\cdot NHNH_2$ and $NH_2CO\cdot$. The rapid decay of $NH_2CO\cdot$ in semicarbazide hydrochloride is surprising in view of its observed stability in other systems (86, 105, 133).

A possible scheme for radiation damage in these systems is:

$$NH_2CSNHNH_2 \overset{\sim}{\longrightarrow} NH_2CSNHNH_2^+ + e \qquad (7)$$

$$NH_2CSNHNH_2^+ + e \longrightarrow NH_2CSNHNH_2^* \qquad (8)$$

$$NH_2CSNHNH_2 + e \longrightarrow NH_2CSNHNH_2^- \qquad (9)$$

The observed species may be formed from each of these precursors.

$$NH_2CSNHNH_2^+ \longrightarrow NH_2CSNHNH\cdot + H^+ \qquad (10)$$

$$NH_2CSNHNH_2^* \longrightarrow NH_2CSNHNH\cdot + H\cdot \qquad (11)$$

$$NH_2CSNHNH_2 + H\cdot \longrightarrow NH_2CSNHNH\cdot + H_2 \qquad (12)$$

$$NH_2CSNHNH_2^- \longrightarrow NH_2CSNH\cdot + NH_2^- \qquad (13)$$

$$NH_2CSNH\cdot + NH_2CSNHNH_2 \longrightarrow NH_2CSNH_2 + NH_2CSNHNH\cdot \quad (14)$$

$$NH_2^- + H^+ \longrightarrow NH_3 \quad (15)$$

In each case the alternative radical, $\cdot NHCSNHNH_2$, could be formed in the same way. Since cleavage of a nitrogen-nitrogen bond has never been observed upon irradiation, reaction (13) appears to be a less probable mode of formation of nitrogen radicals. Reactions analogous to (10)-(12) are unlikely to occur in the hydrochloride because of the presence of the additional proton on the terminal nitrogen atom but reaction (13), involving loss of ammonia is more probable.

It appears however that an alternative sequence of reactions becomes important for the hydrochlorides. The cationic radical is much more likely to recombine with electrons as it is formally doubly charged.

$$NH_2CSNHNH_3^{++} + e \longrightarrow [NH_2CSNHNH_3^+]^* \quad (16)$$

$$[NH_2CSNHNH_3^+]^* \longrightarrow NH_2CS\cdot + \cdot NHNH_3^+ \quad (17)$$

$$[NH_2CSNHNH_3^+]^- \longrightarrow NH_2CS^- + \cdot NHNH_3^+ \quad (18)$$

$$[NH_2CSNHNH_3^+]^- \longrightarrow NH_2CS\cdot + NHNH_3 \quad (19)$$

$$NHNH_3 \longrightarrow NH_2NH_2 \quad (20)$$

$$NH_2CS^- \longrightarrow NCS^- + H_2 \quad (21)$$

The presence of a stable $\cdot NHNH_3^+$ radical in semicarbazide hydrochloride indicates that reactions (17) or (18) are important, and since $NH_2CO\cdot$, which is known to be quite stable, is not observed reaction (18) followed by rapid decay of NH_2CO^- seems more probable. In thiosemicarbazide hydrochloride,

on the other hand, the $NHNH_3^+$ radical is unstable and probably decays either by recombination or by capturing an electron to form hydrazine,

$$NH_2CS^- + \cdot NHNH_3^+ \longrightarrow NH_2CS\cdot + N_2H_4 \quad (22)$$

$$\cdot NHNH_3^+ + e \longrightarrow N_2H_4 \quad (23)$$

This is again consistent with radical formation by way of reaction (18) rather than (17) which produces two quite stable species which are likely to decay at a similar rate.

It therefore seems likely that decay of the anion leads to the observed radicals in the hydrochlorides while decay of the cation or of the electronically excited molecule leads to the observed radicals in the normal semicarbazides.

In thioacetamide no ionic species were observed. At low temperatures it seems likely that the $\cdot CH_2CSNH_2$ radical is produced but this decays by recombination at temperatures below room temperature possibly to form other species which become subject to further radiation damage.

The results of this project show that compounds containing unsaturated carbon-sulphur bonds are very resistant to permanent radiation damage, probably because simple recombination of the primary cations and anions is the favoured mode of decay. An exception to this rule occurs when the molecule can lose a hydrogen atom from an atom not adjacent to the thiocarbonyl group; thus large molecules are more likely to form stable radicals upon irradiation than are small molecules like thiourea or thioacetamide. The primary ions decay below 120°K and even in sodium diethyldithiocarbamate where a cation was observed, the primary anion has apparently undergone further reaction at temperatures below 120°K; and irradiation at room

temperature destroys the planarity and the π-structure of the molecule. Lower temperatures are therefore required to study the primary ions in unsaturated carbon-sulphur systems. Because of the difficulty in assigning structures to species where the unpaired electron is located on a sulphur atom it would be desirable to perform experiments on such compounds enriched with ^{33}S and ^{13}C. This should enable a more accurate estimate of the distribution of the unpaired electron in the radical than can be obtained from the g-value.

These studies have confirmed theories about the nature of nitrogen π-radicals. The radical observed in thiosemicarbazide is only the second radical of this type for which a complete set of tensors have been evaluated, and the radical is found to be substantially different from the other, which is $NHNH_3^+$. Radiation mechanisms have been deduced for the production of the observed radicals, based largely upon circumstantial evidence. Additional experiments at lower temperatures or product analysis of irradiated crystals are required to check these deductions.

APPENDIX 1

A. The g tensor

Consider a system of three orthogonal axes defined with respect to crystal faces. Let the unit vector along the magnetic field be $\bar{\eta} = (\ell,m,n)$ in this laboratory axis system (187-189).

Since $\bar{\bar{g}}$ is symmetric the value of g^2 along $\bar{\eta}$ is given by

$$g_e^2 = (\bar{\eta}.\bar{\bar{g}})\,(\bar{\bar{g}}.\eta)$$

$$= \bar{\eta}.\bar{\bar{T}}.\bar{\eta}$$

where $\bar{\bar{T}}$ is the symmetric tensor $\bar{\bar{g}}^2$. It is possible to define (ℓ,m,n) in terms of two independent angles, θ and ϕ defined in the diagram below.

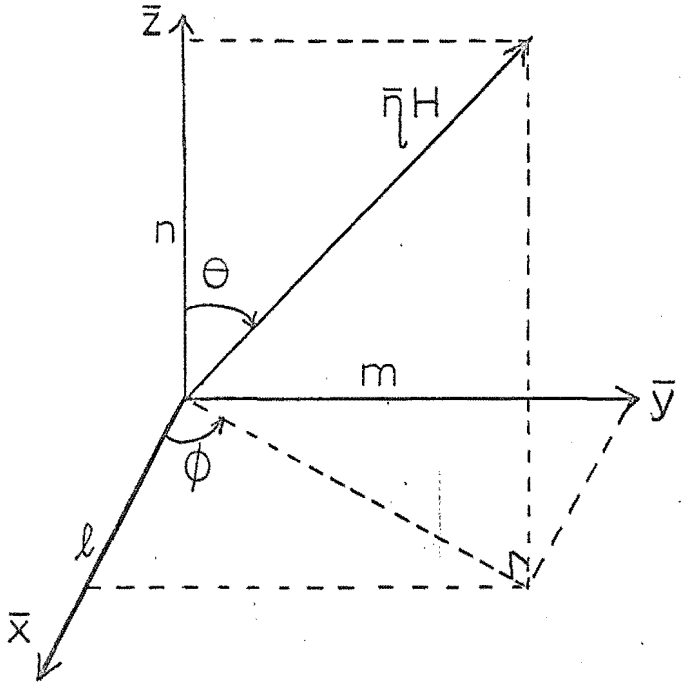

where $\ell = \sin\theta\cos\phi$

$m = \sin\theta\sin\phi$

$n = \cos\theta$

Thus:

$$g^2_{expt} = \sin^2\theta[T_{11}\cos^2\phi + 2T_{12}\sin\phi\cos\phi + T_{22}\sin^2\phi]$$

$$+ 2\sin\theta\cos\theta[T_{13}\cos\phi + T_{23}\sin\phi] + T_{33}\cos^2\theta$$

An exactly analogous equation may be used to calculate the elements of the square of the nuclear hyperfine tensor, $\bar{\bar{A}}$, if it is taken to be symmetric (173).

A least squares optimisation of the T_{ij} is performed and the T matrix is then diagonalised to yield principal values and axes. The principal values of the g tensor are the square roots of these principal values and the directions of the principal axes are the same for the g and T tensors. The g tensor may then be regenerated from the diagonal matrix and the matrix containing the direction cosines of the principal axes with respect to the laboratory axes.

B. Correction for Anisotropy of g

For the first order calculation of the hyperfine tensors, $\bar{\bar{A}}$, associated with each nucleus it is assumed that g is isotropic. The anisotropy of g causes the average direction of the aligned electron spin to differ from $\bar{H}$. The direction of the field effective on the nucleus in the case when the nuclear Zeeman term is negligible is given by:

$$\bar{k}_m = M \sum_{ijk} \left(\frac{g_{jk}A_{ij}}{g}\right) \eta_k \bar{U}_i$$

where: M is the eigenvalue of the projection $\bar{U}_s.\bar{S}$ along the axis of quantisation of the electron spin operator,

η_k is the direction cosine between $\bar{H}$ and the unit vector $\bar{U}_k$ along the k^{th} axis of an arbitrary Cartesian set

$$g = \{\sum_{j=1}^{3} (\sum_{k=1}^{3} g_{jk}\eta_k)^2\}^{\frac{1}{2}}$$

Thus the observed splitting between two hyperfine lines, d, is given by:

$$d^2 = \frac{(\bar{n}.\bar{\bar{g}}.\bar{\bar{A}})(\bar{\bar{A}}.\bar{\bar{g}}.\bar{n})}{g^2_{expt}} = \frac{\bar{n}.\bar{\bar{g}}.\bar{\bar{A}}^2.\bar{\bar{g}}.\bar{n}}{g^2_{expt}}$$

where $g^2_{expt} = \bar{n}.\bar{\bar{g}}.\bar{\bar{g}}.\bar{n}$.

When the elements of the g tensor are known, this equation is used to determine the elements of $\bar{\bar{A}}^2$ by a linear least squares fitting procedure. For thiosemicarbazide the effect was observed to change the elements of the hyperfine splitting tensor by about 0.01G. These calculations were performed by the computer program FOE.

Derivation of First Order ESR Tensors (FOE)

Purpose: This program calculates the first order g- and hyperfine tensors of free radicals in single crystals.

Contents: The main program, FOE, and subroutines DIAG, MATINV, and EIGEN.

Library Routines Used: SQRT, ABS, SIN, COS.

Language: IBM System/360 Fortran IV (BCD).

Method: This program uses input hyperfine splitting and orientation, or magnetic field, microwave frequency and orientation to determine the hyperfine or g-tensor by a linear least squares method. The tensor is then diagonalised to yield principal values and their direction cosines.

Each observation is weighted by the factor g^{-n} or A^{-n} where n is an input integer. For the g-tensor, the magnetic field at the centre of the spectrum is given as input and g is given by:

$$g^2_{expt} = (\bar{n}.\bar{\bar{g}})(\bar{\bar{g}}.\bar{n})$$

where $\bar{n}$ is the unit vector along the magnetic field. For the A-tensor the calculation is the same to a first approximation but if the effect of anisotropy in the g-tensor is included the observed splitting, d, is given by:

$$d^2 = \frac{(\bar{n}.\bar{\bar{g}}.\bar{\bar{A}})(\bar{\bar{A}}.\bar{\bar{g}}.\bar{n})}{g^2_{expt}}$$

Input:

Card No.	Columns	Fortran Symbol	Format	Contents
1	1-72	TITLE	18A4	Title of Calculation
2	1	INDEX	I1	=1 for g-tensor
				=2 for A-tensor
	2	IWGHT	I1	=0, no weighting
				=n, g^2 is weighted by g^{-n}

If INDEX = 2, the effect of anisotropy of the g-value may be incorporated into the calculation of the hyperfine tensor.

2A	1	IINDEX	I1	=2 if the anisotropic g-value is to be included
				=1 otherwise.

If IINDEX = 2,

2B	1-10	GINPUT(1)	F10.4	g_{11} or A_{11}
	11-20	GINPUT(2)	"	g_{12} or A_{12}
	21-30	GINPUT(3)	"	g_{13} or A_{13}
	31-40	GINPUT(4)	"	g_{22} or A_{22}
	41-50	GINPUT(5)	"	g_{23} or A_{23}
	51-60	GINPUT(6)	"	g_{33} or A_{33}

If INDEX = 1, Cards 2A and 2B are omitted.

If IINDEX = 1, Card 2B is omitted.

Card No.	Columns	Fortran Symbol	Format	Contents
3	1	IFILE	I1	blank
	2-10	H(I)	F9.3	If INDEX = 1, H is the magnetic field, in gauss. If INDEX = 2, H is the measured hyperfine splitting, in gauss.
	11-20	SHI(I)	F10.3	the azimuthal angle, ϕ, in degrees.
	21-30	SHETA(I)	F10.3	the polar angle, θ, in degrees.
	31-40	FR(I)	F10.5	the microwave frequency, in MHz.

There is one card of type 3 for each orientation. End of data is signified by a 1 in column 1.

Output:

(1) Title of calculation.

(2) Type of tensor, g or A.

(3) The tensor, T, to be diagonalised.

(4) The input data and the best fit value of A or g.

(5) The diagonalised T tensor.

(6) The direction cosines, stored row-wise.

(7) The principal values.

(8) The A or g tensor in laboratory coordinates.

(9) The isotropic and anisotropic components of A.

(10) The standard deviation in A_{expt} or g_{expt}.

Capacity: The capacity is limited only by the DIMENSION statements which are at present set to deal with a maximum of 250 observations.

Limitations: The program calculates only the first order A-tensor.

```
C
C     ********************************************************************
C
C     PROGRAM FOE - FIRST ORDER ESR ANALYSIS
C
C     ********************************************************************
C
C     PURPOSE- TO COMPUTE THE ESR TENSORS THAT FIT THE EXPERIMENTAL
C     DATA BY A LEAST SQUARES PROCESS, TO THE FIRST ORDER
C
C     CARD 1 ***TITLE
C     CARD 2 *** INDEX IN COLUMN 1
C            *** IWGHT IN COLUMN 2
C       IF INDEX IS 2
C          CARD 2A *** IINDEX IN COLUMN 1
C          CARD 2B *** G11,G12,G13,G22,G23,G33 IN COLUMNS 1-10,11-20,ETC
C     CARDS 3 TO N+2 ** H(I),PHI(I),THETA(I),FR(I) LEAVE COLUMN 1 BLANK
C     CARD N+3  *** A 1 IN COLUMN 1
C
C     INDEX IS 1 FOR G-TENSOR,2 FOR A-TENSOR
C
C     IINDEX IS 2 IF THE ANISOTROPY OF THE G TENSOR IS TO BE INCLUDED
C     IN THE A TENSOR CALCULATION,OTHERWISE IINDEX IS 1
C
C     H IS THE MAGNETIC FIELD IN GAUSS
C     FR IS THE FREQUENCY IN MC/S
C     THETA IS THE POLAR ANGLE
C     PHI IS THE AZIMUTHAL ANGLE
C     FOR THE A TENSOR FR IS IGNORED AND H IS THE HYPERFINE SPLITTING
C
C     FORTRAN PROGRAM NUMBER 5 IS ASSIGNED TO THE CARD READER
C     FORTRAN PROGRAM NUMBER 6 IS ASSIGNED TO THE LINE PRINTER
C
C     ********************************************************************
C
      DIMENSION GSQUAR(500)
      DIMENSION G2(6),GINPUT(6)
      DIMENSION A(49),AI(49),NA(7),TITLE(18),SHI(250),SHETA(250)
      DIMENSION DIFFER(250)
      DIMENSION FR(250),PHI(250),THETA(250),H(250),C(7,250)
      DIMENSION DLS(50),G(9),B(9),AM(49),G2CALC(250)
    2 FORMAT(2I1)
    4 FORMAT(' ',3(F10.4,2X),F5.1,4X,F5.1,4X,F10.3,2X,F10.3)
    5 FORMAT('0',3X,'GE ',9X,'GCALC ',8X,'DIFF',6X,'PHI',4X,'THETA',10X,
     1'H',9X,'FR',8X,' ')
    6 FORMAT('0',21X,'-',I1/' ','WEIGHTING FACTOR IS A')
   10 FORMAT('0','ANISOTROPY OF G-TENSOR INCLUDED')
   13 FORMAT('0','A-TENSOR')
   15 FORMAT('0','STANDARD DEVIATION IS ',F12.5)
   16 FORMAT('0','TENSOR FOR DIAGONALISING')
   17 FORMAT('0','G-TENSOR')
   20 FORMAT('0',21X,'-',I1/' ','WEIGHTING FACTOR IS G')
   22 FORMAT('0',3X,' A ',9X,'ACALC ',8X,'DIFF',6X,'PHI',4X,'THETA',10X,
     1'H')
   23 FORMAT(' ',3(F12.4,10X))
   26 FORMAT(I1,F9.3,2F10.3,F10.5)
   27 FORMAT('0','N= ',I3)
  222 FORMAT(I1)
  600 FORMAT('0',80('*'))
  844 FORMAT('0','ERROR IN MATRIX INVERSION')
  911 FORMAT(18A4)
  912 FORMAT('0',18A4)
  913 FORMAT(6F10.4)
C
C
   96 READ(5,911,END=99) (TITLE(I),I=1,18)
      WRITE(6,912) (TITLE(I),I=1,18)
      READ(5,2) INDEX,IWGHT
      IF(INDEX-1) 28,29,28
   29 WRITE(6,17)
```

```
      WRITE(6,20) IWGHT
      GO TO 8
   28 WRITE(6,13)
      WRITE(6,6) IWGHT
      READ(5,222) IINDEX
      GO TO(8,9),IINDEX
    9 WRITE(6,10)
C
CC    CALCULATE G-TENSOR FOR CLOSER APPROXIMATION TO A-TENSOR
C
      WRITE(6,17)
      READ(5,913) (GINPUT(I),I=1,6)
      WRITE(6,23) GINPUT(1),GINPUT(2),GINPUT(3)
      WRITE(6,23) GINPUT(2),GINPUT(4),GINPUT(5)
      WRITE(6,23) GINPUT(3),GINPUT(5),GINPUT(6)
      G2(1)=GINPUT(1)**2+GINPUT(2)**2+GINPUT(3)**2
      G2(2)=GINPUT(1)*GINPUT(2)+GINPUT(2)*GINPUT(4)+GINPUT(3)*GINPUT(5)
      G2(3)=GINPUT(1)*GINPUT(3)+GINPUT(2)*GINPUT(5)+GINPUT(3)*GINPUT(6)
      G2(4)=GINPUT(2)**2+GINPUT(4)**2+GINPUT(5)**2
      G2(5)=GINPUT(2)*GINPUT(3)+GINPUT(4)*GINPUT(5)+GINPUT(5)*GINPUT(6)
      G2(6)=GINPUT(3)**2+GINPUT(5)**2+GINPUT(6)**2
    8 N=0
C
CC    READ INPUT DATA,CALCULATE G2 OR A2 AND COEFFICIENTS
C
      I=1
    1 READ(5,26) IFILE,H(I),SHI(I),SHETA(I),FR(I)
      IF(SHETA(I).EQ.90.0) SHI(I)=SHI(I)+2.5
      IF(SHI(I).EQ.90.0) SHETA(I)=SHETA(I)+7.2
      I=I+1
      N=N+1
      IF(IFILE) 1,1,11
   11 N=N-1
      WRITE(6,27) N
      ENN=N
      ENM=SQRT(ENN)
      GO TO (18,19),INDEX
   18 WRITE(6,5)
      DO 21 I=1,N
      C(7,I)=FR(I)*0.71449/H(I)
   21 C(7,I)=C(7,I)*C(7,I)
      GO TO 9900
   19 WRITE(6,22)
      DO 9921 I=1,N
 9921 C(7,I)=H(I)*H(I)
 9900 CONTINUE
      DO 12 I=1,N
      PHI(I)=SHI(I)/57.29578
      THETA(I)=SHETA(I)/57.29578
      C(1,I)=SIN(THETA(I))**2
      C(2,I)=2.0*SIN(THETA(I))*COS(THETA(I))
      C(3,I)=COS(PHI(I))*C(2,I)
      C(4,I)=SIN(PHI(I))**2*C(1,I)
      C(5,I)=SIN(PHI(I))*C(2,I)
      C(6,I)=COS(THETA(I))**2
      C(2,I)=2.0*SIN(PHI(I))*COS(PHI(I))*C(1,I)
      C(1,I)=COS(PHI(I))**2*C(1,I)
      IF(INDEX.EQ.1) GO TO 12
      IF(IINDEX.EQ.1) GO TO 12
C
CC    COMPUTE EFFECT OF ANISOTROPY OF G
C
      GSQUAR(I)=C(1,I)*G2(1)+C(2,I)*G2(2)+C(3,I)*G2(3)+C(4,I)*G2(4)+C(5,
     1I)*G2(5)+C(6,I)*G2(6)
      EL=SIN(THETA(I))*COS(PHI(I))
      EM=SIN(THETA(I))*SIN(PHI(I))
      EN=COS(THETA(I))
      AL1=GINPUT(1)*EL+GINPUT(2)*EM+GINPUT(3)*EN
      AL2=GINPUT(2)*EL+GINPUT(4)*EM+GINPUT(5)*EN
      AL3=GINPUT(3)*EL+GINPUT(5)*EM+GINPUT(6)*EN
```

```
      C(1,I)=AL1**2/GSQUAR(I)
      C(2,I)=2.0*AL2*AL1/GSQUAR(I)
      C(3,I)=2.0*AL3*AL1/GSQUAR(I)
      C(4,I)=AL2**2/GSQUAR(I)
      C(5,I)=2.0*AL2*AL3/GSQUAR(I)
      C(6,I)=AL3**2/GSQUAR(I)
   12 CONTINUE
C
CC    INITIALIZE MATRIX AM FOR LEAST SQUARES PROCEDURE
C
      DO 925 L=1,49
  925 AM(L)=0.0
C
CC    SET UP MATRIX AM FOR LEAST SQUARES PROCEDURE
C
      DO 3 I=1,N
      DO 3 L=1,7
      DO 3 M=1,7
      K=7*(L-1)+M
      DLS(K)=C(L,I)*C(M,I)/C(7,I)**IWGHT
    3 AM(K)=AM(K)+DLS(K)
C
CC    INVERT MATRIX AM
C
      CALL MATINV(AM,AM,DET)
      DO 845 I=2,49
  845 AM(I)=AM(I)/AM(1)
      STDDEV=0.0
      IF(ABS(DET)-1.0E-6) 843,843,81
  843 WRITE(6,844)
      GO TO 96
C
CC    CALCULATE BEST FIT G2 OR A2,STANDARD DEVIATION IN G OR A
C
   81 DO 115 I=1,N
      G2CALC(I)=C(1,I)*AM(7)+C(2,I)*AM(2)+C(3,I)*AM(3)+C(4,I)*AM(4)+C(5
     1,I)*AM(5)+C(6,I)*AM(6)
      C(7,I)= SQRT(C(7,I))
      G2CALC(I)=SQRT(ABS(G2CALC(I)))
      DIFFER(I)=ABS(ABS(C(7,I))-ABS(G2CALC(I)))
      STDDEV=STDDEV+DIFFER(I)**2
      IF(INDEX.EQ.1) GO TO 14
      WRITE(6,4)C(7,I),G2CALC(I),DIFFER(I),SHI(I),SHETA(I),H(I)
      GO TO 115
   14 WRITE(6,4)C(7,I),G2CALC(I),DIFFER(I),SHI(I),SHETA(I),H(I),FR(I)
  115 CONTINUE
      WRITE(6,16)
      WRITE(6,23) AM(7),AM(2),AM(3)
      WRITE(6,23) AM(2),AM(4),AM(5)
      WRITE(6,23) AM(3),AM(5),AM(6)
      AM(1)=AM(7)
      AM(7)=AM(3)
      AM(3)=AM(4)
      AM(4)=AM(7)
      STDDEV=SQRT(STDDEV)/ENN
      CALL DIAG(AM,0,INDEX)
      WRITE(6,15) STDDEV
      WRITE(6,600)
      GO TO 96
   99 STOP
      END
```

```
      SUBROUTINE DIAG(G,MV,INDEX)
C*****************************************************************
C
C     SUBPROGRAM DIAG(G,MV,INDEX)
C
C     PURPOSE-DIAGONALISATION OF A G2 OR A2 MATRIX
C     G IS THE MATRIX TO BE DIAGONALISED WITH G1=G11,G2=G12,G3=G22,
C     G4=G13,G5=G23,G6=G33
C     B IS THE MATRIX OF EIGENVECTORS
C     THE G OR A MATRIX IS RECALCULATED IN LABORATORY COORDINATES
C     THE ISOTROPIC AND ANISOTROPIC COMPONENTS OF THE A TENSOR ARE
C     CALCULATED
C
C*****************************************************************
      DIMENSION G(9),B(9),BT(9)
      CALL EIGEN(G,B,3,0)
      WRITE(6,12)
   12 FORMAT('0','DIAGONALISED TENSOR')
      WRITE(6,16) G(1),G(2),G(4)
      WRITE(6,16) G(2),G(3),G(5)
      WRITE(6,16) G(4),G(5),G(6)
   16 FORMAT(' ',3(F12.4,5X))
      IF(G(1)*G(3)) 13,13,15
   15 IF(G(1)*G(6)) 13,13,171
   13 WRITE(6,14)
   14 FORMAT('0','AT LEAST ONE PRINCIPAL VALUE IS NOT REAL'/'  ACALC IS
     1NOT VALID')
  171 WRITE(6,17)
   17 FORMAT('0','DIAGONALISING TENSOR')
      DO 18 I=1,9,3
   18 WRITE(6,19) B(I),B(I+1),B(I+2)
   19 FORMAT(' ',3(F10.4,5X))
   23 G(1)=SQRT(ABS(G(1)))
      G(3)=SQRT(ABS(G(3)))
      G(6)=SQRT(ABS(G(6)))
      WRITE(6,21)
   21 FORMAT('0','PRINCIPAL VALUES')
      WRITE(6,19) G(1),G(3),G(6)
C
C     CALCULATE G IN LABORATORY COORDINATES
C
      BT(1)=B(1)
      BT(2)=B(4)
      BT(3)=B(7)
      BT(4)=B(2)
      BT(5)=B(5)
      BT(6)=B(8)
      BT(7)=B(3)
      BT(8)=B(6)
      BT(9)=B(9)
      G(5)=G(3)
      G(9)=G(6)
      G2=(G(1)+G(3)+G(6))/3.0
      G1=G(1)-G2
      G3=G(3)-G2
      G6=G(6)-G2
      J=1
      DO 704 I=1,9,4
      DO 704 K=1,3
      B(J)=G(I)*B(J)
  704 J=J+1
      DO 705 I=1,7,3
      DO 705 J=1,3
  705 G(I+J-1)=BT(I)*B(J)+BT(I+1)*B(J+3)+BT(I+2)*B(J+6)
      WRITE(6,706)
  706 FORMAT('0',' TENSOR IN LAB COORDINATES XYZ')
      DO 708 I=1,7,3
  708 WRITE(6,707) G(I),G(I+1),G(I+2)
```

```
707 FORMAT(' ',3(F10.4,10X))
 27 FORMAT(6F10.4)
    IF(INDEX.EQ.1) GO TO 99
    WRITE(6,31) G2
 31 FORMAT('0','ISOTROPIC HYPERFINE COMPONENT =',F10.4)
    WRITE(6,32) G1,G3,G6
 32 FORMAT('0','ANISOTROPIC HYPERFINE TENSOR IS ',3F10.4)
 99 RETURN
    END



    SUBROUTINE MATINV(A,AI,DET)
C
CCCC    SUBPROGRAM MATINV(AM,AM,DET)
CCC
C   DET =RESULTANT DETERMINANT OF A
    DIMENSION A(49),AI(49),NA(7)
C
CCC    MOVE A TO AI
C
    DET=1.0
     DO 800 I=1,7
    NA(I)=I
    DO 800 J=I,49,7
800 AI(J)=A(J)
CCC    SEARCH FOR PIVOT ELEMENT LARGEST IN ROW
C
    DO 801 I=1,7
    L=(I-1)*7
    K=L+I
    B=0.0
    DO 813 J=K,49,7
    C=AI(J)
    IF(C) 810,811,811
810 C=-C
811 IF(B-C) 812,812,813
812 B=C
    L1=J-K
813 CONTINUE
CCC    INTERCHANGE COLUMNS IF NECESSARY
C
    IF(L1) 802,803,802
802 L2=L+1
    L3=L2+6
    DO 820 J=L2,L3
    L2=J+L1
    B=AI(J)
    AI(J)=AI(L2)
820 AI(L2)=B
    L2=I+L1/6
    L3=NA(I)
    NA(I)=NA(L2)
    NA(L2)=L3
    DET=-DET
C
CCC    DIVIDE ROW BY PIVOT ELEMENT AND REDUCE MATRIX
C
803 B=AI(K)
    AI(K)=1.0
    DET=B*DET
    DO 830 J=I,49,7
830 AI(J)=AI(J)/B
    DO 801 J=1,7
    L1=J-I
    IF(L1) 831,801,831
```

```
831 L2=L+J
    B=AI(L2)
    AI(L2)=0.0
    DO 832 K=J,49,7
    L1=K-L1
832 AI(K)=AI(K)-B*AI(L2)
801 CONTINUE
C
C   INTERCHANGE ROWS IF NECESSARY
C
    DO 805 I=1,7
    IF(NA(I)-I) 850,805,850
850 DO 852 J=1,7
    IF(NA(J)-I) 852,851,852
851 NA(J)=NA(I)
    L1=J-I
    GO TO 853
852 CONTINUE
853 DO 854 J=I,49,7
    L2=J+L1
    B=AI(J)
    AI(J)=AI(L2)
854 AI(L2)=B
805 CONTINUE
    RETURN
    END
```

```
    SUBROUTINE EIGEN(A,R,N,MV)
C***********************************************************************
C
C       SUBPROGRAM EIGEN
C
C       PURPOSE
C          COMPUTE EIGENVALUES AND EIGENVECTORS OF A REAL SYMMETRIC
C          MATRIX
C
C       USAGE
C          CALL EIGEN(A,R,N,MV)
C
C       DESCRIPTION OF PARAMETERS
C          A - ORIGINAL MATRIX (SYMMETRIC), DESTROYED IN COMPUTATION.
C              RESULTANT EIGENVALUES ARE DEVELOPED IN DIAGONAL OF
C              MATRIX A IN DESCENDING ORDER.
C          R - RESULTANT MATRIX OF EIGENVECTORS (STORED COLUMNWISE,
C              IN SAME SEQUENCE AS EIGENVALUES)
C          N - ORDER OF MATRICES A AND R
C          MV- INPUT CODE
C                    0   COMPUTE EIGENVALUES AND EIGENVECTORS
C                    1   COMPUTE EIGENVALUES ONLY (R NEED NOT BE
C                        DIMENSIONED BUT MUST STILL APPEAR IN CALLING
C                        SEQUENCE)
C
C       REMARKS
C          ORIGINAL MATRIX A MUST BE REAL SYMMETRIC (STORAGE MODE=1)
C    FOR YOUR INFORMATION THIS MEANS UPPER TRIANGULAR FORM
C          MATRIX A CANNOT BE IN THE SAME LOCATION AS MATRIX R
C
C       SUBPROGRAMS AND FUNCTN SUBPROBRAMS REQUIRED
C          NONE
C
C       METHOD
C          DIAGONALIZATION METHOD ORIGINATED BY JACOBI AND ADAPTED
C          BY VON NEUMANN FOR LARGE COMPUTERS AS FOUND IN 'MATHEMATICAL
C          METHODS FOR DIGITAL COMPUTERS', EDITED BY A. RALSTON AND
C          H.S. WILF, JOHN WILEY AND SONS, NEW YORK, 1962, CHAPTER 7
```

```
C
CCC ***********************************************************************
      DIMENSION A(1),R(1)
C
C     ..................................................................
C
C        IF A DOUBLE PRECISION VERSION OF THIS ROUTINE IS DESIRED, THE
C        C IN COLUMN 1 SHOULD BE REMOVED FROM THE DOUBLE PRECISION
C        STATEMENT WHICH FOLLOWS.
C
C     DOUBLE PRECISION A,R,ANORM,ANRMX,THR,X,Y,SINX,SINX2,COSX,
C    1                 COSX2,SINCS,RANGE
C
C        THE C MUST ALSO BE REMOVED FROM DOUBLE PRECISION STATEMENTS
C        APPEARING IN OTHER ROUTINES USED IN CONJUNCTION WITH THIS
C        ROUTINE.
C
C        THE DOUBLE PRECISION VERSION OF THIS SUBROUTINE MUST ALSO
C        CONTAIN DOUBLE PRECISION FORTRAN FUNCTIONS.  SQRT IN STATEMENTS
C        40, 68, 75, AND 78 MUST BE CHANGED TO DSQRT.  ABS IN STATEMENT
C        62 MUST BE CHANGED TO DABS. THE CONSTANT IN STATEMENT 5 SHOULD
C        BE CHANGED TO 1.0D-12.
C
C     ..................................................................
C
C        GENERATE IDENTITY MATRIX
C
    5 RANGE=1.0E-6
      IF(MV-1) 10,25,10
   10 IQ=-N
      DO 20 J=1,N
      IQ=IQ+N
      DO 20 I=1,N
      IJ=IQ+I
      R(IJ)=0.0
      IF(I-J) 20,15,20
   15 R(IJ)=1.0
   20 CONTINUE
C
C        COMPUTE INITIAL AND FINAL NORMS (ANORM AND ANORMX)
C
   25 ANORM=0.0
      DO 35 I=1,N
      DO 35 J=I,N
      IF(I-J) 30,35,30
   30 IA=I+(J*J-J)/2
      ANORM=ANORM+A(IA)*A(IA)
   35 CONTINUE
      IF(ANORM) 165,165,40
   40 ANORM=1.414*SQRT(ANORM)
      ANRMX=ANORM*RANGE/FLOAT(N)
C
C        INITIALIZE INDICATORS AND COMPUTE THRESHOLD, THR
C
      IND=0
      THR=ANORM
   45 THR=THR/FLOAT(N)
   50 L=1
   55 M=L+1
C
C        COMPUTE SIN AND COS
C
   60 MQ=(M*M-M)/2
      LQ=(L*L-L)/2
      LM=L+MQ
   62 IF( ABS(A(LM))-THR) 130,65,65
   65 IND=1
      LL=L+LQ
      MM=M+MQ
```

```
      X=0.5*(A(LL)-A(MM))
   68 Y=-A(LM)/ SQRT(A(LM)*A(LM)+X*X)
      IF(X) 70,75,75
   70 Y=-Y
   75 SINX=Y/ SQRT(2.0*(1.0+( SQRT(1.0-Y*Y))))
      SINX2=SINX*SINX
   78 COSX= SQRT(1.0-SINX2)
      COSX2=COSX*COSX
      SINCS =SINX*COSX
C
CCC      ROTATE L AND M COLUMNS
C
      ILQ=N*(L-1)
      IMQ=N*(M-1)
      DO 125 I=1,N
      IQ=(I*I-I)/2
      IF(I-L) 80,115,80
   80 IF(I-M) 85,115,90
   85 IM=I+MQ
      GO TO 95
   90 IM=M+IQ
   95 IF(I-L) 100,105,105
  100 IL=I+LQ
      GO TO 110
  105 IL=L+IQ
  110 X=A(IL)*COSX-A(IM)*SINX
      A(IM)=A(IL)*SINX+A(IM)*COSX
      A(IL)=X
  115 IF(MV-1) 120,125,120
  120 ILR=ILQ+I
      IMR=IMQ+I
      X=R(ILR)*COSX-R(IMR)*SINX
      R(IMR)=R(ILR)*SINX+R(IMR)*COSX
      R(ILR)=X
  125 CONTINUE
      X=2.0*A(LM)*SINCS
      Y=A(LL)*COSX2+A(MM)*SINX2-X
      X=A(LL)*SINX2+A(MM)*COSX2+X
      A(LM)=(A(LL)-A(MM))*SINCS+A(LM)*(COSX2-SINX2)
      A(LL)=Y
      A(MM)=X
C
CCC      TESTS FOR COMPLETION
C
CCC      TEST FOR M = LAST COLUMN
C
  130 IF(M-N) 135,140,135
  135 M=M+1
      GO TO 60
C
CCC      TEST FOR L = SECOND FROM LAST COLUMN
C
  140 IF(L-(N-1)) 145,150,145
  145 L=L+1
      GO TO 55
  150 IF(IND-1) 160,155,160
  155 IND=0
      GO TO 50
C
CCC      COMPARE THRESHOLD WITH FINAL NORM
C
  160 IF(THR-ANRMX) 165,165,45
C
CCC      SORT EIGENVALUES AND EIGENVECTORS
C
  165 IQ=-N
  185 CONTINUE
      RETURN
      END
```

APPENDIX 2

Nuclear Zeeman Interaction

Consider the spin Hamiltonian:

$$\mathcal{H} = \beta\bar{S}.\bar{\bar{g}}.\bar{H} + \sum_i \bar{S}.\bar{\bar{A}}_i.I_i - \sum_i g_N\beta_N\bar{H}.\bar{I}_i$$

In computing the hyperfine tensor, g may be taken as isotropic to a good approximation and as the second term is small compared with the first, S may be considered to be quantized along the magnetic field, which may be used to define $\bar{X}$, $\bar{Y}$ and $\bar{Z}$ directions. In this approximation

$$\bar{S} = M_s\bar{Z} \qquad \text{where } M_s = \pm\tfrac{1}{2}$$
$$\text{and} \qquad \bar{Z} = \frac{\bar{H}}{H}$$

$$\therefore \quad \mathcal{H} = g\beta HM_s + \sum_i M_s\bar{Z}.\bar{\bar{A}}_i.\bar{I}_i - \sum_i g_{N_i}\beta_N\bar{Z}.I_i$$

This enables the nuclear terms to be separated from one another and from the term expressing the interaction of the electron with the magnetic field.

Unless the nuclear Zeeman term is much smaller than the hyperfine term, the nuclear spin may not be assumed to be quantized along the direction of the field. Thus for each nucleus the nuclear spin part of the Hamiltonian may be expressed in terms of the component spin operators I_x, I_y and I_z where $\bar{X}$ and $\bar{Y}$ are arbitrary directions perpendicular to each other and $\bar{Z}$. The spin Hamiltonian describing the nuclear interaction may therefore be written

$$\mathcal{H} = (M_s\bar{Z}\bar{\bar{A}}\bar{Z} - g_N\beta_N H)I_z + M_s\bar{Z}\bar{\bar{A}}\bar{X}I_x + M_s\bar{Z}\bar{\bar{A}}\bar{Y}I_y$$

or

$$\mathcal{H}(M_s = \pm\tfrac{1}{2}) = \pm\tfrac{1}{2}\{(\bar{Z}\bar{\bar{A}}\bar{Z} \mp 2g_N\beta_N H)I_z + \bar{Z}\bar{\bar{A}}\bar{X}I_x + \bar{Z}\bar{\bar{A}}\bar{Y}I_y\}.$$

Since $\beta_N = 5.0504 \times 10^{-24}$ erg.gauss^{-1}

and H ~ 3300 gauss for X-band esr studies

$$g_N\beta_N H = 2.51 g_N \text{ MHz}$$

$$= 14.0 \text{ MHz for } {}^{1}H$$

$$= 2.1 \text{ MHz for } {}^{2}H$$

$$= 1.4 \text{ MHz for } {}^{35}Cl$$

$$= 1.1 \text{ MHz for } {}^{37}Cl$$

$$= 1.0 \text{ MHz for } {}^{14}N$$

$$= 3.8 \text{ MHz for } {}^{63}Cu$$

$$= 4.1 \text{ MHz for } {}^{65}Cu$$

Thus the effect of the direct field interaction is greatest for protons and is negligible for nitrogen, copper and chlorine except for very small hyperfine coupling constants.

For protons it can be shown that four absorption peaks occur at energies given by

$$E = g\beta H \pm \tfrac{1}{4}(A_+ \pm A_-)$$

where

$$A_\pm = \{(A_{zz} \pm 2g_N\beta_N H)^2 + (A_{zx}^2 + A_{zy}^2)\}^{\frac{1}{2}}$$

These two doublets normally have different intensities as a consequence of the fact that $\bar{I}$ is no longer quantised along $\bar{Z}$ and the normal selection rule, $\Delta M_I = 0$, is therefore not valid.

The two doublets have spacing, $d_\pm$, given by

$$d_{\pm} = \tfrac{1}{2}(A_{+} \pm A_{-})$$

$$= \tfrac{1}{2}\{(ZAZ + 2\nu)^2 + (ZAX)^2 + (ZAY)^2\}^{\frac{1}{2}}$$

$$\pm \tfrac{1}{2}\{(ZAZ - 2\nu)^2 + (ZAX)^2 + (ZAY)^2\}^{\frac{1}{2}}$$

$$= \tfrac{1}{2}\{ZA^2Z + 4\nu^2 + 4\nu(ZAZ)\}^{\frac{1}{2}} \pm \tfrac{1}{2}\{ZA^2Z + 4\nu^2 - 4\nu(ZAZ)\}^{\frac{1}{2}}$$

and the ratio of the intensities of the doublets is given by:

$$\frac{I_{-}}{I_{+}} = \frac{(A_{zx}^2+A_{zy}^2)(A_{+}-A_{-}+4g_N\beta_N H)^2}{(A_{zz}+A_{-}-2g_N\beta_N H)(A_{zz}+A_{+}+2g_N\beta_N H) + (A_{zx}^2+A_{zy}^2)}$$

Thus when the magnetic field is along a principal axis of A the d_{-} doublet has zero intensity. The two doublets are of comparable intensity when A_{zz} is of the order of $2g_N\beta_N H$ provided $A_{zx}^2 + A_{zy}^2 \neq 0$. This is true for protons when $A_{zz} \approx$ 10G. In general where $A_{zz} >$ 10G the d_{+} doublet will be more intense than the d_{-} doublet and the converse will be true when $A_{zz} <$ 10G, although this also depends on the ratio of $A_{zx}^2 + A_{zy}^2$ to A_{zz}^2, a high ratio causing the d_{+} doublet to be the most intense even below 10G (166,179-186).

From the hyperfine coupling tensor calculated by first order equations it was possible to calculate a self consistent tensor for the hydrogen hyperfine coupling using the second order equations given above by a simple least squares procedure. The effect of anisotropy in the g tensor is incorporated in a similar manner to the first order procedure outlined in Appendix 1B.

The general least squares computer program, ORGLS (190) was used to calculate the hyperfine tensor, taking into account the nuclear Zeeman interaction. It was adapted by the addition of two subroutines. DIAG and EIGEN were used as in FOE, to

obtain the principal values and their direction cosines. A subroutine, CALC, substantially the same as that used in ANGCALC, was used to calculate the coupling constants at each orientation from the tensor being adjusted by the non-linear least squares method.

Use was also made of a computer program, ANGCALC, to calculate the g-value or hyperfine coupling constant at any orientation from input tensors. Calculations included the direct field correction and it was possible to compare the experimental and calculated g-values or hyperfine coupling constants.

Angular Variation from Tensors

(ANGCALC)

Purpose: This program calculates g-values or hyperfine coupling constants from an input tensor. Experimental and calculated quantities may be compared and a standard deviation determined. The tensor is diagonalised and the direction cosines evaluated.

Contents: One mainline program, ANGCALC, and the subroutines EIGEN and CALC.

Library Routines Used: SIN, COS, SQRT, ABS.

Language: IBM System/360 Fortran IV(BCD).

Method: This program first calculates the g^2 or A^2 tensor, unless this is given as input, and then diagonalises it to yield the principal values and their direction cosines. g or A is calculated at 5° intervals in the tensorial axis system and if required, experimental and calculated quantities are compared and a standard deviation determined.

Input:

Card No.	Columns	Fortran Symbol	Format	Contents
1	1-10	G(1)	F10.4	g_{11}
	11-20	G(2)	F10.4	g_{12}
	21-30	G(4)	F10.4	g_{13}
	31-40	G(3)	F10.4	g_{22}
	41-50	G(5)	F10.4	g_{23}
	51-60	G(6)	F10.4	g_{33}
	61	ICALCG	I1	=1, if g-value is to be calculated at 5^{o} intervals
				= 0, otherwise.
	62	JCALC	I1	=1, if experimental and calculated quantities are to be compared
				= 0, otherwise
	63	KCALC	I1	= 1, if the experimental quantities used for the last calculation are to be used again
				= 0, if new experimental quantities are to be read
	64	LCALC	I1	= 1, if the g^2 or A^2 tensor is given as input
				= 0, if the g or A tensor is given as input
	71-80	SR	F10.4	coefficient for direct field term which is SR*I
If JCALC = 1 and KCALC = 0				
2	1	IIDEX	I1	= 1 for g-tensor
				= 2 for A-tensor
3	1	KODE	I1	left blank
	2-10	H(I)	F9.4	if IIDEX = 1, H is the magnetic field, in gauss.
				if IIDEX = 2, H is the measured hyperfine splitting, in gauss.

Card No.	Columns	Fortran Symbol	Format	Contents
3	11-20	FHI(I)	F10.4	the azimuthal angle, ϕ, in degrees.
	21-30	FHETA(I)	F10.4	the polar angle, θ, in degrees.
	31-40	FR(I)	F10.4	the microwave frequency, in MHz.

There is one card of type 3 for each orientation. End of data is signified by a 1 in column 1.

Output:

(1) The input tensor

(2) The value of SR

(3) The diagonalising tensor. The direction cosines are stored row-wise.

(4) The principal values

(5) The g-tensor if the g^2-tensor was given as input

(6) The value of A or g at 5° intervals

(7) The calculated and experimental values

(8) The standard deviation.

Capacity: The number of experimental values is limited by the DIMENSION statement, which at present is set for a maximum of 290 observations.

Limitations: The present form of subroutine CALC limits inclusion of the direct field effect to nuclei with nuclear spins of $\frac{1}{2}$.

```
C
CCCCC  ***********************************************************************
C
CCCCC  PROGRAM ANGCALC
C
CCCCC  ***********************************************************************
C
CCCCC  PURPOSE-TO DIAGONALISE A SYMMETRIC MATRIX
CCCCC  INPUT- ONE CARD PER MATRIX
CCCCC  WITH A11,A12,A13,A22,A23,A33 IN F10.4 FORMAT
CCCCC  A 1 IN COLUMN 61 CAUSES G OR A TO BE CALCULATED AT 10 DEGREE
CCCCC  INTERVALS IN THREE ORTHOGONAL PLANES
CCCCC  A 1 IN COLUMN 62 ENABLES CALCULATED G OA A VALUES TO BE COMPARED
CCCCC  WITH EXPERIMENTAL QUANTITIES CALCULATED FROM THE FOLLOWING CARDS
CCCCC  WHICH ARE IDENTICAL TO THE INPUT FOR FOE
CCCCC  A 1 IN COLUMN 63 CAUSES THE SAME EXPERIMENTAL POINTS TO BE USED
CCCCC  FOR THIS INPUT MATRIX
CCCCC  A 1 IN COLUMN 64 IS REQUIRED WHEN THE INPUT TENSOR IS THE SQUARE
CCCCC  OF THE DESIRED TENSOR
CCCCC  COLUMNS 71-80 CONTAIN SR, THE COEFFICIENT OF I IN THE DIRECT FIELD
CCCCC  TERM
C
CCCCC  FORTRAN PROGRAM NUMBER 1 IS ASSIGNED TO THE WORKING FILE
CCCCC  FORTRAN PROGRAM NUMBER 5 IS ASSIGNED TO THE CARD READER
CCCCC  FORTRAN PROGRAM NUMBER 6 IS ASSIGNED TO THE LINE PRINTER
CCCCC  FORTRAN PROGRAM NUMBER 7 IS ASSIGNED TO THE CARD PUNCH
C
CCCCC  ***********************************************************************
C
      DIMENSION FHI(290),FHETA(290),FR(290),H(290),GEXPT(290)
     1,DIFFER(290)
      DIMENSION G(9),B(9),BT(9)
C
    1 FORMAT(6F10.4,4I1,6X,F10.4)
    2 FORMAT('0',' INPUT TENSOR IN LAB COORDINATES')
    3 FORMAT(' ',3(F10.4,4X))
    4 FORMAT('0',' DIAGONALISING TENSOR')
    6 FORMAT(' ',3(F10.4,5X))
    7 FORMAT('0',' PRINCIPAL VALUES')
   16 FORMAT(' ',F10.2,6X,F10.2,6X,F10.4)
   17 FORMAT('0',4X,'PHI',12X,'THETA',10X,'GCALC')
   18 FORMAT('0',' ***********************************************************')
   22 FORMAT(I1,F9.4,3F10.4)
   25 FORMAT('0',' STANDARD DEVIATION IS ',F10.4)
   27 FORMAT('0','  GEXPT        GCALC     DIFFER       PHI         THETA
     1    H          FR          ')
   28 FORMAT(' ',3F10.4,2F10.1,F10.2,F10.3)
   30 FORMAT(I1)
   35 FORMAT('0','  AEXPT        ACALC+    ACALC-       DIFFER       PHI
     1 THETA       H          ')
   38 FORMAT(' ',4F10.4,2F10.1,F10.2)
   39 FORMAT('0',' DIRECT FIELD TERM IS ',F10.5,'I')
C
CC    READ MATRIX ELEMENTS AND CODES.
C
    8 READ(5,1,END=9) G(1),G(2),G(4),G(3),G(5),G(6),ICALCG,JCALC,KCALC,L
     1CALC,SR
      WRITE(6,2)
      WRITE(6,3) G(1),G(2),G(4)
      WRITE(6,3) G(2),G(3),G(5)
      WRITE(6,3) G(4),G(5),G(6)
      WRITE(6,39)  SR
      KKK=0
      IF(LCALC.EQ.1) GO TO 21
   19 IF(ICALCG.EQ.0) GO TO 26
      WRITE(6,17)
C
CC    CALCULATE G OR A AT 5 DEGREE INTERVALS
C
      INDEX=0
```

```
      PHI=0.0
   11 THETA=0.0
   10 GCALC=SQRT((G(1)*G(1)+G(2)*G(2)+G(4)*G(4))*SIN(THETA)**2*COS(PHI)
     1**2+(G(1)*G(2)+G(2)*G(3)+G(4)*G(5))*2.0*SIN(THETA)**2*SIN(PHI)*
     2COS(PHI)+((G(1)*G(4)+G(2)*G(5)+G(4)*G(6))*COS(PHI)+(G(2)*G(4)+
     3G(3)*G(5)+G(5)*G(6))*SIN(PHI))*2.0*SIN(THETA)*COS(THETA)   +(G(2)
     4*G(2)+G(3)*G(3)+G(5)*G(5))*SIN(THETA)**2*SIN(PHI)**2+(G(4)*G(4)+
     5G(5)*G(5)+G(6)*G(6))*COS(THETA)**2)
      SHI=PHI*57.29578
      SHETA=THETA*57.29578
      WRITE(6,16) SHI,SHETA,GCALC
      IF(INDEX.EQ.2) GO TO 14
      THETA=THETA+5.0/57.29578
      IF(INDEX.NE.2) GO TO 15
   14 PHI=PHI+5.0/57.29578
      IF(PHI.LE.3.14158) GO TO 10
      GO TO 26
   15 IF(THETA.LE.3.14158) GO TO 10
      INDEX=INDEX+1
      GO TO(12,13,26), INDEX
   12 PHI=90.0/57.29578
      GO TO 11
   13 THETA=90.0/57.29578
      PHI=0.0
      GO TO 10
   26 IF(JCALC.EQ.0) GO TO 21
C
C     COMPARE CALCULATED AND EXPERIMENTAL VALUES
C
      STDDEV=0.0
      I=1
      IF(KCALC.EQ.1) GO TO 33
      READ(5,30)  IIDEX
   33 IF(IIDEX.EQ.2) GO TO 34
      WRITE(6,27)
      IF(KCALC.EQ.1) GO TO 37
      GO TO 24
   34 WRITE(6,35)
   24 IF(KCALC.EQ.1) GO TO 37
      READ(5,22) KODE,H(I),FHI(I),FHETA(I),FR(I)
      IF(KODE.EQ.1) GO TO 23
   37 PHI=FHI(I)/57.29578
      THETA=FHETA(I)/57.29578
      CALL CALC(SR,PHI,THETA,GCALC,G,GCALC1)
      IF(IIDEX.EQ.2) GO TO 31
      GEXPT(I)=FR(I)/H(I)*0.71449
      GO TO 32
   31 GEXPT(I)=H(I)
   32 DIFFER(I)=ABS(GCALC   -GEXPT(I))
      GG=GEXPT(I)/2.0
      IF(GG.LE.SR) DIFFER(I)=ABS(GCALC1-GEXPT(I))
      STDDEV=STDDEV+DIFFER(I)**2
      IF(IIDEX.EQ.1)  WRITE(6,28) GEXPT(I),GCALC,DIFFER(I),FHI(I),FHETA(
     1I),H(I),FR(I)
      IF(IIDEX.EQ.2)  WRITE(6,38) GEXPT(I),GCALC,GCALC1,DIFFER(I),FHI(I)
     1,FHETA(I),H(I)
      IF(KCALC.NE.1) GO TO 40
      IF(I.EQ.N) GO TO 29
   40 I=I+1
      GO TO 24
   23 N=I-1
   29 STDDEV=SQRT(STDDEV/N)
      WRITE(6,25) STDDEV
C
C     DIAGONALISE MATRIX
C
   21 CALL EIGEN(G,B,3,0)
      WRITE(6,4)
      DO 5 I=1,9,3
    5 WRITE(6,6) B(I),B(I+1),B(I+2)
```

```
      WRITE(6,7)
      WRITE(6,6) G(1),G(3),G(6)
      IF(LCALC.NE.1) GO TO 20
      G(1)=SQRT(ABS(G(1)))
      G(5)=SQRT(ABS(G(3)))
      G(9)=SQRT(ABS(G(6)))
      BT(1)=B(1)
      BT(2)=B(4)
      BT(3)=B(7)
      BT(4)=B(2)
      BT(5)=B(5)
      BT(6)=B(8)
      BT(7)=B(3)
      BT(8)=B(6)
      BT(9)=B(9)
      J=1
      DO 704 I=1,9,4
      DO 704 K=1,3
      B(J)=G(I)*B(J)
  704 J=J+1
      DO 705 I=1,7,3
      DO 705 J=1,3
  705 G(I+J-1)=BT(I)*B(J)+BT(I+1)*B(J+3)+BT(I+2)*B(J+6)
      IF(KKK.EQ.1) GO TO 20
      WRITE(6,2)
      DO 708 I=1,7,3
  708 WRITE(6,3) G(I),G(I+1),G(I+2)
      G(4)=G(3)
      G(3)=G(5)
      G(5)=G(6)
      G(6)=G(9)
      KKK=1
      IF(LCALC.EQ.0) GO TO 20
      GO TO 19
   20 WRITE(6,18)
      GO TO 8
    9 STOP
      END
```

```
      SUBROUTINE CALC(SR,PHI,THETA,Y,P,Y1)
      DIMENSION P(9)
      COMP1(A,B,C,D)=(EL*A+EM*B+EN*C+2.0*SR*D)**2
      COMP2(A,B,C,D)=(EL*A+EM*B+EN*C-2.0*SR*D)**2
      SR=5.18
      EL=SIN(THETA)*COS(PHI)
      EM=SIN(THETA)*SIN(PHI)
      EN=COS(THETA)
      A1=SQRT(COMP1(P(1),P(2),P(4),EL)+COMP1(P(2),P(3),P(5),EM)+COMP1(P(
     14),P(5),P(6),EN))
      A2=SQRT(COMP2(P(1),P(2),P(4),EL)+COMP2(P(2),P(3),P(5),EM)+COMP2(P(
     14),P(5),P(6),EN))
      Y=0.5*(A1+A2)
      Y1=0.5*(A1-A2)
      RETURN
      END
```

```
      SUBROUTINE EIGEN(A,R,N,MV)
C*******************************************************************
C
C     SUBPROGRAM EIGEN
C
C*******************************************************************
C
C  THIS SUBPROGRAM IS IDENTICAL TO THAT USED IN FOE,TO WHICH YOU ARE
C  REFERRED FOR A LISTING
```

APPENDIX 3

Spectral Simulation

Extensive use was made of spectral simulation in determining the nuclear hyperfine tensors. For second order calculations of the spectral parameters an adaptation of program C168 provided by the Argonne National Laboratory (Applied Mathematics Division) was used but as second order effects were usually negligible the first order program, LINPLT, was generally used. This program was able to calculate spectra using line positions derived from second order theory by use of an option where all line parameters were determined with the aid of other programs and given as input for LINPLT.

Simulation of ESR Spectra for Plotting

(LINPLT)

Purpose: This program calculates first order spectra of organic free radicals, in solution or single crystal, from input hyperfine splitting data.

Contents: One mainline program, LINPLT, and the plotting package, PLOTAA.

Library Routines Used: EXP, SIN, COS, SQRT, ABS, PLOTAA.

Language: IBM System/360 Fortran IV (BCD).

Method: This program first calculates the hyperfine splittings for the required orientation by the method appropriate to the option given by KALKOD and then calculates an intensity function for each line. These are summed and the resultant spectrum is printed on either lineprinter or autoplotter, or both. The hyperfine splitting is the only variable in the Hamiltonian used to define the spectrum unless the option is used where all line parameters are given as input.

Input:

Card No.	Columns	Fortran Symbol	Format	Contents
1	1-80	TITLE	80A1	Title of plot. 1-60 plotted.
2	1-2	SHAPE	I2	= 1, Lorentzian lineshape
				= 2, Gaussian lineshape
	3-4	DERIV	I2	= 0, Absorption
				= 1, First derivative
				= 2, Second derivative
	5-6	PHASE	I2	= 1
				= 2
	7-8	SPECYS	I2	Number of different species for which tensors are to be read. Read only if KALKOD = 1 or 2. Up to eight species may be accommodated.
	9-10	KPLOT	I2	= 0, if only printed spectrum is required.
				= 1, if both plot and printed spectra are required.
				= 2, if only a plot is required.
	11-20	PHI	F10.5	azimuthal angle, in degrees.
	21-30	THETA	F10.5	polar angle, in degrees.
	31-40	HEIGHT	F10.5	height of plot, in cm.
	41-50	XMAX	F10.5	maximum width of plot, in cm.
3	1-5	DISPL(1)	F5.2	The displacement (in cm) of the centre of the spectrum for species 1.
	6-10	RELINT(1)	F5.2	The relative intensity of species 1. If RELINT(I) is zero it is reset to equal 1.0.
	11-15	DISPL(2)	F5.2	
	etc.			

Up to eight species may be accommodated.

Input (cntd):

Card No.	Columns	Fortran Symbol	Format	Contents
4	1	KALKOD	I1	= 0, if line parameters are input. = 1, if isotropic hyperfine splittings and nuclear spins are given for each interacting nucleus. = 2, if hyperfine tensors are input.
	2-11	WYDTH	F10.5	linewidth, in cm.
	12-21	SCAN	F10.5	scan width, in gauss per 40 cm.

If KALKOD = 0, line parameters are given as input and WYDTH is ignored unless WIDTH(I) is zero.

5	1	IFILE	I1	blank
	2-11	XCENTR(I)	F10.5	centre of line, in cm.
	12-21	FNTENS(I)	F10.3	relative intensity of line.
	22-31	WIDTH(I)	F10.3	linewidth, in cm.

Card type 5 is repeated for each line in the spectrum. End of data is signified by a 1 in column 1.

If KALKOD = 1, line positions are calculated from input isotropic hyperfine coupling constants, and nuclear spins.

5	1-3	SPIN(1)	F3.1	nuclear spin
	4-10	HFSPLT(1)	F7.3	hyperfine coupling constnat in gauss, of nucleus 1.
	11-13	SPIN(2)	F3.1	nuclear spin
	etc.			

Up to 8 nuclei may be accommodated.

If KALKOD = 2, line positions are calculated from input hyperfine coupling tensors, nuclear spins, and orientation.

Input (cntd):

Card No.	Columns	Fortran Symbol	Format	Contents
5	1-10	SPIN(I)	F10.5	Nuclear spin
	11-20	G(1,I)	F10.5	A_{11}
	21-30	G(2,I)	F10.5	A_{12}
	31-40	G(3,I)	F10.5	A_{13}
	41-50	G(4,I)	F10.5	A_{22}
	51-60	G(5,I)	F10.5	A_{23}
	61-70	G(6,I)	F10.5	A_{33}

There MUST be 8 cards of type 5 if KALKOD = 2, although some may be blank.

In all cases card type 5 is followed by:

6	1	KGEN	I1	= 0, if a new set of data is to be read. = 1, if the same lines are to be plotted with their linewidths incremented by WIDINC.
	2-10	WIDINC	F10.5	linewidth increment, in cm.

Card type 6 may be repeated as often as desired. The last card for each spectrum to be plotted must therefore be blank.

Output:

(1) Title of plot

(2) Phi, Theta, Xmax, Height

(3) Nuclear spin, Hyperfine splitting

(4) Derivative

(5) Number of lines

(6) Line position, width, relative intensity

(7) Lineshape

(8) Punched cards to be used as input for the autoplotter.

Capacity: Capacity is limited to 8 nuclei with nonzero nuclear spins for each of up to eight species, if line-positions are to

be generated. If line positions are input the DIMENSION statements limit capacity to 200 lines, and 75 cm plots.

Limitations: The calculation of line positions is only to a first order approximation.

```
C*************************************************************************
C
C     PROGRAM LINPLT
C
C*************************************************************************
C
C     PURPOSE-TO COMPUTE SPECTRA OF SUPERIMPOSED LINES AND TO PUNCH
C     CARDS TO BE USED AS INPUT FOR THE 1627 PLOTTER
C
C     INPUT-
C     CARD 1   COLUMNS 1-80 TITLE IN A FORMAT
C     CARD 2   COLUMNS 1-2 SHAPE IN I2 FORMAT
C     SHAPE=1   LORENTZIAN LINESHAPE
C          =2   GAUSSIAN LINESHAPE
C              COLUMNS 3-4 DERIV IN I2 FORMAT
C     DERIV=0       ABSORPTION
C     DERIV=1       FIRST DERIVATIVE
C     DERIV=2       SECOND DERIVATIVE
C              COLUMNS 5-6 PHASE IN I2 FORMAT
C     PHASE=1  POSITIVE TO LEFT
C     PHASE=2  POSITIVE TO RIGHT
C              COLUMNS 7-8 SPECYS IN I2 FORMAT (WHEN KALKOD EQ 1 OR 2)
C     COLUMN 10   KPLOT
C     COLUMN 10 IS 0 IF ONLY A PRINTED SPECTRUM IS REQUIRED
C     COLUMN 10 IS 1 IF BOTH PLOT AND PRINTED SPECTRUM ARE REQUIRED
C     COLUMN 10 IS 2 IF ONLY A PLOT IS REQUIRED
C              COLUMNS 11-20 PHI IN F10.5 FORMAT
C              COLUMNS 21-30 THETA IN F10.5 FORMAT
C              COLUMNS 31-40 HEIGHT IN F10.5 FORMAT
C              COLUMNS 41-50 XMAX IN F10.5 FORMAT
C     HEIGHT AND XMAX ARE IN CM
C
C     CARD 3    DISPL(I) AND RELINT(I) IN 16F5.2 FORMAT
C          DISPL(I)
C          THE DISPLACEMENT (IN CM) OF THE CENTRE FOR EACH SPECIES I
C          RELINT(I)
C          THE RELATIVE INTENSITY OF EACH SPECIES I
C
C     CARD 4  KALKOD IN COLUMN 1 WYDTH IN COLUMNS 2-11, SCANN IN COLUMNS
C     12-21 (GAUSS PER 40 CM)
C
C     IF KALKOD IS 0 -LINE PARAMETERS ARE INPUT AND WYDTH IS IGNORED
C     CARDS 5 ON        THIS CARD IS REPEATED FOR EACH LINE
C              COLUMN 1 BLANK
C              COLUMNS 2-10 XCENTR IN  F9.5 FORMAT (IN CM)
C              COLUMNS 11-20 FNTENS IN F10.5 FORMAT
C              COLUMNS 21-30 W IN F10.3 FORMAT(IN CM)
C                IF W=0 THEN WIDTH(I) IS SET EQUAL TO WYDTH
C     END OF DATA IS SIGNIFIED BY A NON-ZERO NUMBER IN COLUMN 1
C
C     IF KALKOD=1   - LINE POSITIONS ARE CALCULATED FROM INPUT
C     NUCLEAR SPINS AND HYPERFINE COUPLING CONSTANTS(ISOTROPIC)
C     CARD 5
C     SPIN(I) IN F3.1 FORMAT IN COLUMNS 1,11,21,ETC
C     HFSPLT(I)  IN F7.3 FORMAT IN COLUMNS 4-10,14-20,24-30, ETC
C     UP TO EIGHT ATOMS MAY BE ACCOMMODATED
C
C      IF KALKOD=2   - HYPERFINE TENSORS IN LABORATORY COORDINATES ARE
C     INPUT AND THE PROJECTIONS ARE CALCULATED
C     CARDS 5 ON
C     SPIN(I) IN COLUMNS 1-10
C      A11,A12,A13,A22,A23,A33 IN COLUMNS 11-20,21-30,31-40( ETC
C      THERE MUST BE 8 OF THESE CARDS, SOME MAY BE BLANK
C
C     CARDS 5 ARE REPEATED FOR ALL SPECIES
C
C     CARD 6 -COMMON TO ALL OPTIONS
C     COLUMN 1- KGEN - IF KGEN IS 1 THE SAME LINES ARE PLOTTED WITH
C     THEIR WIDTHS INCREMENTED BY WIDINC
C     COLUMNS 2-10   WIDINC IN CM
```

```
C    IF KGEN IS 0 A NEW SET OF DATA IS READ
C
C    FORTRAN PROGRAM NUMBER 1 IS ASSIGNED TO THE WORKING FILE
C    FORTRAN PROGRAM NUMBER 5 IS ASSIGNED TO THE CARD READER
C    FORTRAN PROGRAM NUMBER 6 IS ASSIGNED TO THE LINE PRINTER
C    FORTRAN PROGRAM NUMBER 7 IS ASSIGNED TO THE CARD PUNCH
C
C    ***********************************************************************
C
     DIMENSION SAVE(5000),DISPL(20),XCENTR(200),WIDTH(200),FNTENS(200)
     DIMENSION NUMBER(20),SPIN(20),HFSPLT(20),M(20),EM(20,10)
     DIMENSION GG(6,10),G(6,8),RELINT(20)
     DIMENSION FONE(3500),XSAVE(3500)
     DIMENSION COLECT(200),COL(2),KOLECT(3500)
     LOGICAL*1 ILABEL(30),TITLE(90),JLABEL(30)
     INTEGER   SHAPE,DERIV,PHASE,SPECYS
     EQUIVALENCE (ILABEL(1),TITLE(1))
     EQUIVALENCE (JLABEL(1),TITLE(31))
     DATA COL/' ','.'/
C
C
 601 FORMAT(80A1)
4000 FORMAT(4I2,I2,4F10.5)
4001 FORMAT(16F5.2)
4005 FORMAT(I1,F9.5,2F10.5,I1)
4010 FORMAT(80A1)
4012 FORMAT('0',80A1)
4015 FORMAT('0','PHI=',F10.3,20X,'THETA=',F10.5//' ','XMAX=',F10.5,'HEI
    1GHT=',F10.5)
4020 FORMAT('0','FIRST DERIVATIVE IS PLOTTED')
4025 FORMAT('0','ABSORPTION IS PLOTTED')
4026 FORMAT('0','SECOND DERIVATIVE IS PLOTTED')
4030 FORMAT('0','NUMBER OF LINES IS',I3)
4035 FORMAT(' ',F10.3,6X,F10.3, 6X,F10.3)
4036 FORMAT('0 CENTRE OF LINE  LINEWIDTH     RELATIVE INTENSITY'//'
    1     CM                 CM')
4040 FORMAT('0','LORENTZIAN LINESHAPE')
4045 FORMAT('0','GAUSSIAN LINESHAPE')
4050 FORMAT(' ','SAVE(',I5,')=',3(E12.6))
4055 FORMAT(' ',100A1)
4060 FORMAT(I1,F10.5)
4065 FORMAT(I1,F9.5,F10.5)
4070 FORMAT(' ','NUCLEUS',I3,6X,'NUCLEAR SPIN',F6.2,6X,'HYPERFINE SPLIT
    1TING',F10.5,'G')
4075 FORMAT(7F10.5)
C
C
1000 READ(5,4010,END=1001) (TITLE(I),I=1,80)
     READ(5,4000) SHAPE,DERIV,PHASE,SPECYS,KPLOT,PHI,THETA,HEIGHT,XMAX
     READ(5,4001) (DISPL(I),RELINT(I),I=1,8)
     DO 196 I=1,8
     RELIN=RELINT(I)
 196 IF(RELIN.LE.0.0) RELINT(I)=1.0
     WRITE(6,4012) (TITLE(I),I=1,80)
     WRITE(6,4015) PHI,THETA,XMAX,HEIGHT
     XMAX=XMAX*100.0/2.54
     ILONG=XMAX+400.0
     HEIGHT=HEIGHT*100.0/2.54
     PHI=PHI/57.29578
     THETA=THETA/57.29578
     IF(KPLOT.EQ.0) GO TO 3
     YPLOT1=1.0
     KPLOT1=1
     JJ=1+KPLOT1
     GO TO 4
   3 KPLOT1=12
     JJ=1+KPLOT1
     YPLOT1=12.0
   4 CONTINUE
     DERIV=DERIV+1
```

```
      READ(5,4065) KALKOD,WYDTH,SCAN
      GPERIN=SCAN*0.0635
      IF(KALKOD.EQ.1) GO TO 200
      IF(KALKOD.EQ.2) GO TO 197
      J=1
      WRITE(6,4036)
   15 READ(5,4005) IFILE,XCENTR(I),FNTENS(I),W,LPHASE
      IF(LPHASE.EQ.1) FNTENS(I)=-FNTENS(I)
      IF(W.EQ.0.0)  WIDTH(I)=WYDTH
      IF(W.NE.0.0) WIDTH(I)=W
      IF(IFILE.NE.0) GO TO 166
      WRITE(6,4035) XCENTR(I),WIDTH(I),FNTENS(I)
      WIDTH(I)=WIDTH(I)*100.0/2.54
      XCENTR(I)=XCENTR(I)*100.0/2.54
      I=I+1
      GO TO 15
  166 IND=I-1
      GO TO 16
C
C     CALCULATE LINE POSITIONS FROM INPUT TENSORS
C
  197 DO 207 KX=1,SPECYS
      DO 198 L=1,8
      READ(5,4075) SPIN(L),(G(J,L),J=1,6)
      GG(1,L)=G(1,L)*G(1,L)+G(2,L)*G(2,L)+G(3,L)*G(3,L)
      GG(2,L)=(G(1,L)*G(2,L)+G(2,L)*G(4,L)+G(3,L)*G(5,L))*2.0
      GG(3,L)=G(1,L)*G(3,L)+G(2,L)*G(5,L)+G(3,L)*G(6,L)
      GG(4,L)=G(2,L)*G(2,L)+G(4,L)*G(4,L)+G(5,L)*G(5,L)
      GG(5,L)=G(2,L)*G(3,L)+G(4,L)*G(5,L)+G(5,L)*G(6,L)
      GG(6,L)=G(3,L)*G(3,L)+G(5,L)*G(5,L)+G(6,L)*G(6,L)
  198 HFSPLT(L)=SQRT(SIN(THETA)**2*(GG(1,L)*COS(PHI)**2+GG(2,L)*COS(PHI)
     1*SIN(PHI)+GG(4,L)*SIN(PHI)**2)+2.0*SIN(THETA)*COS(THETA)*(GG(3,L)*
     2COS(PHI)+GG(5,L)*SIN(PHI))+GG(6,L)*COS(THETA)**2)
      GO TO 199
  200 DO 207 KX=1,SPECYS
      READ(5,201) SPIN(1),HFSPLT(1),SPIN(2),HFSPLT(2),SPIN(3),HFSPLT(3),
     1SPIN(4),HFSPLT(4),SPIN(5),HFSPLT(5),SPIN(6),HFSPLT(6),SPIN(7),HFSP
     2LT(7),SPIN(8),HFSPLT(8)
  201 FORMAT(8(F3.1,F7.2))
  199 DO 5 I=1,8
      IF(SPIN(I).EQ.0.0) GO TO 6
    5 WRITE(6,4070) I,SPIN(I),HFSPLT(I)
    6 DO 203 I=1,8
      HFSPLT(I)=HFSPLT(I)/GPERIN
      HFSPLT(I)=HFSPLT(I)*100.0
      M(I)=2.0*SPIN(I)+1.05
      MX=M(I)
      DO 203 J=1,MX
      EM(I,J)=-SPIN(I)
  203 SPIN(I)=SPIN(I)-1.0
      M1=M(1)
      M2=M(2)
       M3=M(3)
      M4=M(4)
      M5=M(5)
      M6=M(6)
      M7=M(7)
      M8=M(8)
      IND=1
      WRITE(6,4036)
      DO 204 L1=1,M1
      DO 204 L2=1,M2
      DO 204 L3=1,M3
      DO 204 L4=1,M4
      DO 204 L5=1,M5
      DO 204 L6=1,M6
      DO 204 L7=1,M7
      DO 204 L8=1,M8
      XCENTR(IND)=(XMAX/2.0+HFSPLT(1)*EM(1,L1)+HFSPLT(2)*EM(2,L2)+
     1HFSPLT(3)*EM(3,L3)+HFSPLT(4)*EM(4,L4)                    +HFSPLT(5)
```

```
     2*EM(5,L5)+HFSPLT(6)*EM(6,L6)+HFSPLT(7)*EM(7,L7)+HFSPLT(8)*EM(8,L8)
     3+DISPL(KX))*0.0254
      FNTENS(INO)=1.0*RELINT(KX)
      WRITE(6,4035) XCENTR(INO),WYDTH,F
      XCENTR(INO)=XCENTR(INO)/0.0254
  204 INO=INO+1
  207 CONTINUE
      INO=INO-1
      DO 205 J=1,INO
  205 WIDTH(J)=WYDTH*100.0/2.54
   16 IF(DERIV.EQ.1) GO TO 20
      IF(DERIV.EQ.3) GO TO 21
      WRITE(6,4020)
      GO TO 25
   20 WRITE(6,4025)
      GO TO 25
   21 WRITE(6,4026)
   25 WRITE(6,4030) INO
      NOPTS=XMAX+1.0
      DO 35 J=1,NOPTS
   35 SAVE(J)=0.0
      GO TO(40,45), SHAPE
   40 WRITE(6,4040)
C
C     CALCULATE LINE SHAPE FUNCTIONS
C     CALCULATE  INTENSITY FUNCTION
C
C     LORENTZIAN LINESHAPE
C
      DO 44 K=1,INO
      W=WIDTH(K)**3
      W1=4.0/(3.0*WIDTH(K)**2)
      W4=3.0*WIDTH(K)
      XFIN=W4
      IF(XFIN+XCENTR(K)-XMAX) 442,443,443
  443 XFIN=XMAX-XCENTR(K)
  442 X=XCENTR(K)-W4
      IF(X) 444,445,445
  444 X=0.0
      J=1
      GO TO 448
  445 J=X/YPLOT1
      J=J*KPLOT1+1
      X=J-1
  448 Y=X-XCENTR(K)
   41 IF((W*(1.0+Y*W1)**2*FNTENS(K)).LE.1.0E35) GO TO 447
      FONE(J)=0.0
      GO TO 446
  447 CONTINUE
      GO TO(42,43,51),DERIV
   42 FONE(J)=1.0/(1.0+Y**2*W1)/WIDTH(K)*FNTENS(K)
      SAVE(J)=SAVE(J)+FONE(J)
      GO TO 446
   43  FONE(J)=Y/(W*(1.0+Y**2*W1)**2)*FNTENS(K)
      SAVE(J)=SAVE(J)+FONE(J)
      GO TO 446
   51   FONE(J)=(1.0-3.0*W1*Y**2)/(W*(1.0+W1*Y**2)**3)*FNTENS(K)
      SAVE(J)=SAVE(J)+FONE(J)
  446 Y=Y+YPLOT1
      J=J+KPLOT1
      IF(Y.LE.XFIN) GO TO 41
   44 CONTINUE
      GO TO 55
   45 WRITE(6,4045)
C
C     GAUSSIAN LINESHAPE
C
      DO 50 K=1,INO
      W=WIDTH(K)**3
      W1=-2.0/WIDTH(K)**2
```

```
      W4=3.0*WIDTH(K)
      XFIN=W4
      IF(XFIN+XCENTR(K)-XMAX) 542,543,543
  543 XFIN=XMAX-XCENTR(K)
  542 X=XCENTR(K)-W4
      IF(X) 544,545,545
  544 X=0.0
      J=1
      GO TO 548
  545 J=X/YPLOT1
      J=J*KPLOT1+1
      X=J-1
  548 Y=X-XCENTR(K)
  549 W2=W1*Y**2
      W3=EXP(W2)
   46 IF(W3.GT.1.0E-34) GO TO 449
      FONE(J)=0.0
      GO TO 49
  449 CONTINUE
      GO TO(47,48,52),DERIV
   47 FONE(J)=FNTENS(K)/WIDTH(K)*W3
      SAVE(J)=SAVE(J)+FONE(J)
      GO TO 49
   48 FONE(J)=Y/W*W3*FNTENS(K)
      SAVE(J)=SAVE(J)+FONE(J)
      GO TO 49
   52 IF(ABS(2.0*W1*Y**2+1.0).LE.1.0E-20) GO TO 552
      FONE(J)=FNTENS(K)/W*W3*(1.0+2.0*W2)
      SAVE(J)=SAVE(J)+FONE(J)
      GO TO 49
  552 FONE(J)=0.0
   49 Y=Y+YPLOT1
      J=J+KPLOT1
      IF(Y.LE.XFIN) GO TO 549
   50 CONTINUE
C
C     SCALE SPECTRUM AMPLITUDE
C
   55 FMAX=SAVE(1)
      DO 60 J=JJ,NOPTS,KPLOT1
      IF(FMAX.GT.SAVE(J)) GO TO 60
      FMAX=SAVE(J)
   60 CONTINUE
      FMIN=SAVE(1)
      DO 65 J=JJ,NOPTS,KPLOT1
      IF(FMIN.LE.SAVE(J)) GO TO 65
      FMIN=SAVE(J)
   65 CONTINUE
      DO 70 J=1,NOPTS,KPLOT1
   70 SAVE(J)=SAVE(J)/(FMAX-FMIN)*HEIGHT
      IF(PHASE.NE.1) GO TO 73
      DO 71 J=1,NOPTS,KPLOT1
   71 SAVE(J)=-SAVE(J)
   73 CONTINUE
C
C    PLOT ON LINEPRINTER EVERY 12TH POINT
C
      DO 74 J=1,NOPTS
   74 KOLECT(J)=(SAVE(J)+500.0)/10.0
      READ(5,4060) KGEN,WIDINC
      IF(KPLOT.EQ.2) GO TO 72
      DO 85 J=1,NOPTS,12
      DO 80 L=1,100
      IF(L.EQ.KOLECT(J)) GO TO 75
      COLECT(L)=COL(1)
      GO TO 80
   75 COLECT(L)=COL(2)
   80 CONTINUE
   85 WRITE(6,4055) (COLECT(KK),KK=1,100)
      IF(KPLOT.EQ.1) GO TO 72
```

```
   88 IF(KGEN.EQ.0) GO TO 1000
      DO 87 KI=1,INO
   87 WIDTH(KI)=WIDTH(KI)+WIDINC*100.0/2.54
      GO TO 25
   72 NOLOC=NOPTS-1
C
C     PLOT ON AUTOPLOTTER
C
      CALL AINIT(ILONG)
      CALL ALAB(100,110,ILABEL,30,3,4)
      CALL ALAB(180,110,JLABEL,30,3,4)
      DO 502 I=1,NOLOC
      GO TO(501,500,501),DERIV
  500 SAVE(I)=SAVE(I)+550.0
      GO TO 502
  501 GO TO(512,511),PHASE
  511 SAVE(I)=SAVE(I)+700.0
      GO TO 502
  512 SAVE(I)=SAVE(I)+300.0
  502 XSAVE(I)=I
      CALL ALINE(XSAVE,SAVE,NOLOC,-200.0,0.0,100.0,100.0,1)
      CALL AEND
      GO TO 88
 1001 STOP
      END
```

APPENDIX 4

A. Anisotropy Curves

A computer program, ROADMAP, was written to plot the variation of the line positions as the crystal orientation in the magnetic field was varied in three orthogonal planes.

Plotting of Anisotropy Curves

(ROADMAP)

Purpose: To plot the variation of line positions as a function of crystal orientation in the magnetic field.

Contents: The main program, ROADMAP, and the plotting package, PLOTAA.

Library Routines Used: SQRT, SIN, COS.

Language: IBM System/360 Fortran IV (BCD).

Method: This program generates line positions by a first order calculation using input g- and hyperfine coupling tensors for angles at five degree intervals in three orthogonal planes defined by the tensorial axis system. These are scaled and plotted on the line printer and, if desired, on the autoplotter. The effect of anisotropy of g on the A tensors is included.

Input:

Card No.	Columns	Fortran Symbol	Format	Contents
1	1-80	TITLE(I)	80A1	Title, columns 1-30 are plotted.
2	1-80	TITLE(I)	80A1	Title, all columns are plotted.
3	1-10	GSCAN	F10.3	Scale of plot, in gauss per 40 cm.
	11-20	SCALE	F10.3	An additional multiplicative scaling factor

Input (cntd):

Card No.	Columns	Fortran Symbol	Format	Contents
4	1	INDEX	I1	left blank
	2	JNDEX	I1	= 9, for the last card of each species except the final species. = 0, otherwise.
	3	KNDEX	I1	= 1, if a punched output for plotting is required. = 0, otherwise.
	4-10	SPIN(J)	F7.3	nuclear spin of atom J.
	11-20	G(J,1,K)	F10.4	The elements of the g- or hyperfine tensor in the order $g_{11}, g_{12}, g_{13}, g_{22}, g_{23}, g_{33}$ for atom J of species K.
	21-30	G(J,2,K)		
	31-40	G(J,3,K)		
	41-50	G(J,4,K)		
	51-60	G(J,5,K)		
	61-70	G(J,6,K)		

Card type 4 is repeated for all tensors. The g-tensor must come first for each species, in which case SPIN(J) is disregarded.

This complete set of cards of type 4 is repeated for all species, with the nuclei in the same order each time for each crystallographically inequivalent site. Completely different species may be dealt with by using more cards than are necessary and setting some of the tensors to zero.

A maximum of six species may be used. End of data is signified by a 1 in column 1 but column 3 must contain the appropriate value of KNDEX.

Output:

(1) Title

(2) Scaling factors

(3) G-tensor

(4) A-tensors

(5) The anisotropy curves on the lineprinter (12" wide)

(6) Punched cards to be used as input to the autoplotter.

Capacity: A maximum of six inequivalent species each with a maximum of nine nuclear hyperfine couplings may be used provided however that the total number of lines does not exceed 100.

Limitations: Line positions are calculated without taking into account the nuclear Zeeman interaction.

```
C
C     ************************************************************************
C
C     PROGRAM ROADMAP
C
C     ************************************************************************
C
C     PURPOSE-
C     TO PLOT THE LINE POSITIONS FOR ALL ANGLES IN THREE ORTHOGONAL PLAN
C
C     ************************************************************************
C
C     INPUT
C
C     CARD 1 TITLE(COLUMNS 1-30 PLOTTED)
C     CARD 2     TITLE (PLOTTED)
C     CARD 3      SCALE FACTORS
C     CARD 4CONTAINS CODE NUMBERS, SPIN(I), AND THE TENSOR ELEMENTS
C     THERE ARE CARDS OF THIS TYPE FOR EACH NUCLEUS AND ONE FOR THE G TE
C
C     FORTRAN PROGRAM NUMBER 1 IS ASSIGNED TO THE WORKING FILE
C     FORTRAN PROGRAM NUMBER 5 IS ASSIGNED TO THE CARD READER
C     FORTRAN PROGRAM NUMBER 6 IS ASSIGNED TO THE LINE PRINTER
C     FORTRAN PROGRAM NUMBER 7 IS ASSIGNED TO THE CARD PUNCH
C
C     ************************************************************************
C
      DIMENSION POSITI(100),X(100),Y(100),XX(100,50)
      DIMENSION             G(10,6,6),SPIN(10),G2(10,6,6),EM(10,10)
      DIMENSION COLECT(500),COL(46),M(10),GO(10,6),POSITN(100)
      DATA COL/' ','A','B','C','D','E','F','G','H','I','J','K','L','M','
     1N','O','P','Q','R','S','T','U','V','W','X','Y','Z','1','2','3','4'
     2,'5','6','7','8','9','*',',','=','+','$','-','(','(',')','.'/
      LOGICAL*1 LABEL1(9)/'A-B PLANE'/
      LOGICAL*1 LABEL2(9)/'B-C PLANE'/
      LOGICAL*1 LABEL3(9)/'A-C PLANE'/
      LOGICAL*1 LABEL4(30),LABEL5(80),TITLE(160)
      EQUIVALENCE (LABEL4(1),TITLE(1)),(LABEL5(1),TITLE(81))
C
C
   10 FORMAT(80A1,/80A1)
   20 FORMAT('0',80A1,/'0',80A1)
   30 FORMAT(3I1,F7.3,6F10.4)
   40 FORMAT('0','G-TENSOR'/'0',3F10.4/' ',10X,2F10.4/' ',20X,F10.4/'0',
     1'A TENSORS')
   50 FORMAT('0','NUCLEAR SPIN = ',F6.2/' ',3F10.4/' ',10X,2F10.4/' ',20
     1X,F10.4)
   70 FORMAT(3F10.3)
   80 FORMAT('0',F10.2,'GAUSS PER 40CM'/'0','SCALE FACTOR OF',F10.4)
   90 FORMAT('0',117A1,I3)
  110 FORMAT('0',//60X,'A-B PLANE'//)
  120 FORMAT('0',//60X,'B-C PLANE'//)
  130 FORMAT('0',//60X,'A-C PLANE'//)
C
C
    1 READ(5,10,END=1001) (TITLE(I),I=1,160)
      WRITE(6,20) (TITLE(I),I=1,160)
      IANGLE=0
      READ(5,70) GSCAN,SCALE
      GPERIN=GSCAN*0.0625
      WRITE(6,80)GSCAN,SCALE
      DO 9 J=1,10
      DO 8 K=1,6
    8 GO(J,K)=0.0
      DO 9 I=1,10
    9 EM(I,J)=0.0
      K=1
      J=1
   11 READ(5,30) INDEX,JNDEX,KNDEX,SPIN(J),(G(J,I,K),I=1,6)
      IF(K.GE.JNDEX) GO TO 13
```

```
      K=K+1
      J=1
      GO TO 11
   13 I=J+1
      IF(INDEX.EQ.0) GO TO 11
      NONUC=J-2
      WRITE(6,40) ((G(1,I,L),I=1,6),L=1,K)
      NORAD=K
      DO 31 J=2,NONUC
   31 WRITE(6,50) SPIN(J),((G(J,I,L),I=1,6),L=1,NORAD)
      DO 41 J=2,NONUC
      M(J)=2.0*SPIN(J)+1.05
      MX=M(J)
      DO 41 I=1,MX
      EM(J,I)=-SPIN(J)
   41 SPIN(J)=SPIN(J)-1.0
      M2=M(2)
      M3=M(3)
      M4=M(4)
      M5=M(5)
      M6=M(6)
      M7=M(7)
      M8=M(8)
      M9=M(9)
      M10=M(10)
      KODE=1
      WRITE(6,110)
      IF(KNDEX.EQ.0) GO TO 42
C
CC    INITIALISE PLOTTER
C
      CALL AINIT(400)
      CALL ALAB(100,100,LABEL4,30,3,4)
      CALL ALAB(200,100,LABEL5,80,1,4)
      CALL AEND
      CALL AINIT(1400)
      CALL AGRID(150,50,1,9,1200,100,1,2)
      CALL ASCA(1,50,0,100,0,20,9,2,2)
      CALL ALAB(650,10,LABEL1,9,2,2)
   42 DEGINC=5.0/57.29578
      THETA=90.0/57.29578
      PHI=0.0
C
CC    CALCULATE LINE POSITIONS
C
   59 DO 61 K=1,NORAD
      DO 60 J=1,NONUC
      G2(J,1,K)=G(J,1,K)**2+G(J,2,K)**2+G(J,3,K)**2
      G2(J,2,K)=G(J,1,K)*G(J,2,K)+G(J,2,K)*G(J,4,K)+G(J,3,K)*G(J,5,K)
      G2(J,3,K)=G(J,1,K)*G(J,3,K)+G(J,2,K)*G(J,5,K)+G(J,3,K)*G(J,6,K)
      G2(J,4,K)=G(J,2,K)**2+G(J,4,K)**2+G(J,5,K)**2
      G2(J,5,K)=G(J,2,K)*G(J,3,K)+G(J,4,K)*G(J,5,K)+G(J,5,K)*G(J,6,K)
   60 G2(J,6,K)=G(J,3,K)**2+G(J,5,K)**2+G(J,6,K)**2
      J=1
   61 GO(J,K)=SQRT(SIN(THETA)**2*(G2(J,1,K)*COS(PHI)**2+2.0*G2(J,2,K)*SI
     1N(PHI)*COS(PHI)+G2(J,4,K)*SIN(PHI)**2)+2.0*SIN(THETA)*COS(THETA)*(
     2G2(J,3,K)*COS(PHI)+G2(J,5,K)*SIN(PHI))+G2(J,6,K)*COS(THETA)**2)
      ELL=SIN(THETA)*COS(PHI)
      EMM=SIN(THETA)*SIN(PHI)
      ENN=COS(THETA)
      ALPHA1=G(1,1,K)*ELL+G(1,2,K)*EMM+G(1,3,K)*ENN
      ALPHA2=G(1,2,K)*ELL+G(1,4,K)*EMM+G(1,5,K)*ENN
      ALPHA3=G(1,3,K)*ELL+G(1,5,K)*EMM+G(1,6,K)*ENN
      DO 63 J=2,NONUC
      DO 63 K=1,NORAD
   63 GO(J,K)=SQRT(G2(J,1,K)*ALPHA1**2+G2(J,2,K)*2.0*ALPHA1*ALPHA2+2.0*G
     12(J,3,K)*ALPHA1*ALPHA3+G2(J,4,K)*ALPHA2**2+2.0*G2(J,5,K)*ALPHA2*AL
     2PHA3+G2(J,6,K)*ALPHA3**2)/GO(1,K)
      DO 62 K=1,NORAD
   62 GO(1,K)=6600.0/GO(1,K)-3300.0
```

```
      INO=1
      DO 72 J=1,120
   72 COLECT(J)=COL(1)
      DO 81 L2=1,M2
      DO 81 L3=1,M3
      DO 81 L4=1,M4
      DO 81 L5=1,M5
      DO 81 L6=1,M6
      DO 81 L7=1,M7
      DO 81 L8=1,M8
      DO 81 L9=1,M9
      DO 81 L10=1,M10
      DO 81 K=1,NORAD
      POSITN(INO)=(GO(1,K)+GO(2,K)*EM(2,L2)+GO(3,K)*EM(3,L3)+GO(4,K)*EM(
     14,L4)+GO(5,K)*EM(5,L5)+GO(6,K)*EM(6,L6)+GO(7,K)*EM(7,L7)+GO(8,K)*E
     2M(8,L8)+GO(9,K)*EM(9,L9)+GO(10,K)*EM(10,L10))/GPERIN*10.0*SCALE+55
      L=POSITN(INO)
      IF(KNDEX.EQ.0) GO TO 84
      IAN=IANGLE/5
      POSITI(INO)=10.0*POSITN(INO)+100.0
      LLL=POSITI(INO)
      XX(INO,IAN)=LLL
   84 INO=INO+1
      LL=INO
      IF(INO.GT.46) LL=INO-45
   81 COLECT(L)=COL(LL)
      WRITE(6,90)(COLECT(I),I=1,117),IANGLE
      GO TO(111,121,131),KODE
  111 IF(PHI.GT.3.15158) GO TO 101
      IANGLE=IANGLE+5
      PHI=PHI+DEGINC
      GO TO 59
  101 KODE=2
      IANGLE=0
      WRITE(6,120)
      IF(KNDEX.EQ.0) GO TO 102
   85 I=1
      DO 83 J=1,INO
      DO 82 K=1,37
      X(I)=XX(J,K)+150.0
      Y(I)=5*K
   82 I=I+1
      CALL ALINE(X,Y,37,0.0,-5.0,100.0,20.0,1)
   83 I=1
      GO TO(366,366,367,368),KODE
  366 CALL AEND
      CALL AINIT(1400)
      CALL AGRID(150,50,1,9,1200,100,1,2)
      CALL ASCA(1,50,0,100,0,20,9,2,2)
      CALL ALAB(650,10,LABEL2,9,2,2)
  102 PHI=90.0/57.29578
      THETA=0.0
      GO TO 59
  121 IF(THETA.GT.3.15158) GO TO 103
      IANGLE=IANGLE+5
      THETA=THETA+DEGINC
      GO TO 59
  103 KODE=3
      IANGLE=0
      WRITE(6,130)
      IF(KNDEX.EQ.0) GO TO 104
      GO TO 85
  367 CALL AEND
      CALL AINIT(1400)
      CALL AGRID(150,50,1,9,1200,100,1,2)
      CALL ASCA(1,50,0,100,0,20,9,2,2)
      CALL ALAB(650,10,LABEL3,9,2,2)
  104 PHI=0.0
      THETA=0.0
      GO TO 59
```

```
  131 IF(THETA.GT.3.15158) GO TO 132
      IANGLE=IANGLE+5
      THETA=THETA+DEGINC
      GO TO 59
  132 MODE=4
      IF(KNDEX.EQ.0) GO TO 133
      GO TO 85
  368 CALL AEND
  133 GO TO 1
 1001 STOP
      END
```

B. Calculation of Direction Cosines

A brief computer program, DIRCOS, was used to calculate the direction cosines of atom-atom directions in the crystal. Data from x-ray crystal structure determinations was used as input and it was possible to transform coordinates and to calculate the direction cosines of lines perpendicular to each atom-atom direction and all of the other atom-atom directions in turn.

Calculation of Direction Cosines

(DIRCOS)

Purpose: To calculate the direction cosines of lines connecting atomic positions and of lines perpendicular to any two such lines. Provision is made for changing the axis system from the crystal axis system.

Contents: One main program, DIRCOS.

Library Routines Used: SQRT.

Language: IBM System/360 Fortran IV (BCD).

Method: This program first converts the fractional coordinates of the atoms to real coordinates and then changes the axis system as specified by an input rotation matrix. The direction cosines are calculated in the new axis system for the lines joining all pairs of atoms. The perpendicular to each pair of these lines may also be calculated.

Input:

Card No.	Columns	Fortran Symbol	Format	Contents
1	1-80	TITLE(I)	80A1	the title of the calculation
2A	1-10	P(1,1)	F10.5	The rotation matrix defining
	11-20	P(2,1)	F10.5	the new a*-axis in terms of
	21-30	P(3,1)	F10.5	the crystal a, b and c-axes.
2B	similarly for the b*-axis			
2C	similarly for the c*-axis			
3	1-10	A	F10.5	
	11-20	B	F10.5	
	21-30	C	F10.5	
	31-40	ALPHA	F10.5	the unit cell parameters
	41-50	BETA	F10.5	
	51-60	GAMMA	F10.5	
	61	KODE	I1	= 1, if normals are to be calculated.
				= 0, otherwise.
4	1	IFILE	I1	left blank
	2-10	X(I)	F9.5	the fractional atomic
	11-20	Y(I)	F10.5	coordinates of atom I
	21-30	Z(I)	F10.5	
	31-34	ATOM(I)	A4	an atomic label

Cards type 4 are repeated for each atom position. End of data is signified by a 1 in column 1.

Output:

(1) Title

(2) The rotation matrix

(3) The unit cell parameters

(4) The fractional atomic coordinates

(5) The computed direction cosines

Capacity: The capacity is limited by the DIMENSION statement

to 250 atom positions.

Limitations: The new axis system, a*b*c*, must be orthogonal.

```
C
C    ***********************************************************************
C
C    PROGRAM DIRCOS
C
C    ***********************************************************************
C
C    PURPOSE-
C
C    TO CALCULATE THE DIRECTION COSINES OF LINES CONNECTING ATOMIC
C    POSITIONS
C
C    ***********************************************************************
C
C    INPUT
C    CARD 1        THE TITLE OF THE PROBLEM
C       CARDS 2,2A,2B
C     THE ROTATION MATRIX  OF THE A*,B*,C* AXES IN THAT ORDER ON
C      CONSECUTIVE CARDS IN 3F10.5 FORMAT
C    CARD 3    A,B,C,ALPHA,BETA,GAMMA IN 6F10.5 FORMAT,KODE IN I1 FORMAT
C    CARD 4      LEAVE COLUMN 1 BLANK
C                X(I),Y(I),Z(I), IN COLUMNS 2-10,11-20,21-30
C                A 4 LETTER ATOM IDENTIFICATION LABEL
C     REPEAT CARD TYPE 3 FOR ALL ATOMIC POSITIONS
C      A 1 IN COLUMN1 SIGNIFIES END OF DATA
C
C    FORTRAN PROGRAM NUMBER 5 IS ASSIGNED TO THE CARD READER
C    FORTRAN PROGRAM NUMBER 6 IS ASSIGNED TO THE LINE PRINTER
C
C
C    ***********************************************************************
C
      DIMENSION P(3,3),Q(3,200)
      DIMENSION ATOM(250),TITLE(100),X(250),Y(250),Z(250)
C
105   FORMAT(80A1)
110   FORMAT('0',80A1)
115   FORMAT(6F10.5,I1)
120   FORMAT('0',4X,'A',10X,'B',10X,'C',8X,'ALPHA',8X,'BETA',8X'GAMMA'/'
     1 ',6F10.3)
125   FORMAT(I1,F9.5,2F10.5,A4)
130   FORMAT('0',5X,'ATOM',9X,'X',9X,'Y',9X,'Z')
135   FORMAT(' ',6X,A4,3(2X,F10.5))
140   FORMAT('0','                                          ',A4 ,'      AND      ',
     1A4,'     IS     ',3(F10.5,5X),10X,I5)
160   FORMAT('0','AA=',F9.4,'A+',F9.4,'B+',F9.4,'C')
170   FORMAT('0','BB=',F9.4,'A+',F9.4,'B+',F9.4,'C')
180   FORMAT('0','CC=',F9.4,'A+',F9.4,'B+',F9.4,'C')
190   FORMAT(3F10.5)
200   FORMAT('0','                                                ',I5,'AND',I5,'IS
     1',3(F10.4,6X))
210   FORMAT('0','DIRECTION COSINES BETWEEN'//)
220   FORMAT('0','DIRECTION COSINES OF PERPENDICULAR TO'//)
C
      CALC(D,E,F,G,S,T)=(E*F-G*D)/SQRT((D*T-E*S)**2+(F*T-G*S)**2+(G*D-F*
     1E)**2)
C
   20 READ(5,105,END=1000)  (TITLE(I),I=1,80)
      WRITE(6,110) TITLE
      DO 21 J=1,3
   21 READ(5,190) (P(I,J),I=1,3)
      WRITE(6,160) (P(I,1),I=1,3)
      WRITE(6,170) (P(I,2),I=1,3)
      WRITE(6,180) (P(I,3),I=1,3)
      READ(5,115) A,B,C,ALPHA,BETA,GAMMA,KODE
      WRITE(6,120) A,B,C,ALPHA,BETA,GAMMA
      ALPHA=ALPHA/57.29578
      BETA=BETA/57.29578
      GAMMA=GAMMA/57.29578
      WRITE(6,130)
```

```
      KK=1
      I=1
    1 READ(5,125) IFILE,X(I),Y(I),Z(I),ATOM(I)
      IF(IFILE-1) 10,15,15
   10 WRITE(6,135) ATOM(I),X(I),Y(I),Z(I)
      I=I+1
      GO TO 1
   15 N=I-1
      M=N-1
      WRITE(6,210)
      DO 30 J=1,M
      L=J+1
      DO 30 K=L,N
      XX=(X(J)-X(K))*A
      YY=(Y(J)-Y(K))*B
      ZZ=(Z(J)-Z(K))*C
      DO 97 LL=1,3
   97 Q(LL,KK)=P(1,LL)*XX+P(2,LL)*YY+P(3,LL)*ZZ
      R=SQRT(Q(1,KK)**2+Q(2,KK)**2+Q(3,KK)**2)
      DO 98 LL=1,3
   98 Q(LL,KK)=Q(LL,KK)/R
      WRITE(6,140) ATOM(J),ATOM(K),(Q(LL,KK),LL=1,3),KK
   30 KK=KK+1
      IF(KODE.NE.1) GO TO 20
      KK=KK-2
      WRITE(6,220)
      DO 35 KS=1,KK
      KSS=KS+1
      KJ=KK+1
      DO 35 KT=KSS,KJ
      X1=CALC(Q(3,KS),Q(3,KT),Q(2,KS),Q(2,KT),Q(1,KS),Q(1,KT))
      Y1=CALC(Q(1,KS),Q(1,KT),Q(3,KS),Q(3,KT),Q(2,KS),Q(2,KT))
      Z1=CALC(Q(2,KS),Q(2,KT),Q(1,KS),Q(1,KT),Q(3,KS),Q(3,KT))
   35 WRITE(6,200) KS,KT,X1,Y1,Z1
      GO TO 20
 1000 STOP
      END
```

REFERENCES

1. (i) O'Donnell J.H., Sangster D.F., "Principles of Radiation Chemistry". Edward Arnold Ltd (London), 1970.
   (ii) Spinks J.W.T., Woods R.J., "An Introduction to Radiation Chemistry". John Wiley & Sons, Inc., 1964.
   (iii) "Advances in Radiation Chemistry, V1", edited by Burton M. and Magee J.L. Wiley-Interscience, 1969.
   (iv) Frank J., Rabinovitch E., Trans. Faraday Soc. 70, 120 (1934).
2. Budzinski E.E., Box H.C., J. Phys. Chem. 75, 2564 (1971).
3. Akasaka K., Kominami S., Hatano H., J. Phys. Chem. 75, 3746 (1971).
4. Toriyama K., Iwasaki M., Noda S., Eda B., J. Am. Chem. Soc. 93, 6415 (1971).
5. Box H.C., Freund H.G., Budzinski E.E., J. Chem. Phys. 49, 3974 (1968).
6. Box H.C., Freund H.G., Frank G.W., J. Chem. Phys. 48, 3825 (1968).
7. Box H.C., Budzinski E.E., Gorman T., J. Chem. Phys. 48, 1748 (1968).
8. Box H.C., Freund H.G., J. Chem. Phys. 41, 2571 (1964).
9. Weiner R.F., Koski W.S., J. Am. Chem. Soc. 85, 873 (1963).
10. Box H.C., Freund H.G., Budzinski E.E., J. Chem. Phys. 45, 809 (1966).
11. Moulton G.C., Cernansky B., J. Chem. Phys. 53, 3022 (1970).
12. Bales B.L., Schwartz R.N., Hanna M.W., J. Chem. Phys. 51, 1974 (1969).
13. Bower H., McRae J., Symons M.C.R., J. Chem. Soc. A 2400 (1971).

14. Ayscough P.B., R0y A.K., Tr. Faraday Soc. 63, 1106 (1967).

15. Miyagawa I., Tamura N., Cook J.W. Jr, J. Chem. Phys. 51, 3520 (1969).

16. (i) Carrington A., McLachlan A.D., "Introduction to Magnetic Resonance", Harper and Row and John Weatherhill Inc., 1967.

(ii) Ayscough P.B., "Electron Spin Resonance in Chemistry". Methuen and Co. Ltd, 1967.

(iii) Poole C.P. Jr, Farach H.A., Advan. Mag. Res. 5, 229 (1971).

17. Fraenkel G.K., J. Phys. Chem. 71, 139 (1967).

18. Gordy W., Ard W.B., Shields H., Proc. Natl Acad. Sci. U.S.A. 41, 983 (1955).

19. Luck G.F., Gordy W., J. Am. Chem. Soc. 78, 3240 (1956).

20. Shields H., Gordy W., J. Phys. Chem. 62, 789 (1958).

21. McCormick G., Gordy W., J. Phys. Chem. 62, 790 (1958).

22. Patten F., Gordy W., Proc. Natl Acad. Sci. U.S.A. 46, 1137 (1960).

23. Kurita Y., Gordy W., J. Chem. Phys. 34, 282 (1961).

24. Cipollini E., Gordy W., J. Chem. Phys. 37, 13 (1962).

25. Hahn Y.N., Rexroad H.N., J. Chem. Phys. 38, 1599 (1963).

26. Akasaka K., J. Chem. Phys. 43, 1182 (1965).

27. Kurita Y., Bull. Chem. Soc. Japan 40, 94 (1967).

28. Box H.C., Freund H.G., J. Chem. Phys. 40, 817 (1964).

29. Akasaka K., Ohnishi S., Suita T., Nitta I., J. Chem. Phys. 40, 3110 (1964).

30. Truby F.K., J. Chem. Phys. 40, 2768 (1964).

31. Milliken S.B., Morgan K., Johnsen R.H., J. Phys. Chem. 71, 3238 (1967).

32. Cadena D.G., Rowlands J.R., J. Chem. Soc. B 488 (1968).

33. Almanov G.A., Schastnev P.V., Tsvetkov Yu.D., J. Struct. Chem. 10, 874 (1969).

34. Kurita Y., Gordy W., J. Chem. Phys. 34, 1285 (1961).

35. Griffith O.H., Mallon M.H., J. Chem. Phys. 47, 837 (1967).

36. Henriksen T., "Free Radicals in Biological Systems", ed. Blois M.S. et al. Academic Press, 1961, page 279.

37. Henriksen T., Pihl A., Nature 185, 307 (1960).

38. Henriksen T., Sanner T., Pihl A., Radiation Research 18, 147 (1963); 18, 163 (1963).

39. Henriksen T., J. Chem. Phys. 36, 1258 (1962).

40. Truby F.K., J. Chem. Phys. 36, 2227 (1962).

41. Henriksen T., J. Chem. Phys. 37, 2189 (1962).

42. Truby F.K., MacCallum C., Hesse J.E., J. Chem. Phys. 37, 2777 (1962).

43. Henriksen T., Sanner T., Acta Chem. Scand. 20, 2888 (1966).

44. Box H.C., Freund H.G., Budzinski E.E., J. Chem. Phys. 45, 2324 (1966).

45. Jaseja T.S., Anderson R.S., J. Chem. Phys. 35, 2192 (1961).

46. Bennett J.E., Mile B., Thomas A., Tr. Faraday Soc. 63, 262 (1967).

47. Vedeneyev V.I., Gurvich L.V., Kondrat'yev V.N., Medvedev V.A., Frankevich Ye.L., "Bond Energies and Ionisation Potentials and Electron Affinities", Translated by Scripta Technica Ltd. Edward Arnold Ltd, 1966.

48. Kerr J.A., Chem. Reviews 66, 465 (1966).

49. Hors field A., Morton J.R., Whiffen D.H., Mol. Phys. 5, 115 (1962).

50. Sinclair J.W., Hanna M.W., J. Phys. Chem. 71, 84 (1967).

51. Hors field A., Morton J.R., Whiffen D.H., Mol. Phys. 4, 425 (1961).

52. Morton J.R., Chem. Reviews 64, 453 (1964).

53. Box H.C., Freund H.G., J. Chem. Phys. 44, 2345 (1966).

54. Fujimoto M., Seddon W.A., Smith D.R., J. Chem. Phys. 48, 3345 (1968).

55. Hors field A., Morton J.R., Whiffen D.H., Trans. Faraday Soc. 57, 1657 (1961).

56. Morton J.R., J. Chem. Phys. 41, 2956 (1964).

57. Box H.C., Freund H.G., Budzinski E.E., J. Am. Chem. Soc. 88, 658 (1966).

58. Box H.C., Freund H.G., Budzinski E.E., J. Chem. Phys. 50, 2880 (1969).

59. Ayscough P.B., Roy A.K., Trans. Faraday Soc. 64, 582 (1968).

60. Gvardzhaladze T.L., Korostelenko M.M., Shul'ga S.Z., Ukr. Fiz. Zh. 12, 1104 (1967).

61. Lassmann G., Damerau W., Mol. Phys. 21, 551 (1971).

62. Collins M.A., Whiffen D.H., Mol. Phys. 10, 317 (1965).

63. Morton J.R., J. Am. Chem. Soc. 86, 2325 (1964).

64. Ghosh D.K., Whiffen D.H., J. Chem. Soc. 1869 (1960).

65. Hedberg A., Ehrenberg A., J. Chem. Phys. 48, 4822 (1968).

66. Pasoyan V.G., Kayushin L.P., Pulatova M.K., Biofizika 13, 600 (1968).

67. Shulga S.Z., Ukr. Fiz. Zh. 13, 211 (1968).

68. Lin W.C., McDowell C.A., Mol. Phys. 4, 333 (1961).

69. Sinclair J.W., Hanna M.W., J. Chem. Phys. 50, 2125 (1969).

70. Ghosh D.K., Whiffen D.H., Mol. Phys. 2, 285 (1959).

71. Wardman P., Smith D.R., Can. J. Chem. 49, 1869 (1971).

72. Wardman P., Smith D.R., Can. J. Chem. 49, 1880 (1971).

73. Wood D.E., Lloyd R.V., J. Chem. Phys. 53, 3932 (1970).

74. Lyons A.R., Symons M.C.R., J. Chem. Soc. (Faraday II) 68, 502 (1972).

75. Wood D.E., Lloyd R.V., Pratt D.W., J. Am. Chem. Soc. 92, 4115 (1970).

76. Danen W.C., Kensler T.T., J. Am. Chem. Soc. 92, 5235 (1970).

77. Seddon W.A., Smith D.R., Can. J. Chem. 45, 3083 (1967).

78. Bullock A.T., Burnett G.M., Kerr C.M.L., Eur. Polym. J. 7, 791 (1971).

79. Kashiwagi M., Bull. Chem. Soc. Japan 39, 2051 (1966).

80. Hamrick P.J. Jr, Shields H.W., Parkey S.H., J. Am. Chem. Soc. 90, 5371 (1968).

81. Lontz R.J., Gordy W., J. Chem. Phys. 37, 1357 (1962).

82. Cook R.J., Rowlands J.R., Whiffen D.H., Mol. Phys. 7, 31 (1963).

83. Yonezawa T., Noda I., Kawamura T., Bull. Chem. Soc. Japan 42, 650 (1969).

84. Livingstone R., Zeldes H., J. Chem. Phys. 47, 4173 (1967).

85. Sevilla M.D., J. Phys. Chem. 74, 669 (1970).

86. Smith P., Wood P.B., Can. J. Chem. 44, 3085 (1966).

87. Rogers M.T., Kispert L.D., J. Chem. Phys. 46, 3193 (1967).

88. Yonezawa T., Noda I., Kawamura T., Bull. Chem. Soc. Japan 41, 766 (1968).

89. Shields H.W., Hamrick P.J., Redwine W., J. Chem. Phys. 46, 2510 (1967).

90. Reiss K., Shields H.W., J. Chem. Phys. 50, 4368 (1969).

91. Fox W.M., Smith P., J. Chem. Phys. 48, 1868 (1968).

92. Lund A., Gillbro T., J. Mag. Res. 2, 164 (1970).

93. Lontz R.J., J. Chem. Phys. 45, 1339 (1965).

94. Cyr N., Lin W.C., J. Chem. Soc. D 192 (1967).

95. Cyr N., Lin W.C., J. Chem. Phys. 50, 3701 (1969).

96. Lau P.W., Lin W.C., J. Chem. Phys. 51, 5139 (1969).

97. Lau P.W., Lin W.C., J. Chem. Phys. 54, 823 (1971).

98. Lind G., Kewley R., Can. J. Chem. 49, 2514 (1971).

99. Symons M.C.R., J. Chem. Soc. A. 3205 (1971).

100. Neta P., Fessenden R.W., J. Phys. Chem. 74, 3362 (1970).

101. Lin W.C., Cyr N., Toriyama K., J. Chem. Phys. 56, 6272 (1972).

102. Toriyama K., Lin W.C., J. Phys. Chem. (1972), in press.

103. Rannev N.V., Ozerov R.P., Datt I.D., Kshnyakina A.N., Soviet Phys. Crystall. 11, 177 (1966).

104. Chieh P.C., Subramanian E., Trotter J., J. Chem. Soc. A 179 (1970).

105. Bower H., McRae J., Symons M.C.R., J. Chem. Soc. A 2400 (1971).

106. Hamrick P., Shields H., J. Chem. Phys. 41, 2560 (1964).

107. Cadena D.G., Rowlands J.R., J. Chem. Soc. B. 485 (1968).

108. Shrivastava K.N., Anderson R.S., J. Chem. Phys. 48, 4599 (1968).

109. Reiss K., Gordy W., J. Chem. Phys. 55, 5329 (1971).

110. Hadley S.G., Volman D.H., J. Am. Chem. Soc. 89, 1053 (1967).

111. Ciecierska-Tworek Z., Birrell G.B., Griffith O.H., J. Chem. Phys. 56, 1001 (1972).

112. "Dictionary of Organic Compounds, 4th Edn". Eyre and Spottiswoode Ltd, 1965.

113. Campbell M.J., Grzeskowiak R., J. Chem. Soc. A 396 (1967).

114. Documentation of Molecular Spectroscopy Card File System, Butterworths Scientific Publications.

115. Reference 114, card 16868.

116. Reference 114, card 17303.

117. Boldrini P., Acta Cryst. B27, 860 (1971).

118. (i) Campbell M.J., Grzeskowiak R., J. Inorg. Nucl. Chem. 30, 1865 (1968).

(ii) Reference 114, card 16867.

119. No published melting point of sodium diethyldithiocarbamate could be found in the literature.

120. "Handbook of Chemistry and PHysics, 48th Edn". The Chemical Rubber Co., 1967.

121. Audrieth L.F., Scott, E.S., Kippur P.S., J. Org. Chem. 19, 733 (1954).

122. Braibanti A., Tiripicchio A., Tiripicchio Camellini M., Acta Cryst. B25, 2286 (1969).

123. Mohr E.B., Brezinski J.J., Audrieth L.F., Inorg. Synth. 4, 32 (1953).

124. "Rodd's Chemistry of Carbon Compounds, 2nd Edn", ed. Coffey S. Elsevier, 1964.

125. (i) Pinner A., Ber. 20, 2358 (1887).

(ii) Skinner S., Ruhemann S., J. Chem. Soc. 53, 550 (1888)

(iii) Pellizzari G., Gazz. Chim. Ital. 16, 200 (1886).

126. Zimmer H., Lankin D.C., Horgan S.W., Chem. Reviews 71, 229 (1971).

127. Pilbrow J.A., M.Sc. Hons Thesis, Physics Dept, University of Canterbury, 1960.

128. Faber R.J., Fraenkel G.K., J. Chem. Phys. 47, 2462 (1967).

129. Adams J.Q., Thomas J.R., J. Chem. Phys. 39, 1904 (1964).

130. Peake B.M., Ph.D. Thesis, Chemistry Dept, University of Canterbury , 1971.

131. Weil J.A. Private Communication.

132. Kominami S., J. Phys. Chem. 76, 1729 (1972).

133. Helcké G.A., Fantechi R., J. Chem. Soc. (Faraday II), 912 (1972).

134. Truter M.R., J. Chem. Soc. 163, 997 (1960).

135. Colapietro M., Domenicano A., Vaciago A., J. Chem. Soc., D 572 (1968).

136. Zvonkova Z.V., Povet'eva Z.P., Vozzennikov V.M., Gluskova V.P., Jakovenko V.I., Khvatkina A.N., Acta Cryst. 21, A156 (1966).

137. Domenicano A., Vaciago A., private communication.

138. page 165, reference 16(ii).

139. Akasaka K., J. Chem. Phys. 45, 90 (1966).

140. Bennett J.E., Mile B., Thomas A., Trans. Faraday Soc. 63, 262 (1967).

141. Nikolov G.St., Tyutyulkov N., Inorg. Nucl. Chem. Letters 7, 1209 (1971).

142. Domiano P., Gasparri G.F., Nardelli M., Sgarabotto P., Acta Cryst. B25, 343 (1969).

143. Andreeti G.D., Domiano P., Gasparri G.F., Nardelli M., Sgarabotto P., Acta Cryst. B26, 1005 (1970).

144. McConnell H.M., Chesnut D.B., J. Chem. Phys. 28, 107 (1958).

145. McConnell H.M., Strathdee J., Mol. Phys. 2, 129 (1959).

146. Rowlands J.R., Mol. Phys. 5, 565 (1962).

147. Rowlands J.R., Whiffen D.H., Nature 193, 61 (1962).

148. Smith W.V., Sorokin P.P., Gelles I.L., Lasher G.J., Phys. Rev. 115, 1545 (1959).

149. Iwasaki F.F., Iwasaki H., Saito Y., Acta Cryst. 23, 64 (1967).

150. Iwasaki F.F., Saito Y., Acta Cryst. 23, 56 (1967).

151. Coppens P., Sabine T.M., Acta Cryst. B25, 2442 (1969).

152. Shimizu H., J. Chem. Phys. 42, 3603 (1965).

153. Nardelli M., Fava G., Giraldi G., Acta Cryst. 19, 1038 (1965).

154. Helcké G.A., Fantechi R., J. Chem. Soc. (Faraday II) 912 (1972).

155. Suntsov E.V., Romanov A.M., Ablov A.V., Gérbeléy N.V., J. Struct. Chem. 11, 401 (1970).

156. Wilkinson B.A., Miyagawa I., J. Chem. Phys. 55, 2177 (1971).

157. Hirasawa R., Kon H., J. Chem. Phys. 56, 4467 (1972).

158. van Rens J.G.M., Keijzers C.P., van Willigen H., J. Chem. Phys. 52, 2858 (1970).

159. Kirmse R., Wartewig S., Windsh W., Hoyer E., J. Chem. Phys. 56, 5273 (1972).

160. Boldrini P., Acta Cryst. B27, 242 (1971).

161. Boldrini P., Acta Crystl B27, 860 (1971).

162. Binnie W.P., Monteath Robertson J., Acta Cryst. 2, 180 (1949).

163. "The Chemistry of Amides", edited by Zabicky J. Interscience, 1970.

164. Cook J.B., Elliott J.P., Wyard S.J., Mol. Phys. 12, 185 (1967).

165. Smith D.R., Seddon W.A., Can. J. Chem. 48, 1938 (1970).

166. McConnell H.M., Heller C., Cole T., Fessenden R.W., J. Am. Chem. Soc. 82, 766 (1960).

167. Boldrini P., Acta Cryst. B27, 860 (1971).

168. Braibanti A., Pellinghelli M.A., Tiripicchio A., Tiripicchio Camellini M., Inorg. Chem. Acta 5, 523 (1971).

169. Koch H.P., J. Chem. Soc. 152, 401 (1949).

170. Garif'yanov N.S., Kozyrev B.M., Semenova E.I., Dokl. Akad. Nauk SSR 170, 1322 (1966).

171. Garif'yanov N.S., Kozyrev B.M., Luchkina S.A., J. Struct. Chem. 9, 794 (1968).

172. Ayscough P.B., Mach K., J. Chem. Soc. (Faraday 1) 1139 (1972).

173. Fantechi R., Helcké G.A., J. Chem. Soc. (Faraday II), 924 (1972).

174. Hamilton W.C., Acta Cryst. 18, 866 (1965).

175. Kunchur N.R., Truter M.R., J. Chem. Soc.161, 2551 (1958).

176. Domiano P., Pellinghelli M.A., Tiripicchio A., Acta Cryst. B28, 2495 (1972).

177. Vaughan P., Donohue J., Acta Cryst. 5, 530 (1952).

178. McConnell H.M., Proc. Natl. Acad. Sci. U.S.A. 44, 766 (1958).

179. Miyagawo I., Gordy W., J. Chem. Phys. 32, 255 (1960).

180. Lontz R.J., Gordy W., J. Chem. Phys. 37, 1357 (1962).

181. Atherton N.M., Whiffen D.H., J. Mol. Phys. 3, 1 (1960).

182. Weil J.A., Anderson J.H., J. Chem. Phys. 35, 1410 (1961).

183. Trammell G.T., Zeldes H., Livingstone R., Phys. Rev. 110, 630 (1958).

184. Bleaney B., Phil. Mag. 42, 441 (1951).

185. Poole C.P. Jr, Farach H.A., J. Mag. Res. 4, 312 (1971).

186. Poole C.P. Jr, Farach H.A., J. Mag. Res. 5, 305 (1971).

187. Schonland D.S., Proc. Phys. Soc. 73, 788 (1959).

188. Weil J.A., Anderson J.H., J. Chem. Phys. 28, 864 (1958).

189. Geusic J.E., Carlton Brown L., Phys. Rev. 112, 64 (1958).

190. Busing W.R., Levy H.A., "ORGLS, a general fortran least squares program". Oakridge National Laboratory, contract No. W-7405-eng-26, 1962.